Modeling defective epigenetic inheritance in vascular aging using Hutchinson-Gilford Progeria Syndrome vascular smooth muscle cells

Submitted by

Zhaoyi Chen

A thesis submitted to the University of Ottawa
in partial fulfillment of the requirements for the
Doctorate in Philosophy Cellular and Molecular Medicine

Department of Cellular and Molecular Medicine
Faculty of Medicine
University of Ottawa

ABSTRACT

Cardiovascular disease (CVD) is the leading cause of death due to its prevalence in tandem with the propensity of atherosclerosis to worsen and cause myocardial infarction and stroke. The greatest risk factor for CVD development is age. The multifactorial etiology of atherosclerosis has made CVD difficult to model and consequently little is known about CVD onset and progression. Hutchinson-Gilford Progeria Syndrome (HGPS) is a severe human premature aging disorder caused by a mutation in Lamin A that leads to the accumulation of an aberrant Lamin A protein termed progerin. Patients who harbour this mutation develop atherosclerosis and die from myocardial infarction or stroke at an average age of 13 years old. Autopsies reveal deterioration of vascular smooth muscle cells (VSMCs) in HGPS patients, underlining a strong connection between VSMC loss and predisposition to CVD development. The major aim of this thesis was to model normative vascular aging and disease using HGPS induced pluripotent stem cell (iPSC)-derived VSMCs and monitor the onset of defective epigenetic inheritance *in vitro*. My results indicate reprogramming of patient fibroblasts to restores a normal nuclear phenotype. Patient derived iPSC lines generated from fibroblasts are nearly indistinguishable from healthy controls in terms of pluripotency, nuclear membrane integrity, as well as transcriptional and epigenetic profiles. However, differentiation of HGPS iPSCs to generate HGPS VSMCs recapitulates many aspects of normative vascular aging exemplified by increased ROS, DNA damage and transcriptomic aberrations. Furthermore, using a multi-omic approach including RNA-sequencing,

and accelerated native isolation of protein on nascent DNA, HGPS VSMCs demonstrate loss of histone acetylation due to defective MOF abundance that contributed to impaired engagement with DNA damage repair pathway. This dissertation provides insights on the mechanisms that drive the epigenetic and transcriptomic changes in HGPS vasculature, illuminating druggable pathways that may also drive CVD in the general population.

ABBREVIATIONS

aniPOND	Accelerated native isolation of proteins on nascent DNA
ATM	Ataxia telangiectasia mutated
ATR	Ataxia telangiectasia and Rad3-related
CVD	Cardiovascular disease
DDR	DNA damage repair
DEGs	Differential expressed genes
DSB	Double strand breaks
EB	Embryoid Body
EC	Endothelial cell
ECM	Extracellular matrix
ESI	Electron spectroscopic imaging
FBS	Fetal Bovine Serum
FTI	Farnesyltransferase Inhibitor
GO	Gene ontology
hESCs	Human embryonic stem cells
HR	Homologous repair
INM	Inner nuclear membrane
LADs	Lamin-associated domains
LBR	Lamin B receptor
MMPs	Metalloproteinases
NAC	N-acetyl cysteine
NHEJ	Non-homologous end joining
NPC	Nuclear Pore Complex
NuRD	Nucleosome remodeling and deacetylase
PCA	Principle Component Analysis
PLA	Proximity ligation assay
ROS	Reactive oxygen species
SA-βGal	Senescence-activated β-galactosidase
SSB	Single strand breaks
VSMC	Vascular smooth muscle cell

ACKNOWLEDGEMENTS

To my parents – Thank you for your unconditional love and support, I am very lucky to call you my parents.

To my wonderful labmates – Carole, Lisa, Rich, Sean, Adam, Julien and Angela, I would not be have made it this far without this intelligent and funny body of people. From the late-night drinking sessions to the annual beer runs (mixed with scientific discussions of course), you guys added so much colour and flavour to my life, and for that I am forever grateful.

To my supervisor, Dr. William Stanford - Thank you for taking me under your wings 10 years ago and for your consistent mentorship.

To Kathleen – Thank you so much for your kindheartedness and encouragement. You are a precious soul and I am so lucky to have you in my life.

To Caitlin, Carlie and Doug – Thank you for including me in your family. Your love and support kept me going through many tough times.

To Nayana, Asoka and Shyane – Thank you so much for the unconditional support during the last stretch of my thesis.

To Dylan – No words can describe the amount of kindness and patience you have shown me over the years. Thank you, thank you, and thank you, for being a constant beacon of light through the good and the bad.

To myself from 10 years ago – Relax, you will do just fine.

Table of Contents

CHAPTER 1 – INTRODUCTION

1.1 Vascular aging

Cardiovascular disease (CVD) is currently the leading cause of morbidity worldwide (Virmani et al., 1991). The economic cost of treating CVD patients is significant in both developed and developing world, and is projected to increase substantially in the coming years(O'Donnell and Nabel, 2008). It has been identified that aging plays a central role in development of cardiovascular diseases (Kovacic et al., 2011). Approximately one-fifth of the world population will be aged 65 or older by 2030, with an exponential increase in the prevalence of CVD (Heidenreich et al., 2011). Addressing age-related vascular diseases is of critical importance since the annual cost for treating CVD is projected to increase dramatically in the near future. To develop novel treatments to mitigate the effects of vascular aging and to prevent age-related vascular pathologies, it is essential to understand the cellular and functional changes that occur in the vasculature during aging.

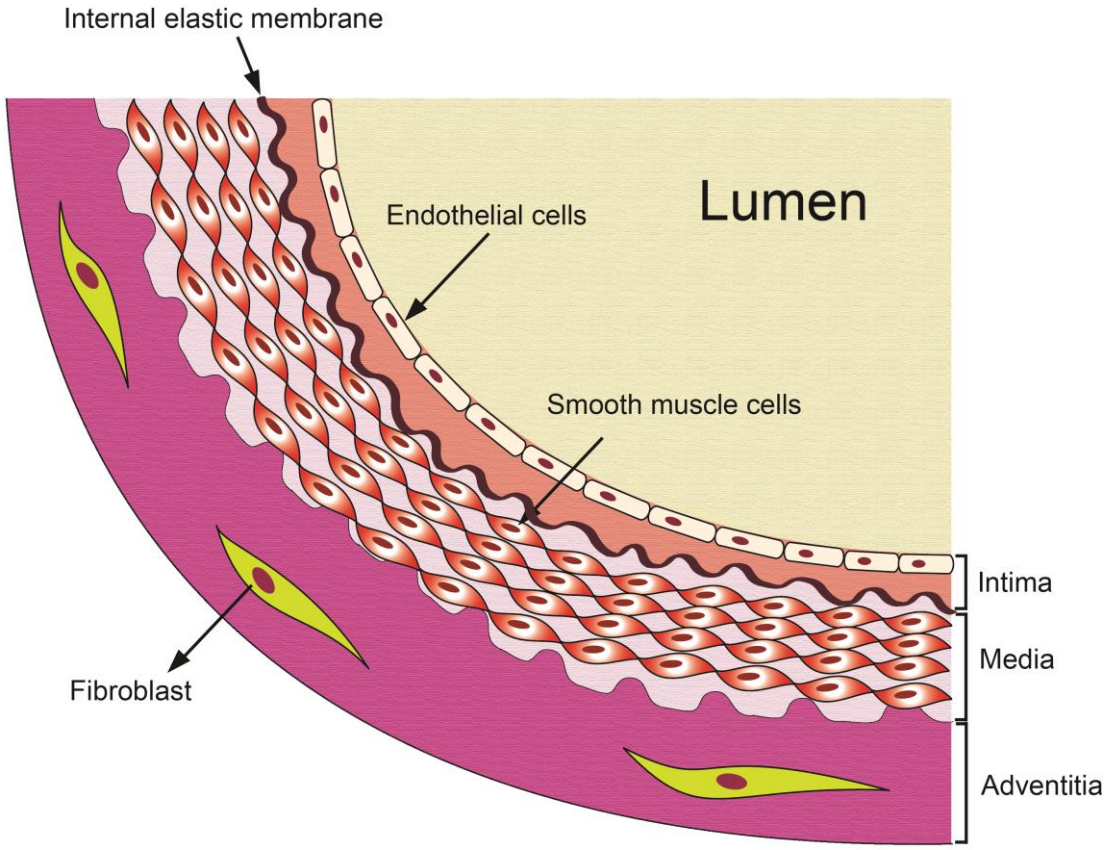

Figure 1.1 Anatomy of the blood vessel wall.

1.1.1 Anatomy of Human Vasculature

The vasculature is made of a circulatory network of blood vessels that deliver blood cells, nutrients and oxygen to the tissues of the body, as well as remove waste and carbon dioxide from the tissues. These blood vessels are composed of extracellular matrix (ECM), vascular smooth muscle cells (VSMCs) and endothelial cells (ECs). These components in the blood vessels are arranged into three concentric layers, which are the intima, media, and adventitia (Tennant and McGeachie, 1990) (Figure 1.1). The adventitia is the outer layer composed of connective tissue and autonomic nerves. The media is the middle layer composed of VSMCs that govern

vasoconstriction and vasodilation, as well as elastic fibres, which propel blood forward through expansion and contraction (Majesky et al., 2011). The innermost layer is the intima, a thin layer abutting the vessel lumen that is composed of a single layer of endothelial cells.

1.1.2 Pathophysiological features of vascular aging

Pathologic vascular aging is a complex and multifactorial process where the vasculature wall increases in thickness and stiffness, while it decreases in vessel compliance. During vascular aging, the blood vessels undergo vascular remodeling, where the vascular wall thickens is due to an increase in collagen deposition and the migration and proliferation of VSMCs from the media to the intima (Gorenne et al., 2006; Virmani et al., 1991). With age, the expression of growth factors that regulate the synthesis of elastic fibers in the ECM also declines. The thickening of vascular wall in tandem with elastic fiber loss in the artery ultimately leads to altered vascular elasticity, increase in lumen size and vascular stiffening in both arteries and veins (Lee and Oh, 2010; Tsai et al., 2012). Since arterial elasticity is a major determinant of blood flow from the heart, stiffened arteries leads to restricted blood flow to organs and tissues, which can leads to many downstream cardiovascular complications such as hypertension, cardiac fibrosis, and atherosclerosis.

Atherosclerosis is one of the most severe consequences of vascular aging. It occurs when a plaque build-up occurs inside a stiffened artery, thereby narrowing the lumen and restricting blood flow (Gorenne et al., 2006). Pathologically, an atherosclerotic plaque is formed when endothelial layer becomes dysfunctional,

accompanied by phenotypic changes in the lumen of aged blood vessels that causes augmented vascular permeability, thereby promoting the infiltration of lipids, cholesterol and inflammatory cells into the subendothelial space (Figure 1.2). Inflammatory cells can engulf lipids to form foam cells, which subsequently releases proinflammatory cytokines to create an inflammatory environment. VSMCs in the medial layer undergo a phenotypic switch, where they hyper-proliferate in response to increased PDGF expression by foam cells and migrate into the intima, where they contribute to the progression of atherosclerotic lesions by depositing ECM and collagen to form the fibrous cap that engulfs the inflamed lipid core. An atherosclerotic plaque becomes unstable when the VSMCs surrounding the fibrous cap undergo premature senescence, releasing more pro-inflammatory cytokines and metalloproteinases (MMPs), promoting further inflammation and ultimately leading to plaque rupture (Wang et al., 2007). Ruptured plaques can induce thrombosis and are a major cause of myocardial infarction and strokes.

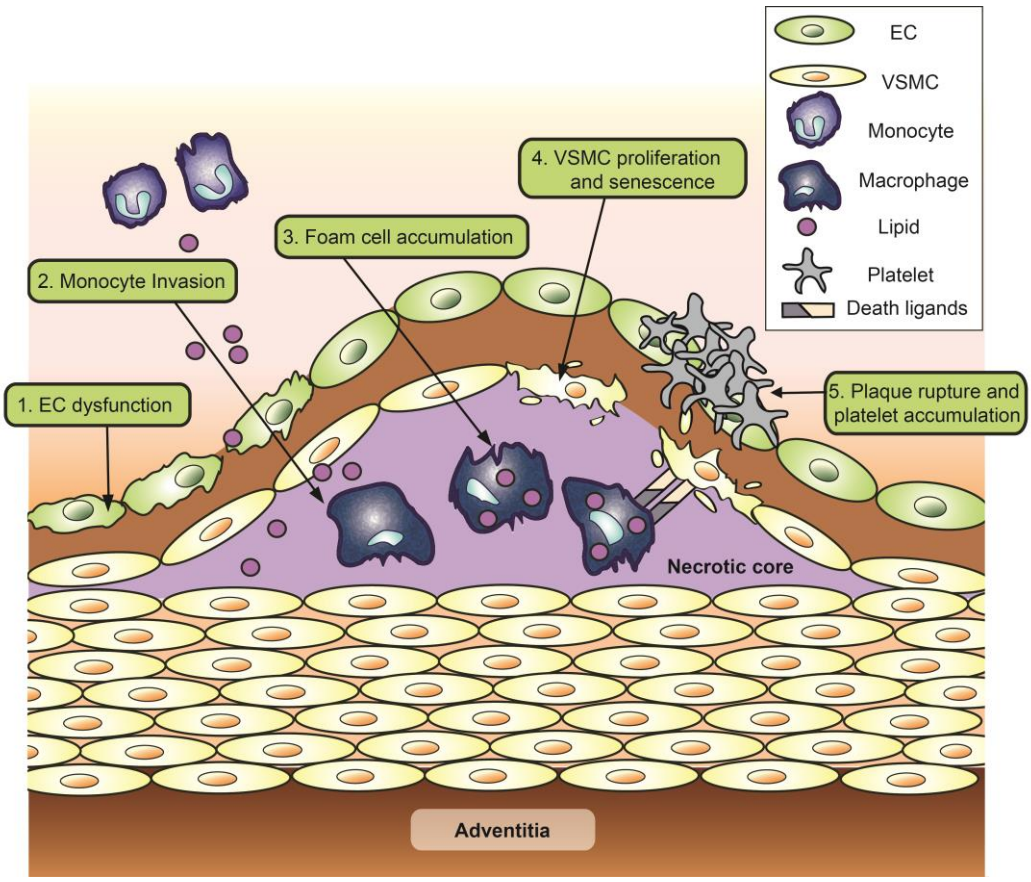

Figure 1.2. Schematic of atherosclerotic plaque. Plaque formation involves a series of events. It is initiated when 1) the endothelial layer becomes dysfunctional and increasing vascular permeability, which promotes the 2) infiltration and attachment of lipid and monocytes into the subendothelial space. 3) Monocytes differentiate into macrophages that engulf lipids to form foam cells and release proinflammatory molecules. 4) VSMCs proliferate and migrate into the intima, where they produce collagen to form a fibrous cap that encloses the lipid core. VSMCs then undergo senescence and further produce inflammatory cytokines to further augment the pre-existing inflammatory environment. 5) Gradual loss of VSMCs and increased matrix-degrading enzymes in the cap result in plaque rupture and subsequent thrombosis.

1.1.3 VSMC alterations in vascular aging

VSMCs play important roles not only in the physiological function of the blood vessels but also in the pathogenesis of vascular diseases. These cells are a major

component the medial layer of the blood vessels, and are critical for regulating contractile tone of arteries, maintaining blood pressure, and arterial repair (Lacolley et al., 2012). VSMCs act as sensors to vasoactive substances in the blood and transduce them into various biochemical signals that regulates blood vessel mechanotransduction (Lacolley et al., 2012; Lacolley et al., 2017). VSMCs are sensitive to said signals as well and can undergo a phenotypic switch to either a proliferative or contractile phenotype. Contractile VSMCs have a spindle-shaped morphology, increased contractile function and reduced proliferative capacity. Conversely, proliferative VSMCs exhibit 'hill and valley' growth, enhanced growth rate, and increase in migration capability (Bennett, 1999). Below summarizes several aspects of how aging affects VSMC behaviour during vascular aging.

1.3.1.1. Premature Senescence: Cellular senescence is defined as the permanent arrest of cell proliferation is coupled with genomic and phenotypic changes, including telomere attrition to the point of dysfunction (Yin and Pickering, 2016). Along with altered expression of cell cycle regulators, senescent cells are characterized by the expression of specific markers, including p16, p21, and senescence-activated beta-galactosidase (SA-βGal) (Dimri et al., 1995).

Cellular senescence plays an essential role in VSMC deterioration associated with vascular aging. VSMCs derived from atherosclerotic plaques exhibit low levels of proliferation compared with cells from normal arterial media (Bennett et al., 1998). Moreover, VSMCs from aged vessels and atherosclerotic plaques exhibit high levels

of SA-βGal, p16, and p21 compared to normal VSMCs (Gorenne et al., 2006). Furthermore, telomere lengths in advanced plaque VSMCs are significantly shorter than normal VSMCs (Matthews et al., 2006), suggesting that these cells exhibit senescence during atherosclerosis.

1.1.3.2. Abnormal Proliferation Rate: VSMCs in healthy vessel walls are in a quiescent non-proliferative phenotype. However, during the early stages of vascular aging, VSMCs exhibit a phenotypic switch from a contractile phase to a proliferative phase. Hyper-proliferative VSMCs can migrate from the media to the intima of the blood vessel, where they deposit ECM and collagen (Lacolley et al., 2012). Several factors present in the atherosclerotic lesions have been shown to further induce VSMC proliferation, including growth factors, low-density lipoproteins, and homocysteine (Zettler et al., 2003). In contrast, VSMCs in advanced atherosclerotic plaques undergo premature senescence and decreased proliferation rates, likely due to altered response to environmental factors and exposure to senescence markers p16 and p21 (Matthews et al., 2006).

1.1.3.3 Oxidative Stress: Oxidative stress is a state of imbalance between free radicals and antioxidants in a cell and is triggered by the sustained production of oxidant molecules or deleterious radicals. The role of oxidative stress has been proposed as a major contributor to the development of cardiovascular disease. Aging vasculature has reduced antioxidative defense in tandem with increased generation of oxidizing reagents and reactive oxygen species (ROS) (Mahmoudi et al., 2006).

Although a basal level of ROS is required for cellular homeostasis and adaptation to stress, overproduction of these radicals can further generate a spectrum of DNA damage including DNA strand breaks and DNA base modifications. Chronic oxidative stress can cause telomere shortening and accelerate cells to become senescent (Matthews et al., 2006). The source of elevated ROS during aging was suggested to be due to defective mitochondrial function and concomitant accumulation of oxidative mitochondria DNA damage (Correia-Melo and Passos, 2015), which accelerates cellular senescence in VSMCs and contributes to overall vascular aging.

A number of studies have demonstrated that oxidative stress contributes to the deterioration of VSMCs. For example, increased ROS production has been observed in aged murine VSMCs compared to younger VSMCs (Moon et al., 2001). In humans, elevated levels of ROS and superoxide has been detected in intima VSMCs in the blood vessels of geriatric subjects (Matthews et al., 2006). Furthermore, VSMCs from patients with coronary artery disease exhibit elevated H_2O_2 due to overexpression of NADPH oxidase 5 (Guzik et al., 2008). Overall, the role of oxidative stress is well documented in VSMC deterioration.

1.1.3.4 DNA Damage: DNA is constantly the target of both endogenous and exogenous insults by agents such as ROS, UV light irradiation and chemical drugs. These agents cause multiple types of DNA damage including single strand DNA break (SSBs) and double strand DNA break (DSBs) (d'Adda di Fagagna et al., 2003).

DSBs are the most severe type of DNA damage, leading to significant genomic instability, however both SSB and DSBs trigger a DNA damage response (DDR). During DDR, repair proteins phosphorylate H2A histone family member X (γ-H2AX) as part of the DDR signalling cascade and together, they accumulate at the site of DNA damage and act to transduce and amplify downstream DDR signals (Rothkamm et al., 2003). DDR also activates p53, which in turn up-regulates p21 to promote a transient cell cycle arrest for the duration of the repair (Herbig et al., 2004). However, failure to amend DSBs can result in sustained activation of DDR and may induce cellular senescence, where sustained DDR signalling activates p53, which in turn up-regulates cell cycle checkpoint proteins and induces growth arrest.

1.1.3.4.a The amplification of DDR signals to repair DSBs: The occurrence of DSBs can be recognized by a series of proteins in a sequential manner during the initiation of DDR (Figure 1.3). First, DNA damage sensor proteins including the XRCC5-XRCC6 and Mre11-Rad50-Nbs1 (MRN) complexes, as well as poly-(ADP-ribose) polymerase 1 (PARP1) bind to DSB break ends and initiate the recruitment of downstream factors (Bunting et al., 2010). Subsequently, recruitment of signalling proteins and repair factors at the site of DNA damage enables the amplification of DDR signal. For example, the DDR signal protein ataxia telangiectasia mutated (ATM) binds to DSBs via interaction with MRN complex, where it undergoes auto-phosphorylation and self-activation to phosphorylate histone H2A.X, yielding γ-H2AX (Rothkamm et al., 2003; Sancar et al., 2004). The presence of γ-H2AX further triggers additional accumulation of MRN complex via the facilitation of MDC1 protein, which recruits

more ATM at the site to phosphorylate more H2A.X, creating a feedback loop to amplify DDR signals and propagate the spread of γ-H2AX to form a cryptogenic focus (Rothkamm et al., 2003; Sancar et al., 2004).

Following the amplification of the DDR signal, DSBs are repaired through two major pathways: non-homologous end joining (NHEJ) and homologous recombination (HR). NHEJ is the predominant DSB repair pathway that is activated throughout the entire cell cycle, although it is favoured in the G1 phase (Chapman et al., 2012). NHEJ takes place when DNA damage sensors XRCC5/6 binds to DNA and serve as a docking site for additional protein recruitment. One of these factors is DNA-PKc, a kinase that undergoes auto-phosphorylation, which favours the processing of DNA ends by endonuclease Artemis. Finally, processed DNA ends are then rejoined through XRCC4-Ligase IV complex (Lieber, 2010). Essentially, NHEJ mediates the direct ligation of two random DNA break ends at proximity in a template independent manner and is thus error-prone, often resulting in small insertions or deletions of DNA (Chapman et al., 2012).

In contrast, when DSBs occur in S/G2 phase of the cell cycle, DNA repair is done via the error-free HR pathway. HR pathway is activated when PARP1 first binds to the DSB and competes with XRCC5/6 binding to DNA ends. The MRN complex is then recruited to DSB in conjunction with BRCA1 to mediate DSB resection through endonuclease Exo1 that mediates DNA degradation, resulting in long stretches of single-stranded DNA (ssDNA). The resulting ssDNA are then coated by Rad51

filaments to form a structure termed “nucleofilaments”. Rad51 together with other HR factors then mediate nucleofilament homology search and strand invasion, a process where resected nucleofilament searches and invades into corresponding homologous template in the sister chromatid. DNA polymerization then occurs using sister chromatid as template to produce an exact copy of the template where the DSB was generated. Unlike NHEJ, HR is mutation free and can accurately amend DSBs that arise from different causes such as ionized irradiation and replication fork collapse.

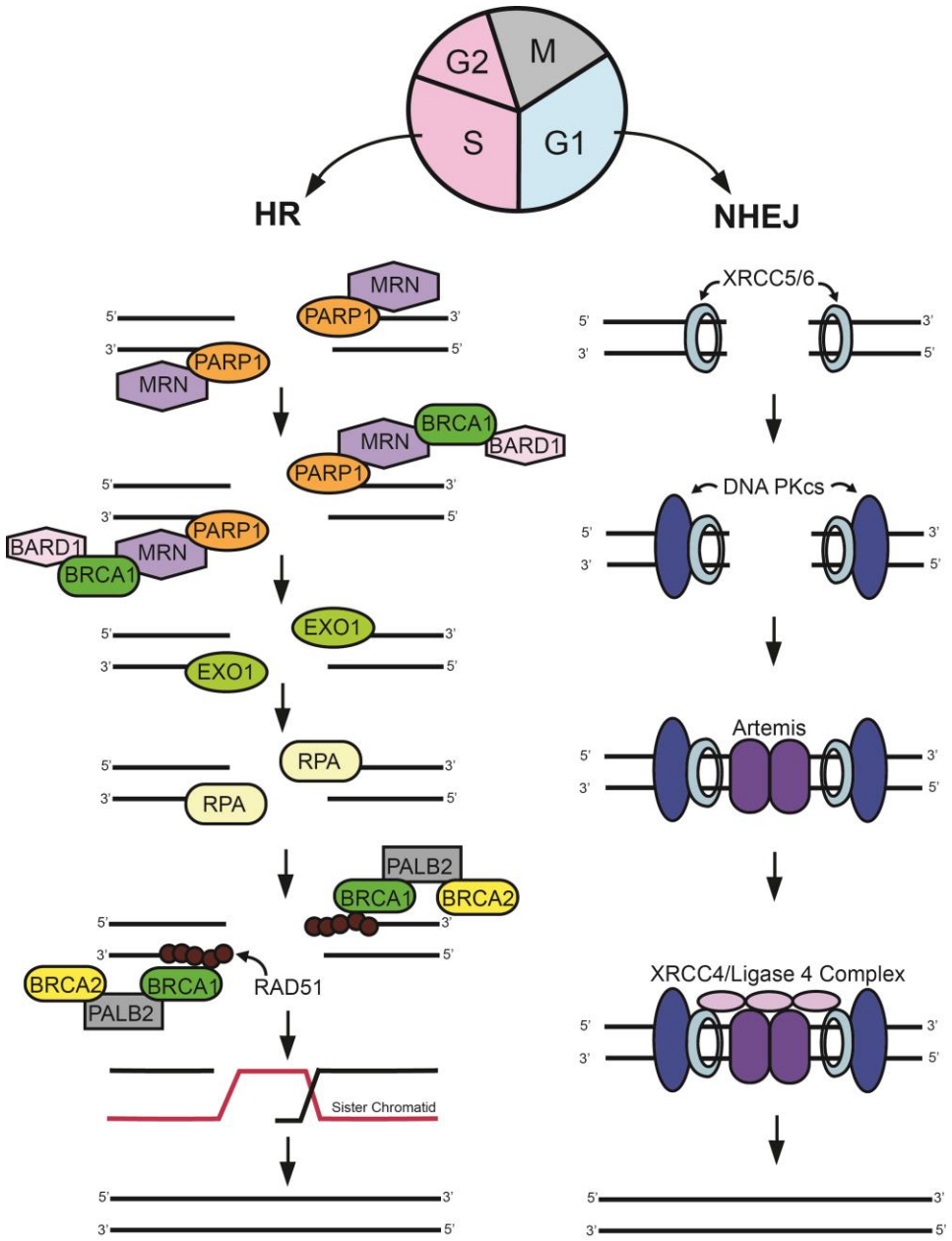

Figure 1.3. Schematic for non-homologous End Joining (NHEJ) (left) and Homologous repair (HR) (right). DNA double-strand breaks (DSBs) are repaired via NHEJ during G1 phase. This process involves 1) XRCC5/6 heterodimer detects and binds to the DSB site; 2) XRCC5/6 recruits DNA PKcs holoenzymes; 3) DNA PKcs undergo autophosphorylation and activates Artemis, a nuclease that is also recruited by XRCC5/6 to the DSB site. Artemis processes the DNA ends by cutting the overhangs at the DNA sites; 4) XRCC4/DNA ligase 4 complex ligates the processed DNA ends. In contrast, when DSB occurs during S and G2 phase, the HR pathway is the preferred. 1) PARP1 binds to DSB and

competes with XRCC5/6 binding. 2) the MRN complex is recruited to the DSB (in conjunction with CtIP, BRCA1 and BARD1) to mediate DSB resection; 3) DNA resectioning is catalyzed by EXO1, resulting in a long stretch of single-stranded DNA (ssDNA); 4-5) ssDNA is coated by RPA, which is replaced by Rad51 filaments via BRCA2/PALB2/BRCA1 complex. 6) RAD51 induces strand invasion into homologous DNA sequences, where DNA polymerization occurs using sister chromatid as a template to produce an exact copy of the template where DSB occurred.

1.1.3.4.b. Signs of DNA damage in aged VSMCs: Many studies suggest that vascular aging and atherosclerotic progression are accompanied by extensive DNA damage. For instance, atherosclerotic plaque VSMCs exhibit increased ATM and γ-H2AX expression both *in vivo* and *in vitro*, which is indicative of extensive DNA damage taking place during disease progression (Mahmoudi et al., 2006). Complementarily, knockout of DDR proteins such as ERCC1 induces premature vascular senescence and vascular stiffness due to defective VSMC function in mice (Durik et al., 2012), highlighting the importance of proper DDR in maintaining VSMC health.

1.1.4 Current efforts in CVD-related research

Aging is tightly linked to the onset and the progression of many CVDs including atherosclerosis. Therefore, a deeper understanding of the complex process of vascular aging enables the development of therapeutic strategies to prolong the lifespan of patients with CVDs. The specific focus on VSMC aging was highlighted due to its apparent role in mediating the aging phenotype in the vasculature, as VSMC dysfunction is thought to be the major trigger of vascular stiffening.

Improving our knowledge of the mechanisms underlying VSMC aging is therefore critical to the development of new strategies to reduce disease burden in the elderly. Much of the molecular hallmarks in VSMC aging were defined through comparisons of young and normally aging animal models or histology studies. In order to derive better drug targets for developing new therapies and improve CVD prevention, a complementary human model is needed to identify which of the VSMC aging hallmarks contribute the most to age-associated cardiovascular damage.

1.2 Cardiovascular disease in HGPS patients

The studies of progeroid disorders have shed light on the cellular and molecular mechanisms driving normative vascular aging and associated CVDs. Amongst them, Hutchinson-Gilford Progeria Syndrome (HGPS) is the most severe progeroid syndrome with a prevalence rate of 1 in 4 million births worldwide (Hennekam, 2006). The typical clinical characteristics observed in HGPS patients are growth retardation, skeletal muscle atrophy, alopecia, decreased subcutaneous fat, and loss of hearing (Hennekam, 2006; Merideth et al., 2008). Mortality is largely due to premature vascular complications causing terminal atherosclerosis in HGPS patients, which leads to fatal cardiovascular diseases such as heart attacks and strokes (Hennekam, 2006), and ultimately causing premature death at an average age of 14 years.

HGPS is caused by a single-point mutation in the *LMNA* gene. After undergoing alternative splicing, the precursor protein prelamin A undergoes several post-

translational modifications to yield mature lamin A (Lin and Worman, 1993; Worman, 2012) (Figure1.4). In HGPS, a single-point mutation within *LMNA* exon 11 (C1824T) that activates a cryptic splice site between exons 11-12, leading to an internal 50 amino acid deletion near the C-terminus of the prelamin A transcript which encompasses the ZMPSTE24 cleavage site. This results in the synthesis of mutant protein termed "progerin" that remains permanently farnesylated and carboxymethylated (Eriksson et al., 2003). Due to the continuous presence of the farnesyl group, progerin remains anchored in the INM leading to abnormalities in nuclear shape and function (Gonzalo et al., 2017).

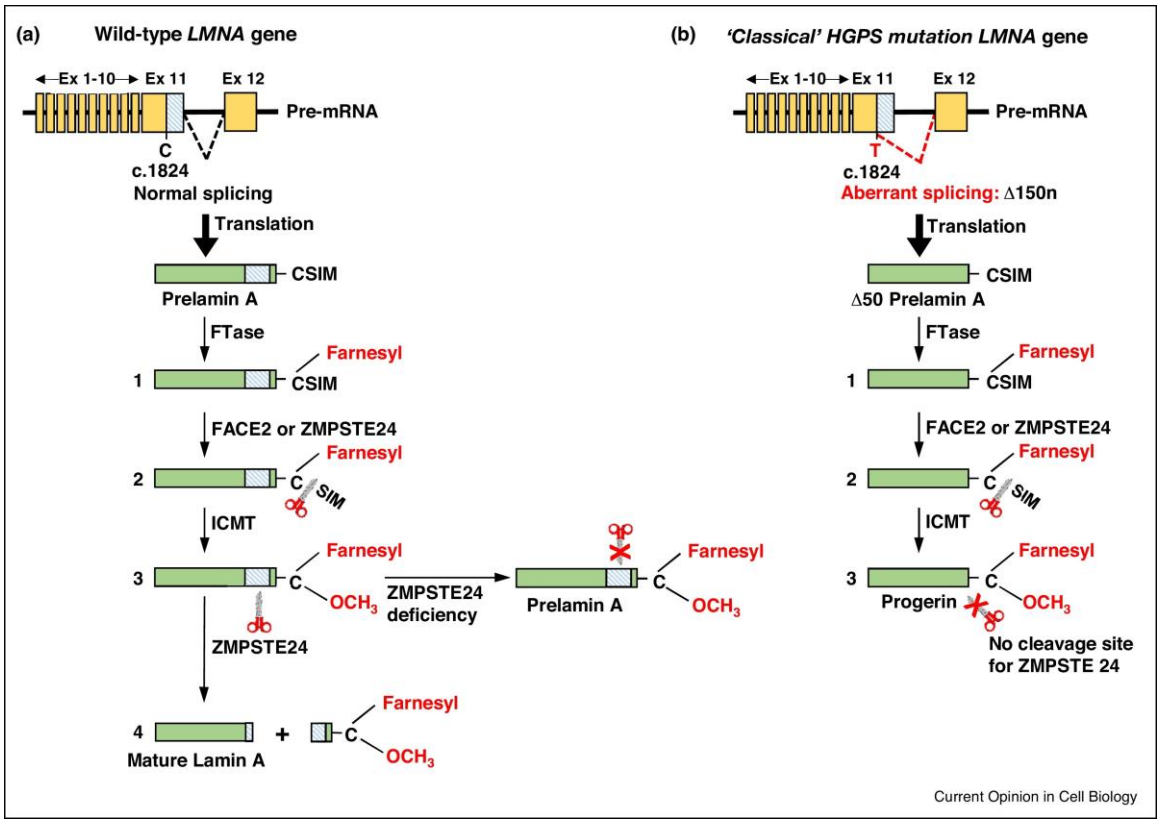

Figure 1.4 Prelamin A processing in normal and HGPS cells (Dorado and Andres, 2017). A) In control cells carrying wildtype *LMNA* sequence, normal splicing between exon 11 and 12 give rise to

prelamin A, which undergoes post-translational modifications to yield mature Lamin A protein. B) Classic HGPS is caused by *de novo* mutation in the *LMNA* gene which results in aberrant splicing between exon 11-12 and the synthesis of progerin. The 50 amino acid residue deletion in progerin encompasses the ZMPSTE24 cleavage site, preventing the removal of progerin C-terminus, which remains permanently farnesylated. Abbreviations: CSIM, cysteine-serine-isoleucine-methionine; FACE-2, farnesylated protein-converting enzyme-2; FTase, farnesyltransferase; ICMT, isoprenylcysteine carboxyl methyltransferase; ZMPSTE24, zinc metallopeptidase STE24. Reprint from . Current Opinion in Cell Biology vol 46, 17-25, B. Dorado and V. Andres, "A-type lamins and cardiovascular disease in premature aging syndromes ", 2017, with permission from Elsevier.

1.2.1 Connection between HGPS and normative vascular aging

The phenotypes and mechanisms underpinning disease progression are markedly similar between HGPS and normative vascular aging (Olive et al., 2010). An immunohistochemistry study on the arterial phenotypes in HGPS patients who succumbed to myocardial infarction identified many classical features of advanced vascular pathology that were also observed in conventional atherosclerosis, including VSMC loss, adventitial thickening and fibrosis, extensive vascular calcification and plaque build-up (Olive et al., 2010).

In addition, several normative vascular aging-associated cellular phenotypes have been observed in HGPS. Similar to aged VSMCs, HGPS cells express hallmarks of premature senescence such as SA-β-gal and p21, indicative of persistent cell cycle arrest (Ragnauth et al., 2010). HGPS cells also show many traits of genomic instability that are observed in aged vasculature from healthy aged individuals, including elevated oxidative stress and increased γ-H2AX foci (Liu et al., 2008).

Interestingly, progerin also accumulates in normal aging individuals. It was discovered that primary cells from normal geriatric patients exhibit a sporadic utilization of the classic HGPS cryptic splice donor site that results in progerin accumulation (Scaffidi and Misteli, 2006). Prelamin A and progerin are widely present in cells and tissues of non-HGPS aging individuals and increases with advancing age (McClintock et al., 2007; Olive et al., 2010), including cells within the coronary atherosclerotic lesions (Olive et al., 2010), implicating the progressive accumulation of progerin as an important contributor to age-induced vascular dysfunction. Collectively, since HGPS vascular deterioration phenocopies normative vascular aging, understanding the molecular mechanisms underpinning cardiovascular alterations associated with HGPS could shed light on novel therapeutic approaches for the treatment of CVDs.

1.3. The importance of lamins in cellular function and disease manifestation

Lamin A plays diverse and important structural and regulatory roles in many essential cellular functions such as nuclear pore formation, chromatin organization and gene regulation. Subtle differences in Lamin A processing or production can therefore result in critical alterations in cellular function. Laminopathies is the term given to a heterogeneous group of diseases caused by mutations in genes encoding for lamins or lamin-binding proteins. They are most frequently caused by mutation in the *LMNA* gene with over 500 currently reported mutations (Gonzalo et al., 2017). Laminopathies include diseases affecting striated muscle, lipodystrophies and

accelerated aging disorders, of which HGPS is the best studied and the most severe type of laminopathy (Smith et al., 2005).

To understand how the mutation in lamin A can manifest into such detrimental effects in HGPS cells, it is important to understand how the nuclear lamina is organized and its function in the nucleus. Below summarizes the structure and the biological functions in lamins.

1.3.1 The structure of nuclear lamina

The nuclear envelope is a lipid bilayer consisting of an outer (ONM) and inner nuclear membrane (INM) connected through nuclear pore complexes (NPC) (Figure 1.5). The ONM connects with the endoplasmic reticulum and is heavily associated with proteins that link the nucleus to the cytoskeleton, while the INM harbours numerous nuclear envelope transmembrane proteins.

The nuclear lamina is a filamentous protein network underlying the INM of the nuclear envelope (Gruenbaum and Medalia, 2015) (Figure 1.5). It is composed of lamins, which are type V intermediate filaments that provide nuclear structural support, and aid in heterochromatin organization, DNA damage repair, gene transcription, and mitosis (Kennedy et al., 2000; Shumaker et al., 2006; Zuela et al., 2012). In mammalian cells, three lamin genes termed *LMNA, LMNAB1,* and *LMNB2* encode for four major and three minor lamin isoforms. The lamins are grouped into A-type lamins (lamin A and C as well as CΔ10 and C2 minor isoforms) that are transcribed from *LMNA* distinctly via an alternative RNA splicing event within exon

10(Lin and Worman, 1993), and B-type lamins (lamin B1 and B2) that are transcribed from *LMNB1* and *LMNB2*. *LMNA* is mainly expressed in differentiated cells, whereas all cells express at least one B-type lamin (Rober et al., 1989). Since different tissues express different sets of lamin-associated proteins, this provides a potential explanation to the tissue-specific phenotypes observed in various laminopathies. Indeed, some of the lamin-associated proteins have been linked to lamin-related diseases.

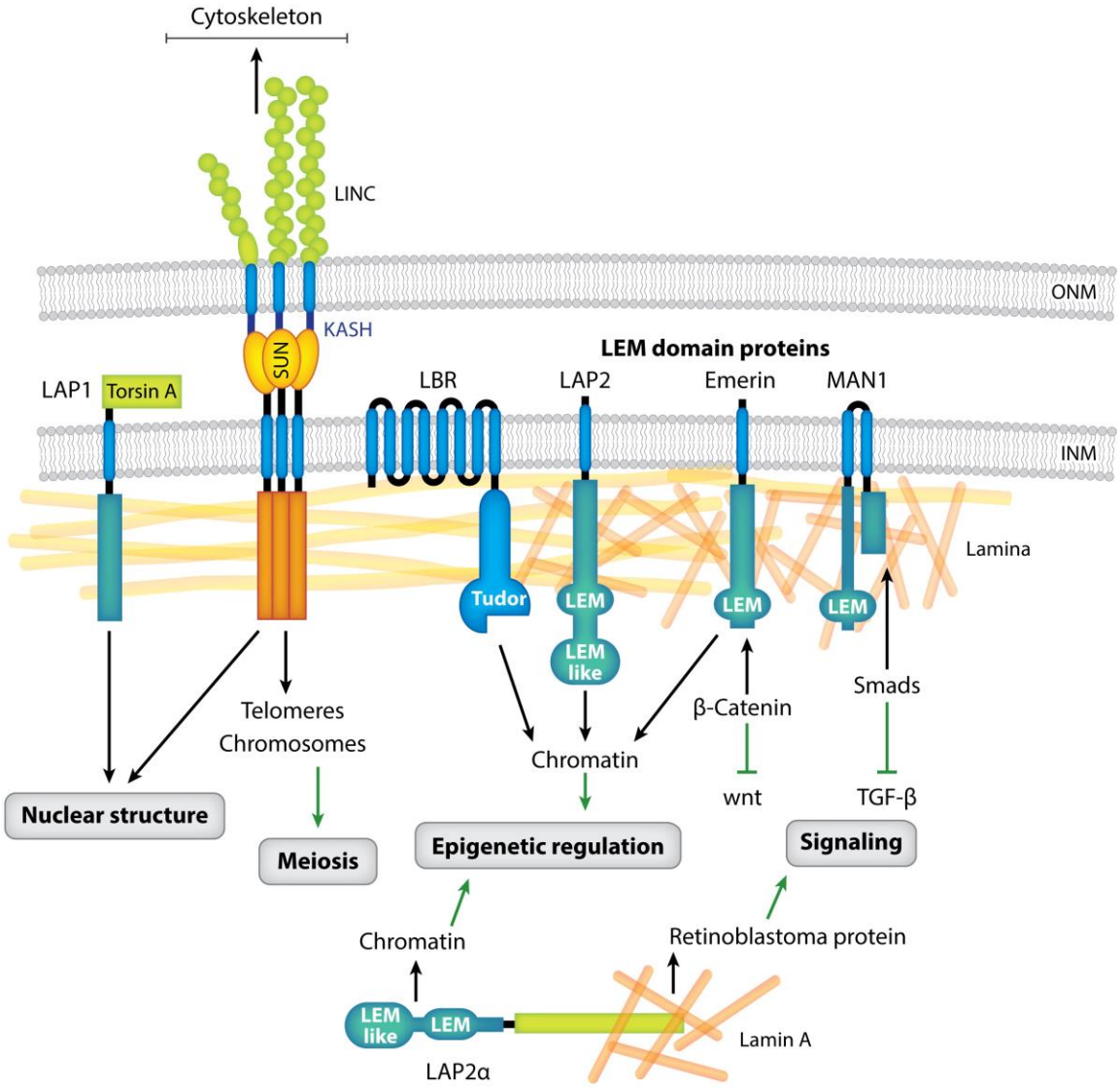

Gruenbaum Y, Foisner R. 2015.
Annu. Rev. Biochem. 84:131–64

Figure 1.5. Lamin-binding proteins and their respective functions (Gruenbaum and Medalia, 2015). Reprinted from Lamins: the structure and protein complexes, Vol 32, Y. Gruenbaum and O. Medalia, Title of article / title of chapter, 7-12., Copyright (2015), with permission from Elsevier.

1.3.2. Functions of Lamins in Nucleus

1.3.2.1. Protein interactions: The nuclear lamina has been found to interact with a plethora of proteins in the INM and the nucleoplasm that contribute to nuclear

architecture as well as to chromatin tethering and organization. For instance, lamins can bind to the LEM group of proteins, which, together with lamins, anchors chromatin to the nuclear lamina through BAF and by directly interacting with the DNA (Figure 1.5). Another group of lamin-interacting proteins is the SUN-domain group. Together with KASH domain proteins, they form the LINC complexes that are found in all eukaryotes (Figure 1.5), where they form a bridge that mediates interactions between the nuclear lamina and with major cytoskeletal structures in the cytoplasm such as actin, tubulin and intermediate filaments to mediate nuclear anchorage (Link et al., 2014).

1.3.2.2. Mechanical: Lamins are the predominant structural component of the nucleus and are essential contributors to the biophysical and mechanical properties of the nucleus. Interestingly, A-type and B-type lamins contribute to the integrity of the nuclear membrane in different manners. B-type lamins have been shown to provide mainly elastic properties, allowing for significant deformation of the nuclear envelope, while A–type lamins confer deformation-resistant stiffness to nuclei (Broers et al., 2005). Lamin ratios can impact cellular function, for example increased levels of lamin A to lamin B in cancer cells impair cell migration as a result of reduced deformability of the nucleus (Harada et al., 2014). Moreover, cells with reduced lamin A levels can lead to rupture of the nucleus (De Vos et al., 2011; Hatch et al., 2013), suggesting that the ratio of A-type versus B-type lamins govern the biomechanical properties of the nucleus. It has been discovered that the interactions between the lamina with the cytoskeletons via SUN domain proteins

and nesprins allows force transmission from the ECM through cell adhesion complexes and the cytoskeleton into the nucleus and contributes to mechanosignal transduction (Lombardi et al., 2011). This force transmission can regulate the levels of lamins (specifically lamin A) produced in the nucleus, allowing for changes in the biophysical properties of the nucleus (Swift et al., 2013) during cell migration and differentiation in response to mechanical stimuli.

1.3.2.3. Lamin Regulates Chromatin Organization: Early electron microscopy has revealed that in eukaryotic nuclei, condensed heterochromatin is mainly localized at the nuclear periphery, while light-staining euchromatin occupies the nuclear interior (Fawcett, 1966). Further advances using the DamID technique revealed that approximately 40% of the human genome is organized into lamin-associated domains (LADs) that have lower gene density, less transcriptional activity, and enriched in heterochromatin marks (Guelen et al., 2008). These regions often replicate in late S-phase and are gene poor. These studies provided strong evidence to the concept that the lamins associate primarily with heterochromatic regions of the genome.

The nuclear lamina was found to physically interact with heterochromatin and in doing so regulate several different biological processes. First, lamins can directly interact *in vitro* with specific regions of the DNA, as Lamin A can artificially bind to gene promoter regions (Lee et al., 2009), and depending on the chromatin modifications in the local genome, binding of lamin A to promoter regulates gene

expression(Lund et al., 2013). In addition, lamin-binding proteins in the INM were shown to tether heterochromatin to the nuclear lamina and mediate gene silencing. The lamin B receptor (LBR) binds to histone modification H3K9me3 via heterochromatin-binding protein 1 (HP1) (Ye and Worman, 1996) as well as to H4K20 via its Tudor domain (Hirano et al., 2012). Furthermore, members of the LEM-protein family such as LAP2β and emerin interact with chromatin via BAF. Both LEM-proteins as well as LBR tethers heterochromatin to the nuclear periphery in a redundant manner in mammalian cells (Solovei et al., 2013). Overall, lamins acts as an essential link in anchoring heterochromatin to the nuclear lamina.

1.3.2.4. Nuclear lamina in DNA damage repair: Several studies have highlighted the role of lamin A/C in DNA damage repair. For instance, lamin A has been shown to stabilize DNA damage repair foci by engaging with the damaged chromosome via binding to DSB-induced γ-H2AX (Mahen et al., 2013). Lamin A/C interacts with components of both NHEJ and HR DNA repair pathways by regulating DNA repair protein balance. Knockdown of lamin A via short hairpin RNA (shRNA) results in cysteine protease Cathepsin L-mediated degradation of p53 binding protein 1 (53BP1) - an important promoter of NHEJ pathway – as well as a transcriptional reduction of BRCA1 and RAD51 – two essential regulators of the HR pathway (Gibbs-Seymour et al., 2015). Mechanistically, lamin A/C binds to 53BP1 via its Tudor domain, suggesting that the nuclear lamina is involved in regulating 53BP1 activity (Gibbs-Seymour et al., 2015). Overall, these studies illustrate a critical role of lamin A/C in DNA damage response.

1.4. HGPS Cellular and Molecular Phenotypes

Due to the regulatory role A-type lamins play in regulating multiple cell functions, progerin-mediated disruption in the production and the assembly of lamins leads to catastrophic defects. Below is a summary of the molecular mechanisms by which progerin accumulation causes defects in HGPS cells.

1.4.1 Nuclear morphological abnormalities

One of the hallmarks of HGPS-derived cells is the nuclear morphological abnormalities (Figure 1.6). Primary HGPS fibroblasts exhibit nuclei that appear to be dysmorphic, with severe nuclear blebbing and invaginations (Eriksson et al., 2003; Goldman et al., 2004). These morphological defects are exacerbated when HGPS fibroblasts are passaged *in vitro*, concomitant with the accumulation of progerin at the nuclear lamina (Driscoll et al., 2012). Progerin accumulation has been shown to exert a dosage-dependent effect on altering nuclear architecture in normal human fibroblasts (Chojnowski et al., 2015). In fact, the farnesyl tail of progerin enhances its binding to the INM protein SUN1, causing SUN1 to accumulate at the nuclear envelope and potentially alter nuclear structure (Chen et al., 2012; Chen et al., 2014). HGPS cells also exhibit increased nuclear stiffness and greater sensitivity to mechanical strain compared to normal cells (Dahl et al., 2006), leading to altered mechanotransduction functions and ultimately leads to nuclear fragility and senescence (Verstraeten et al., 2006). The altered responses to force could be the underlying cause for tissue-specific effects of progerin, where rapid

deterioration in tissues that are subjected to high levels of mechanical stress, such as skeletal muscle, heart, and the vasculature, are more affected in HGPS patients.

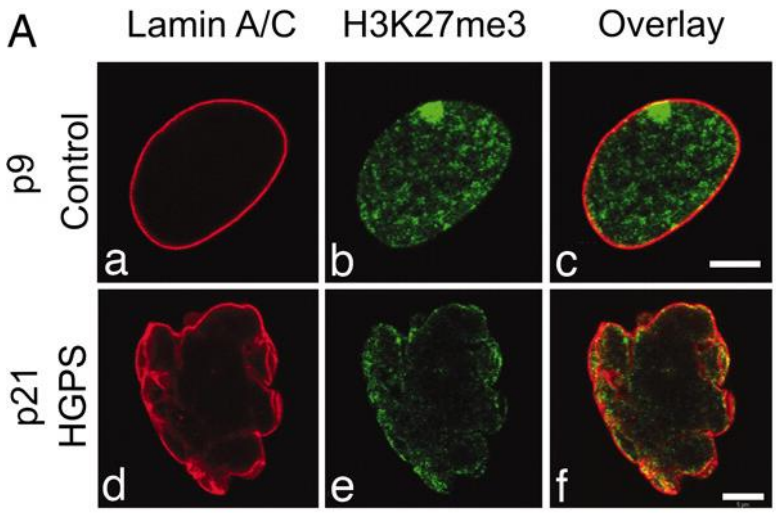

Figure 1.6. Immunofluorescence staining with antibodies against Lamin A/C and H3K27me3 in control and HGPS cells. Control cell nuclei at passage 9 (p9) display a distinctly clear nuclear lamina. HGPS cells exhibit a change in nuclear morphology by p21 and an overall loss of H3K27me3 (Shumaker et al., 2006). Copyright (2004) National Academy of Sciences, U.S.A.

.

1.4.2. Epigenetic Changes

The distortion of the nuclear lamina in HGPS is accompanied with a severe loss of chromatin organization and compartmentalization. Particularly, HGPS cells display a progressive loss of peripheral heterochromatin with increasing progerin accumulation (Dechat et al., 2008; Kubben et al., 2012) (Figure 1.7). Indeed, multiple reports have shown that HGPS cells exhibit abnormal histone modifications, DNA methylation and chromatin-modifying activities. Progressive changes in histone methylation associated with heterochromatic regions are

frequently observed, including a down-regulation of the facultative heterochromatin marker H3K27me3 and constitutive heterochromatin marker H3K9me3 (Figure 1.7), as well as an up-regulation of H4K20me3 (McCord et al., 2013; Scaffidi and Misteli, 2005; Shumaker et al., 2006). These chromatin changes in tandem with progerin expression are also observed in physiological aging, suggesting that epigenetic landscape alterations may play a role in the pathophysiology of aging (Scaffidi and Misteli, 2006).

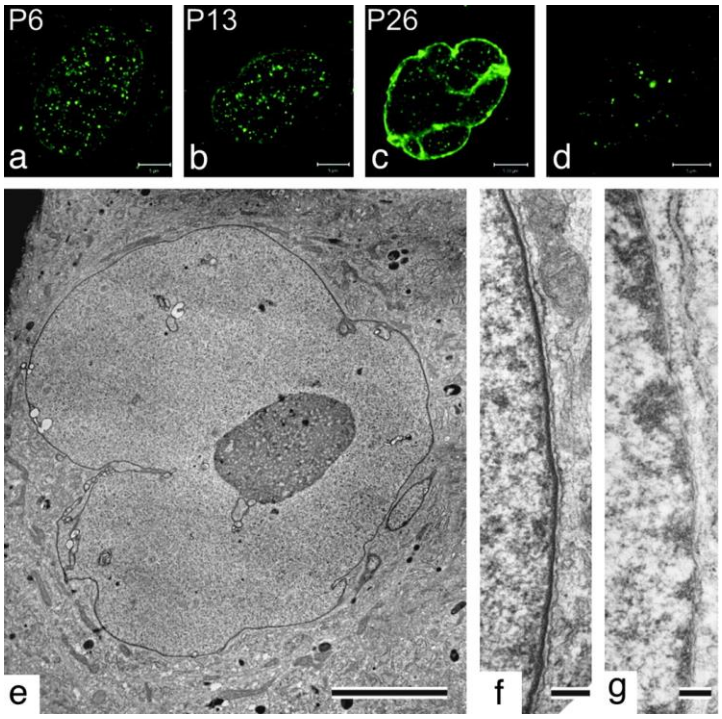

Figure 1.7 Prelamin A accumulation in HGPS cells causes loss of peripheral heterochromatin(Goldman et al., 2004). (A-D) HGPS fibroblasts exhibit gradual increase in prelamin A accumulation with increase passaging (A-C) vs lack of progerin accumulation in control fibroblast (D). (E) Electron microscopic images of HGPS fibroblasts at passage 26 exhibit extensive lobulations. (F-G) High magnification view of the nuclear envelope in a normal fibroblast shows a normal array of heterochromatin (dark-coloured) next to the nuclear envelope (G) while HGPS fibroblast at passage

26 shows a loss of peripheral heterochromatin (F). Copyright (2004) National Academy of Sciences, U.S.A.

The underlying cause of abnormal histone methylations in HGPS and how they contribute to disease progression is a topic of ongoing research over the past decade. For instance, the mechanism that causes H3K9me3 loss has been correlated with reduced level of histone methyltransferase SUV39H1 activity in HGPS cells (Liu et al., 2013b). It has also been shown that a significant down-regulation of heterochromatin protein 1 α (HP1α), a histone-binding protein that binds to and is critical for the maintenance the abundance of H3K9me3 (Dechat et al., 2008; Scaffidi and Misteli, 2005), causes a significant loss of H3K9me3 in HGPS cells (Zhang et al., 2015). Loss of H3K27me3 in HGPS cells has been linked to decreased expression of methyltransferase EZH2, a part of the Polycomb Repressive Complex 2 (PRC2) that is responsible for establishing H3K27me3 marks (Shumaker et al., 2006). H3K27me3 enrichment at specific gene promoter regions was significantly correlated with downstream gene expression alterations in HGPS cells, suggesting a causal link between H3K27me3 enrichment and altered gene expression in HGPS cells(McCord et al., 2013). Since the nuclear lamina tethers to heterochromatin, the incorporation of progerin is suggested to affect the interaction and the regulation of various heterochromatin-associated proteins that leads to the consequential alteration in histone marks.

In addition to histone methylation, abnormal histone acetylation levels have been linked to progeria. HGPS patient cells exhibit reduced expression of components of

the NuRD (Nucleosome Remodeling Deacetylase complex)(Pegoraro et al., 2009). In addition, SIRT6, a member of the sirtuin family that modulates acetylation of histone H3, is significantly compromised in HGPS cells (Ghosh et al., 2015). Moreover, H4 lysine 16 hypoacetylation is observed in Zmpste24$^{-/-}$ mouse embryonic fibroblasts (MEFs that mimic HGPS by producing unprocessed prelamin A) due to deficiency in the histone acetyltransferase MOF, further suggesting a direct role of progerin accumulation in abnormal acetylation activities in HGPS cells. There are many evidences pointing to a central role of acetylation/deacetylation patterns and related modifying proteins in HGPS cells, however the data remain controversial.

1.4.3. DNA damage response and Genomic Instability

As previously mentioned, the nuclear lamina serves as an important regulator in DNA damage repair. Consequently, functional disruption of the nuclear lamina via progerin accumulation leads to defective DNA damage repair and increased genomic instability. Abnormal activation of the NHEJ pathway was observed in smooth muscle cells derived from HGPS patients (Zhang et al., 2014; Zhang et al., 2011), suggesting that defective DNA damage response contributes to progerin-driven VSMC death. Moreover, fibroblasts derived from HGPS patients display a delayed recruitment of NHEJ regulator 53BP1, as well as RAD51, a component in HR pathway, at the damaged DNA lesions upon ionized irradiation (Liu et al., 2005). Instead, there is an aberrant accumulation of the nucleotide excision repair protein XPA at the sites of DNA damage. As a result, HGPS fibroblasts display an increased sensitivity towards DNA damage inducing agents and slow recovery rate compared

to control fibroblasts (Liu et al., 2005). HGPS cells also exhibit delayed recruitment of the MRN complex necessary for sensing DNA lesions, and an aberrant level of DNAPK holoenzyme components (DNAPKcs, XRCC5/6)(Liu et al., 2011), which are necessary for the proper recruitment of NHEJ components.

The presence of progerin has been mechanistically shown to disrupt DNA damage repair by interfering with lamin A/C functionality. Unprocessed prelamin A in ZMPSTE24 knock-out mice caused decrease in the overall level of histone transferase MOF, and subsequently impairs 53BP1 foci formation at DNA lesions (Krishnan et al., 2011). Progerin was also shown to reduce retinoblastoma binding proteins 4 and 7 (RBBP4 & and RBBP7) and histone deacetylase (HDAC), all of which are components of NuRD complex (Pegoraro et al., 2009). The loss of acetylation landscape induced by prelamin A accumulation could render a more condensed chromatin structure and create a physical barrier preventing DNA repair factors to access damaged sites.

1.4.3.1 Oxidative stress: Progerin also increases DNA damage via increased level of ROS. Specifically, it has been reported that HGPS fibroblasts exhibit increased levels of ROS that cause DNA breaks and increase subsequent sensitivity to oxidative stress, which impaired proliferation capacity by activating replicative senescence(Richards et al., 2011; Xiong et al., 2016). Treatment of HGPS fibroblasts with farnesylation inhibitors prevented onset of oxidative stress, supporting the idea that accumulation of farnesylated prelamin A contributes to overall oxidative

stress. Progerin accumulation in the nuclear lamina was also shown to impair NRF2 pathway, which contributes to elevated oxidative stress in HGPS (Kubben et al., 2016). Normally, NRF2 binds to antioxidant-responsive elements (ARE) motifs and in turn activates antioxidant genes. Progerin has been shown to have a high affinity to NRF2, causing NRF2 subnuclear mislocalization and disrupting its interaction with ARE motifs. Consequently, NRF2-ARE targeted genes are repressed in HGPS, leading to altered oxidative stress response in the cell (Kubben et al., 2016). Although the levels of oxidative stress have been shown to clearly resemble those observed in atherosclerotic plaques, there is a lack of mechanistic insight into the source and the effect of ROS. In particular, how does elevated ROS induce DNA damage and oxidative stress remains to be examined.

1.4.3.2 Epigenome changes in response to DNA damage during aging: Epigenetic inheritance is the process by which the epigenetic marks on the parental DNA is transmitted to the nucleosomes on the daughter DNA strands (Margueron and Reinberg, 2010). There is correlative evidence suggesting that the persistent DNA damage leads to defective epigenetic inheritance. Indeed, the DNA damage response is accompanied by significant alterations of chromatin structure, affecting both intrinsic chromatin components and epigenetic marks, since change in chromatin state is required to allow the recruitment of DDR factors at the sites of DSBs. For instance, many ATP-dependent chromatin remodelers such as CHD2 are recruited to damaged chromatin to change chromatin compaction and increase histone mobilization (Luijsterburg et al., 2016). Polycomb Group proteins, histone

deacetylases and methyltransferases also accumulate at DNA damaged sites either to modify chromatin or as part of the post-damage signalling cascade (Liu et al., 2005; Luijsterburg et al., 2016; Lukas et al., 2011; O'Hagan et al., 2008; Pegoraro et al., 2009; Rothkamm et al., 2003). Persistent DDR activation in HGPS cells could alter the epigenome through a failure to remove imparted epigenetic changes during DSB repair, however this mechanism of defective epigenetic inheritance remains to be elucidated in HGPS cells.

1.5 Therapeutic approaches for HGPS

Given the pathological implication of farnesylated prelamin A and progerin in the nuclear abnormalities in HGPS cells, the prevailing treatment for HGPS patients currently is the administration of a farnesylation inhibitors (FTI) Lonafarnib, which inhibits the processing of prelamin A to progerin (Yang et al., 2006). Treating HGPS fibroblasts or normal fibroblasts overexpressing progerin with Lonafarnib was able to improve overall nuclear morphologies (Capell et al., 2005). *In vivo* studies on HGPS mouse models also demonstrated that Lonafarnib treatment rescues a variety of disease phenotypes such as growth retardation and VSMC loss (Capell et al., 2008; Yang et al., 2006). These results motivated the launch of the first Lonafarnib clinical trials for HGPS patients (Gordon et al., 2012; Varela et al., 2008). Administration of Lonafarnib for two years improved various symptoms in HGPS patients, including improving the incidence of stroke, headaches, and seizures (Gordon et al., 2012). However, FTI administration only extended survival by 1.6 years compared to matched patients from untreated group (Gordon et al., 2014). As a result, new clinical trials are currently underway to determine whether combination therapies

with FTI could further improve survival outcome. An ongoing trial includes statins and bisphosphonates in conjunction with Lonafarnib in order to inhibit multiple steps in the farnesyl biosynthetic pathway.

In addition to prenylation inhibitors, other therapeutic strategies have shown to rescue HGPS phenotypes in both mouse HGPS cell models of progeria. For example, rapamycin and sulforaphane were shown to improve progerin solubility and clearance via mTOR inhibition in HGPS fibroblast cultures (Cao et al., 2011; Gabriel et al., 2015). However, a recent comparative study evaluated the different drug combinations between rapamycin, FTI and zoledronate, and pravastatin on mesenchymal stromal cells derived from HGPS stem cells found that while all treatments improved nuclear morphology, differences in rescuing DNA damage a cellular proliferation were observed (Blondel et al., 2014). Some combinations even yielded cytotoxic effects that worsened cellular growth. Also, the ROS scavenger N-acetylcysteine (NAC), which reduces free radicals and is a synthetic precursor to antioxidant enzyme glutathione, was shown to reduce the level of unrepairable DNA damage caused by increased ROS (Richards et al., 2011). This suggest that oxidative stress is a major contributor to genomic instability in HGPS cells, and that combination of NAC with FTI could improve HGPS phenotypes in a synergistic manner.

Compounds that target histone modifiers also demonstrated therapeutic potential in HGPS models. For instance, remodelin, an inhibitor of N-acetyltransferase-10

(NAT10), rescues abnormal morphology and proliferation defects in HGPS fibroblasts (Larrieu et al., 2018). Remodelin not only rebalances the nuclear Ran localization in HGPS cells, but also increases chromatin compaction and rescued abnormal gene expression (Larrieu et al., 2018). In addition, supplementing *Zmpste24*$^{-/-}$ mice with sodium butyrate in their diet extended their life span significantly (Krishnan et al., 2011), suggesting that reversal of epigenetic marks such as histone methylation and acetylation could make an attractive therapeutic target against progeroid pathologies.

Overall, the best treatment for HGPS patients remains a matter of debate. Understanding the full spectrum of defects in HGPS patients and the functional effects of each drug will shed light on uncovering effective strategies to rescue HGPS phenotypes while minimizing cellular toxicity.

1.6 Remaining Questions in elucidating HGPS pathology

Emerging evidence suggests that oxidative stress plays a major role in HGPS disease progression, however mechanistic elucidation on how progerin accumulation induces elevated oxidation and how oxidative stress affects HGPS VSMCs remain to be studied. Additionally, loss of heterochromatin and epigenetic marks in HGPS cells is poorly understood. It is suspected that sustained DSB repair could cause defective epigenetic regulation in HGPS cells, but this theory remains to be tested. Most importantly, unraveling the molecular mechanisms that link progerin accumulation to vascular cellular dysfunction could lead to novel therapeutic

approaches to improve overall cardiovascular health in HGPS patients as well as the aging population. Therefore, elucidating disease mechanisms in HGPS vascular cells such as the VSMC is essential.

1.7 Using patient specific iPSCs to study HGPS

Studies of HGPS disease progression have historically relied on primary culture of HGPS donor fibroblasts, ectopic expression of progerin in human cell lines, or *in vivo* studies of HGPS rodent models. The vast majority of HGPS studies utilized HGPS patient-derived skin fibroblasts that are close to the limit of their replicative span and are therefore not ideal to examine the initiation of molecular defects in these cells. Furthermore, HGPS is a segmental disorder that affects only certain cell types, VSMCs being the most severely affected. However, due to the small cohort of HGPS patients worldwide, vascular biopsies are rare and incapable of supporting larger scale studies.

A powerful model to study HGPS vascular aging is the use of patient specific stem cell cells. In 2007, Yamanaka's group demonstrated that human fibroblasts can be reprogrammed into embryonic-stem-like cells, termed induced pluripotent stem cells (iPSCs), using a cocktail of transcription factors (Figure 1.8)(Takahashi et al., 2007). iPSCs quickly became a widely-used tool for disease modeling due to their ability to recapitulate patient-specific disease phenotypes in disease relevant cell types *in vitro.* Indeed, established patient-specific iPSC lines can theoretically be differentiated into any cell types in the human body, which enables the elucidation

of tissue specific disease mechanisms. iPSCs can be expanded to support a wide range of studies, which is often problematic for primary cells. iPSC reprogramming has the potential to restart the epigenetic signature of the cell, allowing investigation of the initiation of HGPS progression.

iPSCs and iPSC-derived cells has been previously reported to model different aspects of HGPS disease progression. iPSCs from HGPS fibroblasts were first derived to show that the nucleoskeletal and epigenetic alterations were erased upon reprogramming (Liu et al., 2011; Xiong et al., 2016; Xiong et al., 2013; Zhang et al., 2011). Upon differentiation of HGPS iPSCs into SMCs, ECs, and adipocytes premature senescence phenotypes became evident (Liu et al., 2011; Xiong et al., 2016; Xiong et al., 2013; Zhang et al., 2014). iPSCs have also been used to to investigate the molecular underpinnings of the absence of neuronal deterioration in HGPS patients, revealing that the restricted expression of miR-9 in neural cells protected this cell lineage from progerin accumulation in HGPS (Nissan et al., 2012). iPSCs have also been used to test several pharmacological agents on HGPS iPSC-derived mesenchymal stem cells (MSCs) (Blondel et al., 2014), which highlighted the usefulness of iPSC-derived cells as powerful tools for comparative pharmacological studies.

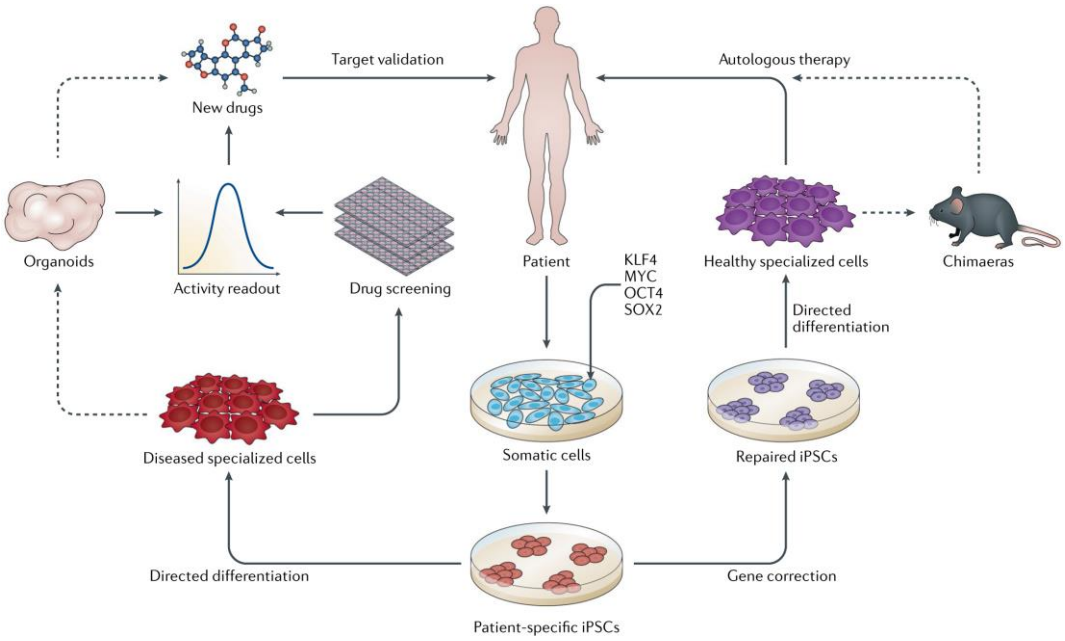

Figure 1.8. Schematic of iPSC derivation from patient somatic cells and its applications (Rowe and Daley, 2019). Somatic cells derived from an individual can be reprogrammed into iPSCs using a cocktail of transcription factors (KLF4, SOX2, OCT4, and cMyc). Reprogrammed iPSCs can be directly differentiated into diseased specialized cells, which can be utilized to create organoids or design drug screens for identifying potential therapeutic targets. Recent advances in autologous iPSC-based therapy also incorporates the use of CRISPR-Cas9 technology to enable repair of disease-causing genetic mutations. Adapted by permission from Springer Nature: Nature Reviews Genetics – Induced Pluripotent stem cells in disease modelling and drug discovery, R Grant et. al., 2019.

1.8 Significance of this Dissertation

The deterioration of VSMCs and subsequent terminal atherosclerosis is the leading cause of death in HGPS. Current therapeutic approaches primarily targets progerin clearance by blocking the farnesylation step in the prelamin A post-translational modification pathway. However, these treatments can only extend the lifespan in HGPS patients by a couple of years. Understanding the molecular mechanisms underlying genomic defects in HGPS VSMCs could help in identifying novel drug targets for improving the cardiovascular health in HGPS patients.

The primary goal of this dissertation was to model HGPS pathophysiology in HGPS VSMCs and monitor the onset of defective epigenetic inheritance *in vitro.*

The over-arching hypothesis of my project is that reprogramming HGPS fibroblasts will reset the epigenetic clock, enabling the modeling of HGPS-affected VSMCs from disease initiation to the onset of molecular and cellular phenotypes**.**

My sub-hypotheses are:

1. Reprogramming HGPS fibroblasts will make bona-fide iPSCs and reset the epigenetic landscape of HGPS cells.
2. ROS accumulation leads to replicative stress and senescence in HGPS–affected VSMCs, which can be rescued by ROS scavengers.

3. ROS-induced DNA damage leads to DNA translesion synthesis and defective epigenetic inheritance.

Chapter 2 – Methods

2.1 Generation of iPSCs from fibroblasts via retroviral reprogramming

HGPS and control iPSCs were reprogrammed from donor fibroblasts from the Progeria Research Foundation biobank and Coriell. Prior to reprogramming, HGPS and normal patient fibroblasts were maintained in fibroblast medium (DMEM supplemented with 10% FBS, Glutamax, and Gentamycin). For reprogramming, retrovirus was generated using constructs pMXs-hOCT4, pMXs-hSOX2, pMXs-hKLF4, pMXs-hc-MYC (Addgene)(Chang et al., 2013; Hotta et al., 2009). To generate VSV-G pseudotyped retrovirus, Plat-GP cells were transfected with 15 mg of expression vector and 5 mg of pVSV-G. Two days post-transfection, retrovirus was collected and filtered through a 0.45 mm filter cap. Transduction of $5x10^5$ patient fibroblasts was performed by the addition of polybrene to a final concentration of 4 mg/ml to a retroviral cocktail either containing a combination of 4 factors. After transduction, fibroblasts were maintained in fibroblast medium for 6 days, then trypsinized and replated onto fresh MEFs. Fibroblast media was then replaced with hESC media that was changed daily. Approximately 20 days later, colonies resembling hESCs in morphology were mechanically picked and replated onto fresh matrigel. These iPSCs were mechanically dissociated for a few passages and then adapted to collagenase IV passaging every 4-5 days onto fresh matrigel. Both H9 hESCs and iPSCs were maintained on Matrigel in E8 medium (DMEM/F12 supplemented with L-ascorbic acid, sodium selenite, bFGF, TGF-β1, sodium bicarbonate, holo-

transferrin, and gentamycin). The majority of the reprogramming experiments were performed by Dr. Wing Y. Chang.

2.2 Embryoid Body and Teratoma Assays

To assess germ layer differentiation in vitro, EBs were generated from hESCs and iPSCs by treating with collagenase IV for 30min at 37^{o}C and gently dislodged with a cell scraper, followed by plating in suspension in low cluster plate for 7-10 days in E6 media ((DMEM/F12 supplemented with L-ascorbic acid, sodium selenite, sodium bicarbonate, holo-transferrin, and gentamycin) with 10% FBS. Afterwards, EBs were plated onto 0.1% gelatin-coated plates for 5 days in E6+10% FBS medium for EB outgrowth induction. EB outgrowths were stained with antibodies against β-III tubulin, smooth muscle actin, and Gata 4 to represent all three germ layers (See table 2.1). For teratoma assays, 3 wells of a 6-well plate iPSC culture at 70-80% confluency were treated with collagenase IV for 30 min. The cells were isolated with a cell scraper, pelleted, and resuspended in 50% Matrigel and injected intramuscularly into NOD/SCID mice. After 8-10 weeks, tumours were removed, fixed in formalin, sectioned with hematoxylin and eosin staining.

2.3 Vascular smooth muscle-like cell differentiation

Differentiation of hESC H9 (WiCell) and iPSCs to VSMCs was essentially conducted as described by Xie et al. (2007) with minor modifications. Briefly, embryoid bodies (EBs) were generated by treating hESCs and iPSCs with collagenase IV for 5 min before being gently dislodged using a cell scraper. Suspended EBs were cultured in low cluster plates in E6 media (DMEM/F12 supplemented with L-ascorbic acid,

sodium selenite, sodium bicarbonate, holo-transferrin, and gentamycin) with 10% FBS. After 7 days, EBs were plated onto 0.1% gelatin-coated plates for 5 days in E6+10% FBS medium for EB outgrowth induction. EB outgrowths were then trypsinized and cells were replated on Matrigel in Medium 231 with addition of smooth muscle growth supplement (Life Technologies) containing FBS, bFGF, EGF, Heparin, IGF-I and BSA, and were passaged when cell culture reached confluency. To differentiate VSMCs into a more contractile phenotype, cells were plated on gelatin-coated plates and grown in VSMC differentiation medium (Medium 231, differentiation supplement (Life technologies) containing FGF and heparin for 7 days.

2.4 Immunofluorescence staining

Cultured cells were washed gently in PBS before being fixed in formalin for 15 min at room temperature. Cells were then permeabilized with 0.1% Triton X-100 mixed with 0.1% BSA for 20min, blocked with 3% skim milk in PBS for 1 hour, and incubated with primary antibodies (**Table 2.1**) diluted in PBS diluted with 5% goat serum overnight at 4^{o}C. On the following day, cells were washed with PBS 3 times for 5 minutes each before incubated with secondary antibodies (**Table 2.1**) in for 1 hours at room temperature. Samples were then washed 3 times in PBS, in which Hoechst 33342 was included in the final wash step. Individual images were captured using Observer Z1 fluorescence microscope or Zeiss LSM510 Confocal Microscope. High content imaging analyses was performed using the Thermo Scientific ArrayScan VTI HCS platform and Studio software. Target activation

algorithm and unbiased quantification analyses were incorporated for quantifying fluorescent signals in each image.

Name	Company	Catalogue number	Dilution
53BP1	New England Biolabs	4937S	1:1000
8-Oxoguanine	Cedarlane	4354-MC-050	1:250
AlexaFluor Goat anti-mouse (H+L) 488	Life Technologies	A11034	1:1000
AlexaFluor Goat anti-mouse (H+L) 555	Life Technologies	A21424	1:1000
BrdU	BD Biosciences	555627	1:200
Calponin	Cedarlane	M3556	1:500
DNA PKc	Millipore	MABC1236	1:250
FITC-conjugated Avidin	Sigma-Aldrich	A2050-2ML	1:200
GAPDH	Abcam	Ab8245	1:1000
Gata4	R&D Systems	MAB2606	1:250
H3K27me3	New England Biolabs	9733S	1:1600
H3K4me3	New England Biolabs	9727S	1:1600
H4K16ac	Sigma Aldrich	07-329	1:500
Hoechst 33342	Life Technologies	H3570	1:5000
Lamin A/C	Millipore	MAB3540	1:500
MOF	Sigma Aldrich	PLA0161-100UL	1:500
Progerin	Millipore	05-1231	1:500
SM22α	Abcam	ab14106	1:200
Smooth Muscle Actin	Millipore	CBL171	1:500
SSEA4	Millipore	MAB4304	1:500
Tra-1-60	Millipore	MAB4360	1:500
Tra-1-81	Millipore	MAB4381	1:500
β-III tubulin	Cedarlane	801202	1:500
γ-H2A.X	Cell Signaling	9718S	1:500

Table 2.1 List of antibodies information used in this dissertation.

2.5 β-galactosidase staining

Protocol for staining was performed as described in the kit (Abcam Ab102534). Cell culture medium was removed, and cells were washed 3 times with PBS without calcium and magnesium (denoted as -/-). Cells were fixed with 0.5mL of fixative solution provided by the kit for 15 minutes and room temperature before being washed 3 times in PBS -/-. Cells were then stained in staining solution containing staining supplement and X-gal and incubated at 37^{o}C for 1 hour before being washed with PBS -/-. Images were taken using Leica DC200 light microscope once blue colour was developed in the wells.

2.6 Alkaline Phosphatase Staining

hESC and iPSC clones were fixed in neutral formalin buffer containing 3.8% formalin for 45 min and washed 3 times with PBS -/-. Staining solution was constituted using naphthol AS-MX phosphate, N,N-dimethylformamide, and fast red violet LB salt dissolved in 0.2M Tris-HCl buffer and filtered through Whatman's paper immediately before staining. Cells were incubated in the staining solution for 30 minutes before being washed 3 times with PBS -/- and imaged using Leica DC200 light microscope.

2.7 Microarray Analyses

Total RNA was isolated from cell pellets using the Nucleospin® RNA kit (Machery-Nagel) according to the manufacturer's instructions. Integrity and quantity of the isolated RNA was measured using the Bioanalyzer RNA 6000 nanochip (Agilent). 300ng of total RNA was labeled and hybridized to GeneChip Human Gene 2.0 ST

arrays (Affymetrix) according to the manufacturer's protocol and scanned on a GeneChip Scanner 3000 7G (Affymetrix). Two replicates were performed for each sample. Gene expression data from Affymetrix HuGene 2.0 microarrays were normalized using the RMA function of the R oligo package. Quality analysis of the microarrays was performed using the R arrayQualityMetrics package. Fold change and significance for transcript cluster identifiers between conditions was determined using the R limma package and annotated using the hugene20sttranscriptcluster.db (v2.14.0).

2.8 ROS induction and measurement

ROS levels in cultured cells were measured using the Image-iT ™ LIVE Green Reactive Oxygen Species Detection Kit (I36007, Life Technologies). Briefly, cells were incubated with 25uM carboxy-H2 DCFDA diluted in warm HBSS (Life Technologies) for 30 minutes at 37^{o}C in the dark. HOECHST was added at 1.0uM final concentration to the solution 5 minutes prior to the end of the incubation period. For ROS induction, control cells were treated with TBHP at a concentration of 100uM for 1 hour at 37^{o}C before the addition of 25uM carboxy-H2 DCFDA. Treated cells were washed twice with warm HBSS before being image using an epifluorescence microscope or through a high-content imaging system for downstream analysis.

2.9 Drug treatment

To assess extent of rescue for nuclear defects in HGPS VSMCs, VSMCs were administered with 1.5uM FTI diluted in VSMC differentiation medium and cultured

for 72 hours before phenotype characterization. For NAC treatment, cells were treated with NAC at 20uM for 72 hours before being harvested for further experiments.

2.10 Comet assay

In preparation for the comet assay, 1% low melting-point agarose (LMA) was was melted by being submerged in a beaker of boiling water with cap loosened, followed by a cooling period of 20 min in 37^{o}C for at least 20 minutes prior to use. Cell samples were typsinized and combined with warm LMA at a ratio of 1:10 10 cells:LMA, and 120uL of the mixture was immediately pipetted onto labelled Gelbond film strip (Lonza, #53740). Cells were applied to the hydrophilic side of the film into a circle of approximately 25mm in diameter. Films with the gel were then placed flat in the dark at 4^{o}C for 10 minutes until the gel solidified. The films were then immersed in pre-chilled Lysis solution and incubated at 4^{o}C for 45 minutes. Following lysis, the films were immersed into freshly made Alkaline Unwinding solution (6g NaOH, 250uL 200mM EDTA in 1L solution with dH_2O) for 45 minutes in the dark. The films were then transferred to a horizontal electrophoresis apparatus where the films were placed equidistant from each electrode in alkaline electrophoresis solution (12g NaOH, 1mM EDTA pH 8 in 1L solution with dH_2O), and electrophoresis was run at 30V for 30min at constant amperage of 300mA. During electrophoresis, temperature fluctuations were minimized by placing the apparatus in a walk-in refrigerator. Following electrophoresis, films were dried in a dessicated container overnight at room temperature. The next day, the slides were stained by submerging in SYBR Green stain at 1:10000 dilution in TE buffer pH 7 for 5 minutes.

The films were then air dried and mounted with coverslips for visualization by fluorescence microscopy using the GFP channel. Comet moments were analyzed using the OpenComet Plugin in ImageJ.

2.11 Proximity Ligation Assay (PLA)

After cell cultures reached 80% confluency, cells were washed twice in PBS and fixed in 3.7% paraformaldehyde for 10 minutes at room temperature. Fixed cells were subsequently permeabilized in 0.1% Triton X-100 (Sigma Aldrich) for 20 minutes and blocked with Duolink Blocking reagent (Sigma Aldrich) for 1 hour at room temperature. Cells were incubated with primary antibodies diluted in Duolink antibody diluent (Sigma Aldrich) at 4^{o}C overnight. Next day, samples were washed 3 times in PBS, followed by incubation with Duolink In Situ PLA Probe Anti-Mouse PLUS and Anti-Rabbit MINUS (Sigma Aldrich) for 1 hour at 37^{o}C in a humidity chamber. After incubation, cells were washed 3 times for 10min in Buffer A (Sigma Aldrich) and incubated with DNA ligase in diluted ligase buffer (Sigma Aldrich) for 30min at 37^{o}C in a humidity chamber. Subsequently, cells were washed again 3 times for 10 minutes each in Buffer A, and incubated with DNA polymerase diluted in polymerase buffer with far red fluorescence-labelled oligonucleotides (Sigma Aldrich) for 90min in a humidity chamber, before being washed and mounted in DAPI mounting medium (Duolink, Sigma Aldrich) for imaging and foci analysis.

2.12 Quantitative PCR (qPCR)

To perform qPCR on iPSCs and VSMCs, cells were washed 3 times in PBS before being lysed using lysis buffer with β-mercaptoethanol. mRNA was extracted using the NucleoSpin RNA isolation kit (Macherey-Nagel). Isolated RNA was quantified using Thermo Fisher Nanodrop and was converted to cDNA using SuperScript® II Reverse Transcriptase (Thermo Fisher Scientific). RT-qPCR was conducted using SYBR® Green PCR Master Mix's protocol (Thermo Fisher Scientific) and a Roche LightCycler 480 Real-Time PCR system, with genomic DNA used as a dilution standard control. Measured transcript levels were normalized to GAPDH.

2.13 ChIP-qPCR

ChIP was performed as previously described with slight modifications (Walker et al., 2010). iPSCs were grown to 80% confluency. Afterwards, 500,000 iPSCs were cross-linked with 1% formaldehyde for 10 minutes at room temperature before being sheared using Covaris S2 Sonicator for 10 minutes (Cycle burst=200; time: 480 minutes, temperature: 4^{o}C; peak power 175) until DNA reaches a final size of 300bp. Sheared DNA were then incubated with Magnetic A beads (Millipore) with H3K4Me3 or H3K27Me3 antibody overnight. After incubation, beads were collected and washed with low salt buffer (0.1% SDS, 1% Triton X-100, 2mmol/L EDTA, 20mmol/L Tris-HCl pH8, 150 nmol/L NaCl). 10% of the pull-down was saved as input. Pull-downs were reverse-crosslinked using Eppendorf Thermomixer at 1,250g at 65^{o}C for 15minutes and precipitated using phenol-chloroform. DNA quantity was measured using the Bioanalyzer RNA 6000 nanochip (Agilent). qPCR was performed as described above and repeated two times for each gene.

2.14 ChIP-sequencing (ChIP-seq)

H3K4me3 and H3K27me3: ChIP was performed as previously described(Chang et al., 2006) with some modifications. Briefly, nuclei pellets were resuspended in TC13 tubes (Covaris) with 2mL of lysis buffer 3 (10mM Tris-HCl pH 8, 100mM NaCl, 1mM EDTA, 0.5mM EGTA, 0.1% Na-Deoxycholate, 0.5% Na-Laurylsarcosine) and sheared using a Covaris S2 sonicator (20% duty cycle, intensity 5, 200 cycles/burst) for 9 minutes per sample. 300ug of chromatin was used for each sample. Before addition of antibodies, an aliquot of each sample was reserved for input control. Antibodies used were as follows: rabbit H3K4Me3 (Millipore), rabbit H3K27Me3 (Cell signaling Technology), and normal rabbit IgG (Cell Signaling Technology). After reverse cross-linking and cleanup, approximately 20ng of each sample was prepared for sequencing using the ChIP-seq sample rep kit (Illumina) according to the manufacturer's instructions. Samples were sequenced on an Illumina GAIIx (Illumina).

Alignment of ChIP-seq to the human genome (hg19) data was performed using bowtie 1.1.0 with the following parameters: "-l 32 --strata --best -y --chunkmbs 3072 -n 2 -m 1". Duplicate reads were removed using the RMDUP function of samtools. In the case of SRA format files from the Short Reads Archive, the NCBI SRA toolkit versions 2.4.3 was used to convert the files for alignment with the above parameters. Known human genes were downloaded from ENSEMBL 74 to determine gene ENSEMBL identifiers, symbols, gene start, gene end strand and gene biotype. Analysis was limited to genes on standard chromosomes (1-23,X,Y).

DiffReps (Shen et al., 2013) was used to identify genomic regions differentially enriched for H3K27me3 and H3K4me3. ChIP-seq BAM files reads were converted to BED files. Fragment lengths used for input into BIDCHIPS were the average of the fragment lengths of the treatment and control files as estimated by MaSC (Ramachandran et al., 2013). The different histones were analyzed with parameters as recommended in the paper. H3K4me3 used the —nsd "sharp" setting and the "peak" mode as it has sharper more localized enrichment, while H3K27me3 used the —nsd "broad" setting and "block" mode as it has broader more distributed enrichment. The "broad" mode uses a 10kb window and step size while the "peak" setting uses a 1kb window and step size. The resulting output identifies windows in the genome where the histone reads are significantly different between treatment and control, taking into account the IgG background.

For PCA analyses and read pileups, known protein-coding genes, reads in the region -5kb/+2kb around the gene start were counted from H3K4me3 and reads over the full gene were counted for H3K27me3. The *r prcomc* function was used to determine the first two principal components, which were then plotted. Depths of reads for each data set for the regions around gene starts were determined to generate the pileup plots. ChIP-seq alignment and PCA analyses were performed by Gareth Palidwor.

H4K16ac ChIP: Patient and control cells were expanded *in vitro* to generate passage 7 and passage 14 cell cultures. When sufficient cell amounts were reached, cells were trypsinized and washed with PBS. Native Chromatin immunoprecipitation (N-ChIP) was performed according to a published protocol. At the step of antibody incubation with hydroxyapatite-purified chromatin, 3µg chromatin and 3ul of rabbit anti-H4K16ac (Table 2.1) were used for each pull-down. Genome-wide sequencing on ChIP DNA was performed on an Illumina HiSeq 2000 at the McGill University and Génome Québec Innovation Centre (Montréal, Québec, Canada). Reads were aligned to the human reference genome hg38 from UCSC genome browser with BWA version 0.7.10 using default options.

2.15 RNA-sequencing (RNA-seq)

VSMCs from passage 7 and 14 were trypsinized and pelleted at 250g for 5min, before total RNA was extracted using Nucleospin RNA isolation kit (Macherey-Nagel). RNA extraction was performed in two batches as technical replicates according to the manufacturer's protocol. RNA concentration was estimated using NanoDrop 2000 spectrophotometer (Thermo Fisher) and ERCC spike was added (Thermo Fisher) to normalize for cell number. Quality control of RNA integrity and total RNA concentration was then verified using the Bioanalyzer Eukaryote Total RNA Pico kit (Agilent). Validated RNA samples were sequenced on the Illumina NextSeq500. Reads were then assigned to transcripts from GENCODE and differentially expressed genes were identified using DESeq2 v1.20.0. DESeq2 identified fold change between HGPS and control VSMCs at both passages. Volcano

plots were generated by plotting log2FoldChange against –log10(*pvalue).* Points in red have a padj <0.05. Gene ontology enrichment analyses was generated on DAVID while Rrevigo was used to condense redundant GO terms and generate visualization maps.

2.16 Western Blot

Whole cell lysates were prepared by dissolving cells in Cell Lysis Buffer (50mM Tris-HCl, 150mM NaCl, 1mM EDTA, 10% glycerol. 1% Triton X-100) and sonicated for 10 seconds. Cell lysates were mixed with Laemmli sample buffer containing 2-mercaptoethanol (Life Technologies) and heated at 70°C for 10 minutes before loading. Blots were blocked with 5% milk and probed for protein in question overnight. The next day, blots were washed 3 times in PBST and treated with secondary antibody for 1 hour before being washed again and imaged using the LI-COR Odyssey Infrared Imager. Band density was analyzed using ImageJ.

2.17 aniPOND coupled with Mass Spectrometry

Accelerated native isolation of proteins on nascent DNA(aniPOND) was performed as previously published(Leung et al., 2013) Approximately $1x10^7$ proliferative VSMCs were labeled with 10μM 5-ethynyl-2'-deoxyuridine (EdU) for 1 hour before being lysed using ice-cold nuclear extra buffer containing 1.5% NP-40 detergent for 15 minutes. Lysed cells were scraped and transferred into a 15mL tube and spun down into nuclei pellets at 3000g for 10 minutes. Supernatants were discarded and samples were washed in 5mL of ice-cold PBS -/- before being spun down again at 30000g for 10 minutes. Pellets were then resuspended in click-reaction buffer

containing Sodium L-ascorbate, CuSO4, and biotin-azide and spun at 4°C for 1 hour. Pellets were then centrifuged for 10 minutes at 3000g at 4°C and washed once in ice-cold PBS -/- before being spun down again to remove PBS supernatant. 500uL of ice cold buffer B1 with protease inhibitor was resuspended with each sample and content was transferred into a 1.5mL Eppendorf tube. Content was then sonicated at 10 seconds on ice using Fisher Scientific 500 sonicator. Pellets were spun down at 4°C for 10 minutes and supernatants were removed. Sample was resuspended with B1 buffer and sonicated once again as previous step. Pelleted sample was then resuspended once again with B1 buffer and sonicated 12 x 10 seconds before centrifuged at max speed for 10 minutes at 4°C. Supernatant was transferred to a new Eppendorf tube mixed with ice cold buffer B2. Input controls were taken before biotinylated DNA with bound protein was captured. Proteins were captured using Streptavidin Agarose Resin (Thermo Scientific) for 16 hours. After extensive washing, the protein-bound DNA was resolved using Laemmli buffer (Bio-Rad) with β-mercaptoethanol (Bio-Rad) by boiling at 95°C for 15 minutes. The samples were then subjected to Western blot analysis or Mass Spectrometry analysis.

Following chromatin extraction, replication fork proteins were identified through mass spectrometry that was performed at the Ottawa Hospital Research Institute Proteomics Core Facility (Ottawa, Canada). Proteins were digested in-gel using trypsin (Promega) according to the method of Shevchenko(Shevchenko et al., 2006). Peptide extracts were concentrated by Vacufuge (Eppendorf). LC-MS/MS was performed using a Dionex Ultimate 3000 RLSC nano HPLC (Thermo Scientific) and

Orbitrap Fusion Lumos mass spectrometer (Thermo Scientific) with 15 cm long PepMap C18 column with 75 micrometer internal diameter (Thermo Scientific). MASCOT software version 2.6.2 (Matrix Science, UK) was used to infer peptide and protein identities from the mass spectra. The observed spectra were matched against human sequences from SwissProt (version 2018-05) and also against an in-house database of common contaminants. The results were exported to Scaffold (Proteome Software, USA) for further validation and viewing.

Differentially abundant proteins were identified based on Fisher's exact test ($p<0.05$) between control and HGPS proteins. Protein networks were identified using STRING protein database, and significant protein complexes were analyzed on the basis of gene ontology using Metascape (Zhou et al., 2019).

2.18 DsiRNA transfection for gene expression knockdown

Transfection protocol was adopted from RNAiMAX Transfection Procedure (Life Technologies). DsiRNAs for MOF were purchased from IDT. Cells were plated until reaching 80% confluency before being transfected with DsiRNAs using RNAiMAX (Life Technologies) and its suggested dilution format. Expression of MOF was tested using qPCR 3 days post transfection.

CHAPTER 3 – RESULTS

3.1 Reprogramming HGPS fibroblasts produced bona-fide iPSCs, resetting their epigenetic landscape

3.1.1 HGPS fibroblasts exhibit nuclear abnormalities and premature senescence in culture

HGPS fibroblasts have been prevalently reported to display severe cellular and nuclear defects (Dechat et al., 2008; Goldman et al., 2004; Shumaker et al., 2006). To assess the nuclear defects in patient cells, I first characterized nuclear defects in HGPS fibroblasts. Amongst the three HGPS fibroblast lines and three fibroblasts from unaffected individuals, a familial trio of two unaffected parents and one affected progeny was included, which enables the direct comparison between related individuals (Table 3.1). To characterize nuclear defects, I performed immunofluorescence staining for Lamin A and quantified abnormal nuclear shape. Significantly more HGPS fibroblasts displayed abnormal nuclear morphology compared to control (Figure 3.1A &C). Significantly more HGPS fibroblasts also stained for the DDR marker γH2A.X (Figure 3.2A & C), suggesting that HGPS fibroblasts exhibit increased DNA damage and repair, consistent with other reports on HGPS fibroblasts (Goldman et al., 2004; Liu et al., 2008).

Patient	Cell Line	iPSC Clones
HGPS	HGADFN167	1J, 1Q
	HGADFN003	1B, 1C
	AG01972	1B, 1D
Control	HGMDFN090	1B, 1C
	HGFDFN168	1D2, 1P
	BJ	1C, 1D

Table 3.1. List of HGPS patients and control fibroblast lines, and their derived iPSC clones. Two clones were used from each individual in this study. Patient HGFDFN168 and HGMDFN090 are the unaffected parents of HGPS patient HGADFN167. Reprinted from John Wiley and Sons – Aging Cell – Reprogramming progeria fibroblasts re-establishes a normal epigenetic landscape, Z. Chen, W.L.Stanford et. al., 2017.

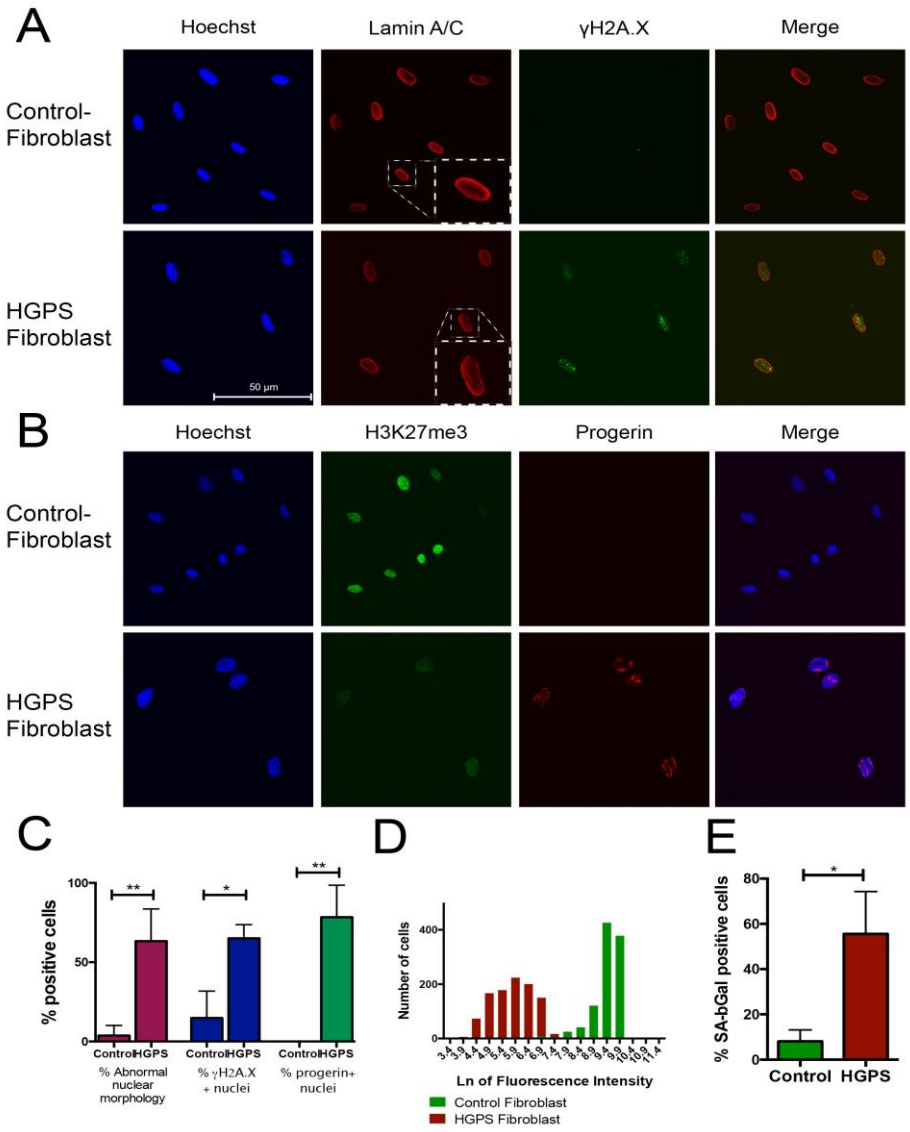

Figure 3.1 HGPS fibroblasts exhibit severe nuclear defects. (A) Immunofluorescence (IF) analysis of Lamin A/C reveals abnormal nuclear morphology in HGPS fibroblasts. HGPS fibroblasts also have increased γH2A.X compared to control. **(B)** IF imaging demonstrates reduced H3K27me3 marks and expression of Progerin in HGPS fibroblast nuclei compared to control. **(C)** Quantification of fibroblasts demonstrating increased abnormal nuclear morphology, accumulation of DNA damage, and expression of Progerin in HGPS fibroblasts compared to control fibroblasts. Results were assessed by immunofluorescence microscopy and Image J software. **(D)** High-content imaging and

fluorescence quantification on a natural log scale showing a loss of H3K27me3 in HGPS fibroblast nuclei compared to control fibroblasts. **(E)** An increased number of HGPS fibroblasts are positive for SA-β-gal compared to control fibroblasts, as assessed by flow cytometry. * indicates $p<0.05$, ** indicates $p<0.005$ where statistical significances were observed. A minimum of 3 biological replicates was performed for each experiment.

It has been demonstrated that progerin accumulation in HGPS fibroblasts is associated with loss of repressive histone marks such as H3K27me3 (Shumaker et al., 2006)). Through high-content-imaging analysis, I detected that 78% of HGPS fibroblasts expressed nuclear progerin as opposed to control fibroblasts that contained almost no detectable progerin levels (Figure 3.1B & C). Immunofluorescence staining coupled with high content imaging also revealed a significant decrease in H3K27me3 fluorescence intensity in HGPS fibroblast nuclei compared to control (Figure 3.1B & D), consistent with a loss of heterochromatin. HGPS fibroblasts also exhibit premature senescence and express senescence-associated β-galactosidase (SA-β-gal)(Goldman et al., 2004). I observed via flow cytometry that less than 10% of control fibroblasts expressed SA-β-gal, while more than 50% HGPS fibroblasts were SA-β-gal positive (Figure 3.1E). Collectively, these results demonstrated that prior to reprogramming, HGPS patient fibroblasts exhibit hallmark nuclear defects, heterochromatin loss and premature senescence.

3.1.2 Reprogrammed HGPS iPSCs express hallmark pluripotent markers

To study HGPS progression from disease onset, fibroblasts from patients and unaffected controls were reprogrammed into iPSCs. Using retroviral

reprogramming, we derived and characterized six iPSC clones, with two clones from each individual (Table 3.1). Upon reprogramming, both control and HGPS iPSCs were morphologically indistinguishable from human embryonic stem cells (hESCs). All iPSC clones expressed typical pluripotent markers TRA-1-60, TRA-1-81, SSEA-4, as well as alkaline phosphatase (ALP) at similar levels to hESCs (Figure 3.2A). The G608G mutation within HGPS iPSC lines was verified using Sanger sequencing to confirm that the C to T mutation is retained in all HGPS clones (Figure 3.2B). All iPSC clones also exhibited normal karyotypes following reprogramming (Figure 3.2C). To determine cell potency, I differentiated iPSCs through embryoid body (EB) formation and detected cells representative from each of the three germ layers, exemplified by the expression of markers of ectoderm (βIII-tubulin), mesoderm (smooth muscle actin, SMA) and endoderm (α-fetoprotein, AFP) (Figure 3.2D). *In vivo* assays further demonstrated that these iPSCs can form teratomas that are comprised of tissues representative of the three germ layers (Figure 3.2D). Together, these data suggest that iPSC clones were successfully derived from both control and HGPS patients.

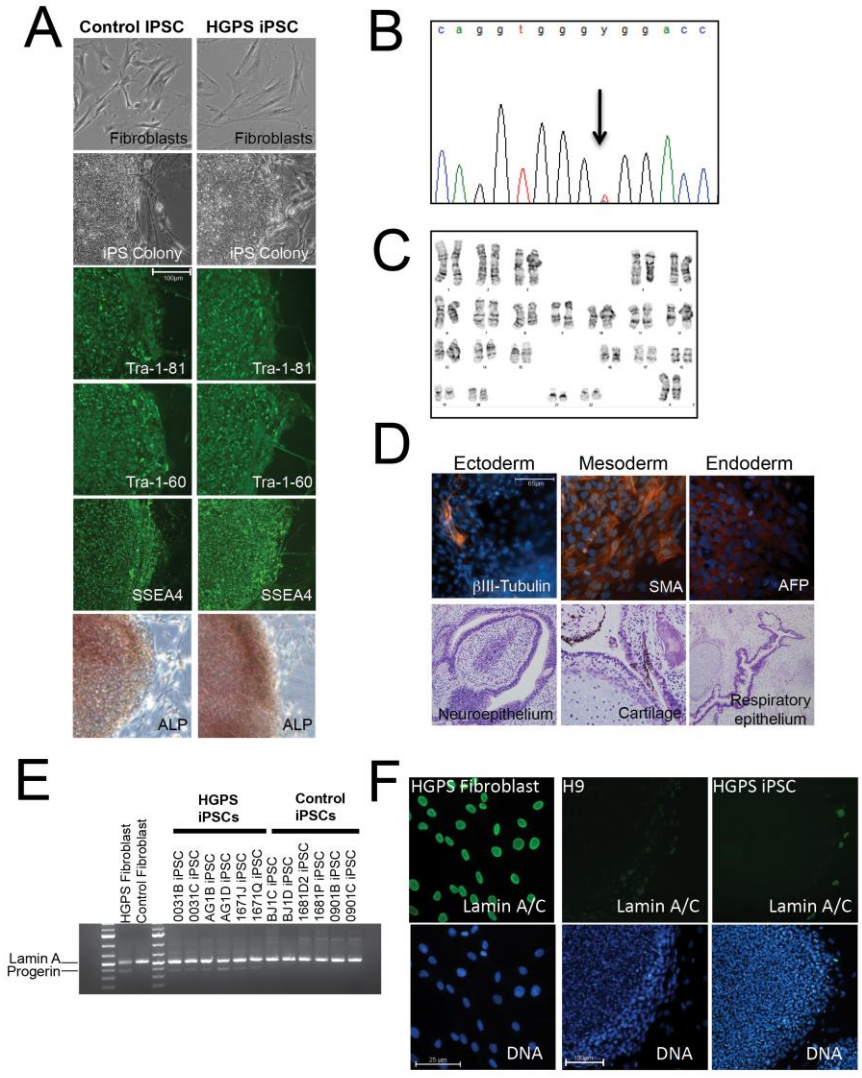

Figure 3.2 iPSCs derived from HGPS patients and control individuals' fibroblasts are pluripotent. (A) iPSC clones derived from both control and HGPS fibroblasts were morphologically indistinguishable from each other. These iPSCs expressed Tra1-81, Tra-1-60, SSEA4, as well as alkaline phosphatase (ALP). **(B)** Sanger sequencing confirmed G606G mutation retained in the iPSC clones derived from HGPS fibroblasts. **(C)** Karyotyping of both control and HGPS iPSCs revealed no gross chromosomal abnormalities following reprogramming. **(D)** Top row: *in vitro* differentiation assay via EB formation confirmed that iPSCs can differentiate into cells from the three germ layers,

including ectoderm (βIII-Tubulin), mesoderm (Smooth Muscle Actin, SMA), and endoderm (α-fetoprotein, AFP). Bottom row: *in vivo* differentiation by teratoma formation confirmed that HGPS iPSCs can differentiate into tissues from all three germ layers. Representative H&E stained micrographs are shown. **(E)** RT-PCR analysis using primers for the full Lamin A transcript and the truncated progerin product in both fibroblasts and iPSCs. The mRNA product of the progerin is expressed in HGPS fibroblasts but not in their iPSC clones. **(F)** Lamin A/C are expressed in HGPS fibroblasts but not in undifferentiated HGPS iPSC and hESC (H9) colonies. Blue represents DAPI stain. Reprinted from John Wiley and Sons – Aging Cell – Reprogramming progeria fibroblasts re-establishes a normal epigenetic landscape, Z. Chen, W.L.Stanford et. al., 2017.

It has been reported that Lamin A is not expressed by undifferentiated human pluripotent stem cells (Constantinescu et al., 2006; Rober et al., 1989). Thus, I next examined Lamin A expression at both mRNA and protein levels. RT-PCR analyses using primers that detect both full-length *LMNA* transcript and truncated progerin transcript confirmed that *progerin* transcripts were only present in HGPS iPSCs while both HGPS and control cultures express *LMNA* (Figure 3.2E). Immunostaining revealed that at the protein level, Lamin A/C is expressed in fibroblasts but absent in pluripotent cells. I found that only differentiated cells at the edge of iPSC colonies expressed detectable levels of Lamin A/C, while the central undifferentiated region of the colonies did not express Lamin A/C (Figure 3.2F). This demonstrates that *LMNA* and progerin expression were downregulated in HGPS iPSCs upon reprogramming.

3.1.3 Reprogramming restored a normal transcriptional profile in HGPS iPSCs

HGPS cells exhibits changes in global gene expression due to progerin accumulation (Dechat et al., 2008; McCord et al., 2013). To examine whether reprogramming re-establishes a wild-type transcriptional landscape, I performed microarray analyses to examine global mRNA expression in all HGPS and control fibroblast lines and their iPSC clones. To determine how progerin affected transcription in diseased and wild-type fibroblast, differential gene expression analysis was conducted between control and HGPS fibroblasts. I found that global gene expression profiles are grossly different between the two groups, as indicated by Pearson correlation analysis (Figure 3.3A). Upon reprogramming, global gene expression profiles between HGPS and control iPSCs with their fibroblast counterparts are starkly different (Figure 3.3A), where 12341 genes were differentially expressed. However, control and HGPS iPSC gene expression profiles are very similar to each other, as well as to hESCs (Figure 3.3A). Only 5 differentially expressed genes (DEGs) between HGPS iPSCs and hESCs and 28 DEGs between control iPSCs versus hESCs were identified, suggesting that the transcriptomic profile is extremely similar between iPSCs and hESCs.

Furthermore, unsupervised hierarchical clustering of reprogrammed iPSCs with their parental fibroblast samples separated the fibroblasts from the iPSCs as expected (Figure 3.3B), while control and HGPS iPSCs did not separate definitively. iPSCs from the parents (168, 090) and the affected progeny (167) did not segregate by hierarchical clustering analysis nor principle component analysis (PCA) (Figure

3.4A & B), demonstrating that reprogramming erases major transcriptional differences between related and unrelated controls and HGPS patients. These results suggest that despite the nuclear defects associated with progerin accumulation, HGPS fibroblasts can be reprogrammed into iPSCs with transcriptomes that are highly similar to control iPSCs and hESCs.

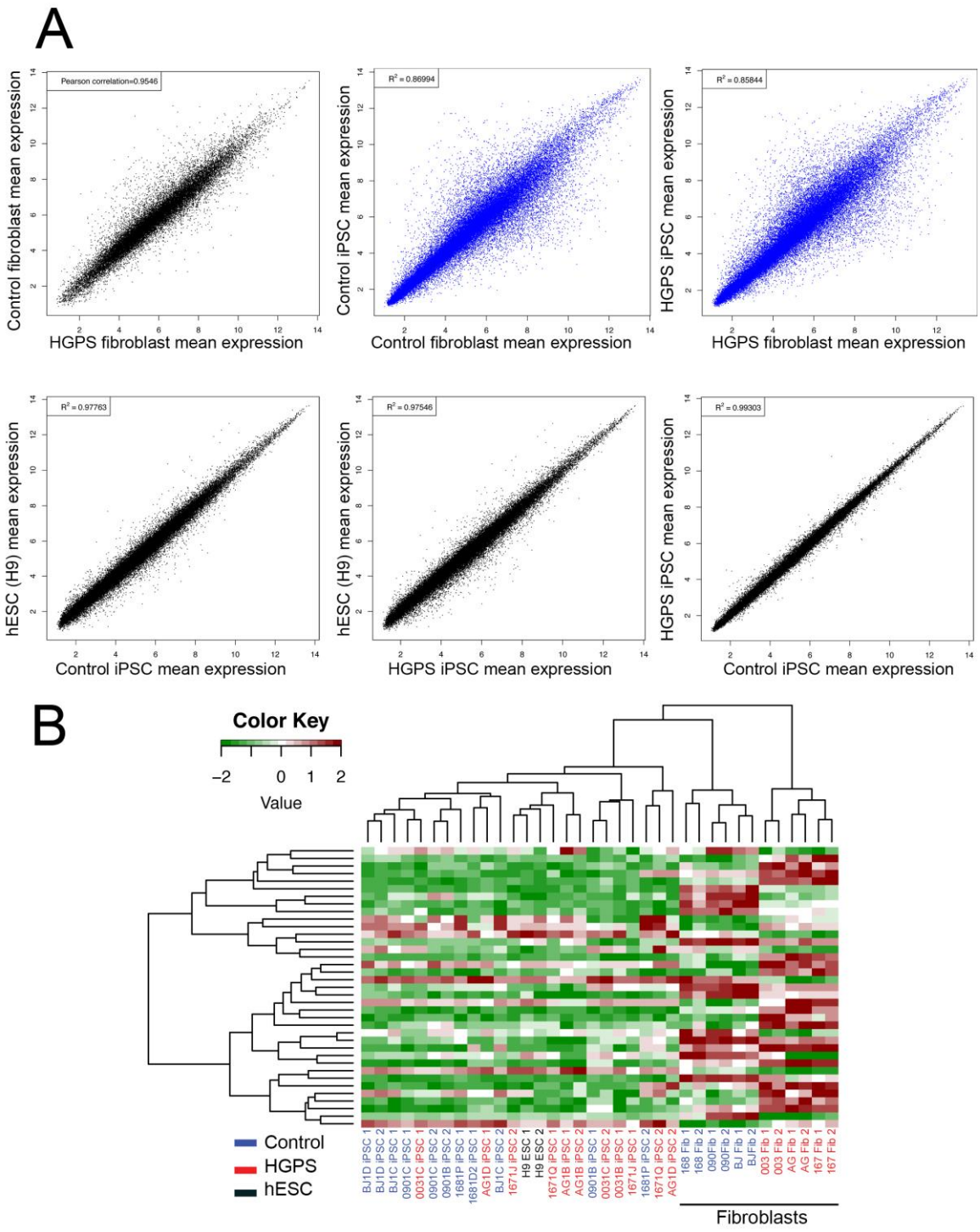

Figure 3.3. Transcriptomic landscape in HGPS iPSCs has been reset following reprogramming. **(A)** Microarray correlation profiles of HGPS iPSCs and control iPSCs compared to their parental fibroblasts and hESCs (H9). **(B)** Hierarchical cluster analyses of all transcriptome profiles demonstrate that HGPS iPSCs cluster closely control iPSCs and hESCs but are markedly different than

parental fibroblasts from either normal or HGPS patients. The names of the cell lines are color-coded to indicate the genotype: hESC lines, black; HGPS lines, red; and unaffected control lines, blue. Bioinformatic analysis including correlation plots and unsupervised clustering were performed by Gareth Palidwor. Reprinted from John Wiley and Sons – Aging Cell – Reprogramming progeria fibroblasts re-establishes a normal epigenetic landscape, Z. Chen, W.L.Stanford et. al., 2017.

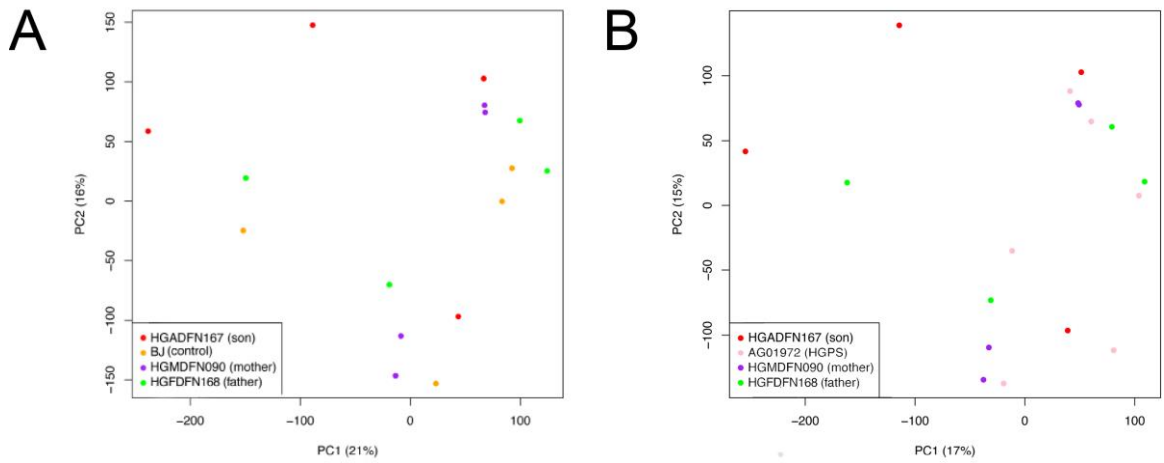

Figure 3.4 PCA of iPSC microarray profiles of familial trio. HGFDN168: father, HGMDFN090: mother, HGDFN167: son, HGPS: unrelated HGPS patient). All PCA graphs were generated by Gareth Palidwor. Reprinted from John Wiley and Sons – Aging Cell – Reprogramming progeria fibroblasts re-establishes a normal epigenetic landscape, Z. Chen, W.L.Stanford et. al., 2017.

3.1.4 Chromatin distribution and histone marks are rescued in HGPS iPSCs upon reprogramming

Defining characteristics of HGPS fibroblasts are the loss of both peripheral heterochromatin and the active histone mark H3K4me3 and repressive mark H3K27me3 (Liu et al., 2013b; Shah et al., 2013; Shumaker et al., 2006). I next investigated whether reprogramming rescued histone mark distribution by examining H3K4me3 and H3K27me3 levels using quantitative high-content

immunofluorescence imaging of our fibroblast and iPSC lines. The fluorescence intensity level of both marks was decreased in parental HGPS fibroblasts compared to controls (Figure 3.5A & B). However, the abundance of both marks was restored in HGPS iPSCs (Figure 3.5A & B), and the levels of both marks were much higher in HGPS iPSCs compared to their parental fibroblasts ($p<0.0001$). Heterochromatin distributions in HGPS fibroblasts and iPSCs were also inspected using electron spectroscopic imaging (ESI). It was observed that HGPS iPSCs exhibit uniform chromatin density with modestly increased density near the periphery, in contrast to the irregular distribution observed in HGPS fibroblasts (Figure 3.6). This suggests that the abnormal chromatin density characteristic of HGPS fibroblasts was restored after reprogramming.

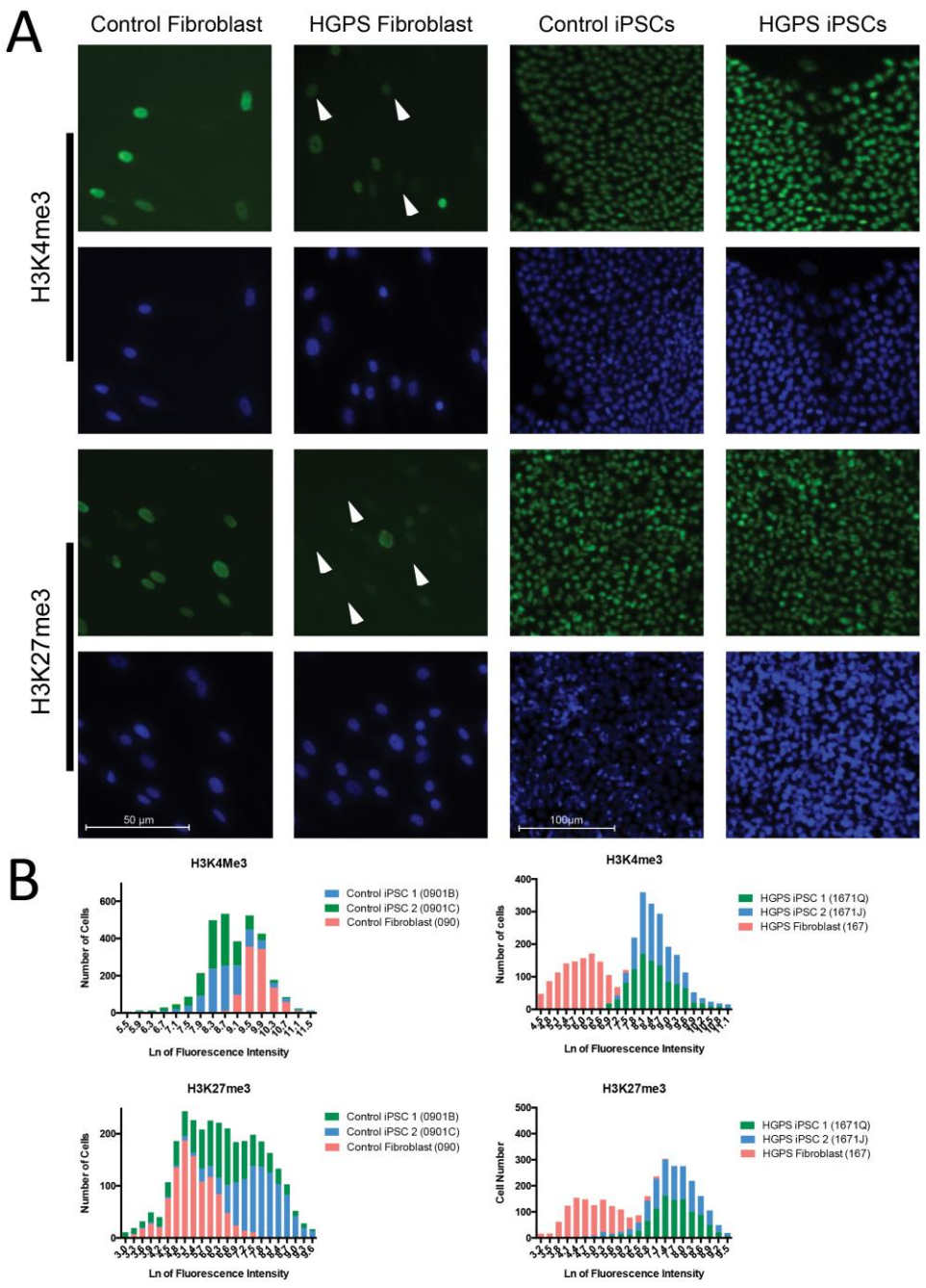

Figure 3.5 Active and repressive histone marks are rescued in HGPS iPSCs following reprogramming. (A) High content imaging of histone marks H3K4me3 and H3K27me3 in HGPS and control fibroblasts, as well as their iPSC derivatives. Arrows indicate nuclei with diminished

H3K4me3 and H3K27me3 fluorescence signal. **(B)** Intensity of H3K4me3 and H3K27me3 expression in fibroblasts (red bars) and corresponding iPSCs (green and blue bars) from normal and HGPS patients was quantified using high content imaging values compared on a natural log scale. Distribution analyses using one-way ANOVA reveal that reprogramming significant restored H3K4me3 and H3K27me3 marks in both control and HGPS iPSCs ($p<0.0001$). A minimum of 2 replicates were performed for each line. Reprinted from John Wiley and Sons – Aging Cell – Reprogramming progeria fibroblasts re-establishes a normal epigenetic landscape, Z. Chen, W.L.Stanford et. al., 2017.

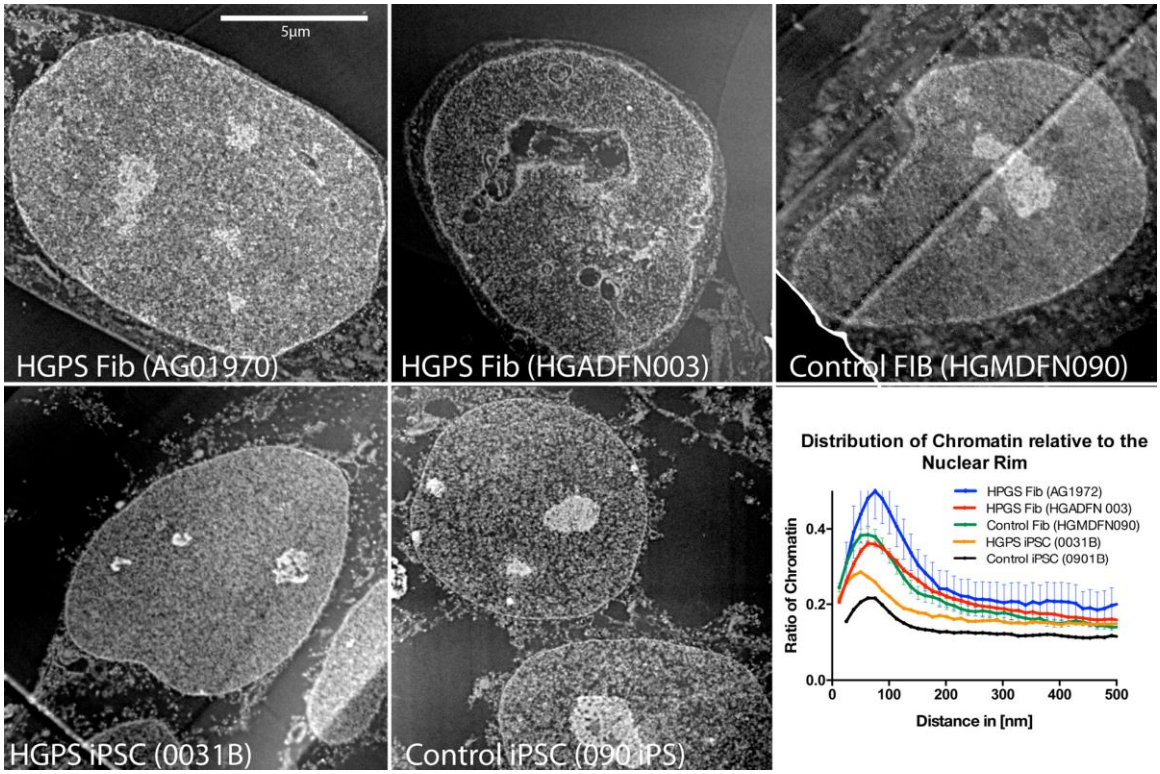

Figure 3.6. ESI images of the distribution of chromatin in fibroblasts and iPSCs. Chromatin of HGPS cells is remodeled to a normal pluripotent state by reprogramming. The images show 175 eV energy loss images (phosphorus enriched) where chromatin and nucleoli show enhanced contrast (white on a black background). *Graph:* The distribution of chromatin was quantified and plotted

relative to the nuclear periphery. The x-axis shows the periphery (left-most part of graph) moving towards the center (right-most part of the graph). The proportion of chromatin relative to total is plotted. The initial peak in the plot reflects the peripheral heterochromatin with higher values reflecting greater densities of heterochromatin associated with the nuclear lamina. White arrows indicate convolutions, green arrows holes and yellow arrows indicate condensed chromatin. ESI experiments and images were performed by Michael Hendzel's lab. Reprinted from John Wiley and Sons – Aging Cell – Reprogramming progeria fibroblasts re-establishes a normal epigenetic landscape, Z. Chen, W.L.Stanford et. al., 2017.

Since HGPS fibroblasts have altered epigenetic landscape, I next examined whether iPSC reprogramming rescued epigenetic landscape. Chromatin immunoprecipitation-sequencing (ChIP-seq) was performed on two HGPS iPSC clones and two unaffected iPSC clones to examine changes in genome-wide H3K4me3 and H3K27me3 as a result of reprogramming. PCA was performed on ChIP-seq iPSC data in relation with publicly available hESCs (BG01, WIBR1, HUES48, and HUES64), and normal iPSCs (A1, C1, A6, 4, 18c, and 15b) H3K4me3 and H3K27me3 datasets. When examining the similarity within -5kb and +2kb of the transcription start site (TSS) region in all known-coding genes, the reprogrammed HGPS iPSC lines clustered well with most of the publicly available hESC and iPSC data (Figure 3.7A). The heterogeneity between control and HGPS iPSCs is less than the inherent heterogeneity amongst other groups of normal pluripotent cells (Figure 3.8A&B). Using enrichment profiling on the average reads of all RefSeq genes, I compared all the iPSCs with hESC H9 and iPSC A7 datasets and found that the H3K4me3 and H3K27me3 enrichment profiles were highly similar between all

the datasets (Figure 3.7B), demonstrating that reprogramming efficiently resets the H3K4me3 and H3K27me3 marks associated with promoter proximal regions in HGPS iPSCs.

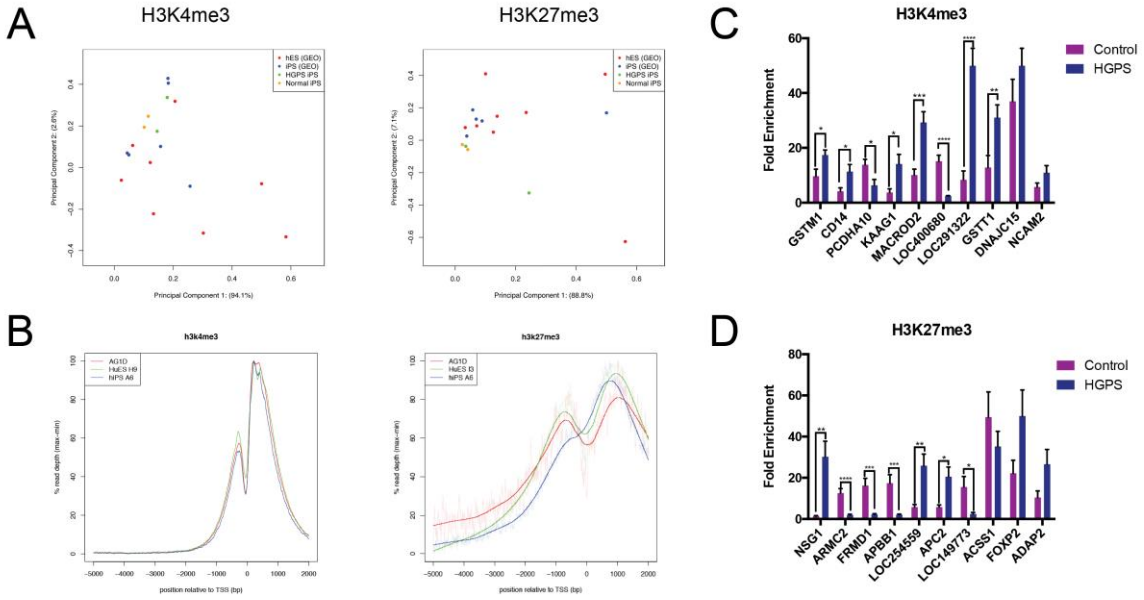

Figure 3.7 ChIP-seq analyses of HGPS iPSCs reveal that H3K4me3 and H3K27me3 profiles were restored upon reprogramming (A) PCA analyses comparing H3K4me3 and H3K27me3 ChIP-seq profiles of two HGPS (green) and two control iPSC lines (yellow), which were then compared to publicly available hESC (red) and normal iPSC (blue) lines. All HGPS and control iPSC lines generated grouped together with minimal variance. **(B)** The composite of average promoter proximal (-5kb to +2kb of the TSS) reads of H3K4me3 and H3K27me3 for all RefSeq genes were compiled between the control and HGPS iPSC lines and compared to that of publicly available profiles of control hESC and iPSC cell lines. **(C)** A 50kb sliding window across the genome to scan the ChIP-seq data to differentiate genomic regions with differential enrichment between Progeria and control iPSCs identified 106 non-promoter proximal differentially methylated regions associated with RefSeq genes across the whole genome. **(D)** ChIP-qPCR of differentially enriched target genes was

performed in all iPSC lines. Error bars represent SEM using student t-test. * indicates P<0.05, ** indicates P< 0.005, *** indicates P<0.001, **** indicates *P*<0.0001. A minimum of 2 biological replicates was performed for each experiment. PCA analyses and composite graphs were generated by Gareth Palidwor. Reprinted from John Wiley and Sons – Aging Cell – Reprogramming progeria fibroblasts re-establishes a normal epigenetic landscape, Z. Chen, W.L.Stanford et. al., 2017.

Furthermore, I examined whether regions with differential H3K4me3/H3K27me3 enrichment also impacted differential transcription in iPSCs. To identify genomic regions with differential enrichment between HGPS and control iPSCs, ChIP-seq datasets were further analyzed beyond the promoter regions using a 50kb sliding window. This strategy yielded 106 non-promoter proximal regions associated with RefSeq genes that are differentially enriched for H3K4me3, and 38 regions for H3K27me3. I then performed ChIP-qPCR to validate the top 10 differentially methylated regions for each histone mark in control and HGPS iPSCs. 8 of 10 H3K4me3 and 7 of 10 H3K27me3 marks were validated as differentially enriched between control and HGPS iPSCs (Figure 3.7C&D). No correlation was found between H3K4me3 and H3K27me3-enriched genes and differential gene expression between control and HGPS iPSCs as confirmed by RT-qPCR (Figure 3.9B). This suggests that the altered epigenetic marks outside promoter regions did not affect gene expression. Therefore, our ChIP-seq and transcriptional microarray analyses together support the notion that epigenetic landscape of HGPS fibroblasts has been reverted to a normal pluripotent state comparable to that in control iPSCs after reprogramming.

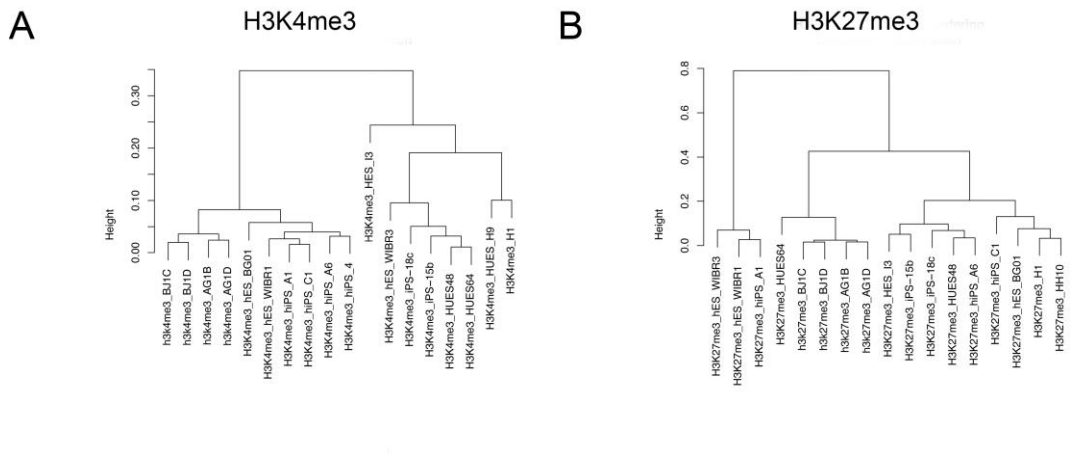

Figure 3.8. Unsupervised clustering of ChIP-seq profiles of HGPS iPSCs with publicly available datasets. Hierarchical clustering of HGPS iPSCs, control iPSCs, and publicly available iPSC and hESC cell lines for both H3K4me3 **(A)** and H3K27me3 **(B)** ChIP-seq profiles. The heterogeneity between control and HGPS iPSCs is less than the inherent heterogeneity amongst other groups of normal pluripotent cells. Reprinted from John Wiley and Sons – Aging Cell – Reprogramming progeria fibroblasts re-establishes a normal epigenetic landscape, Z. Chen, W.L.Stanford et. al., 2017.

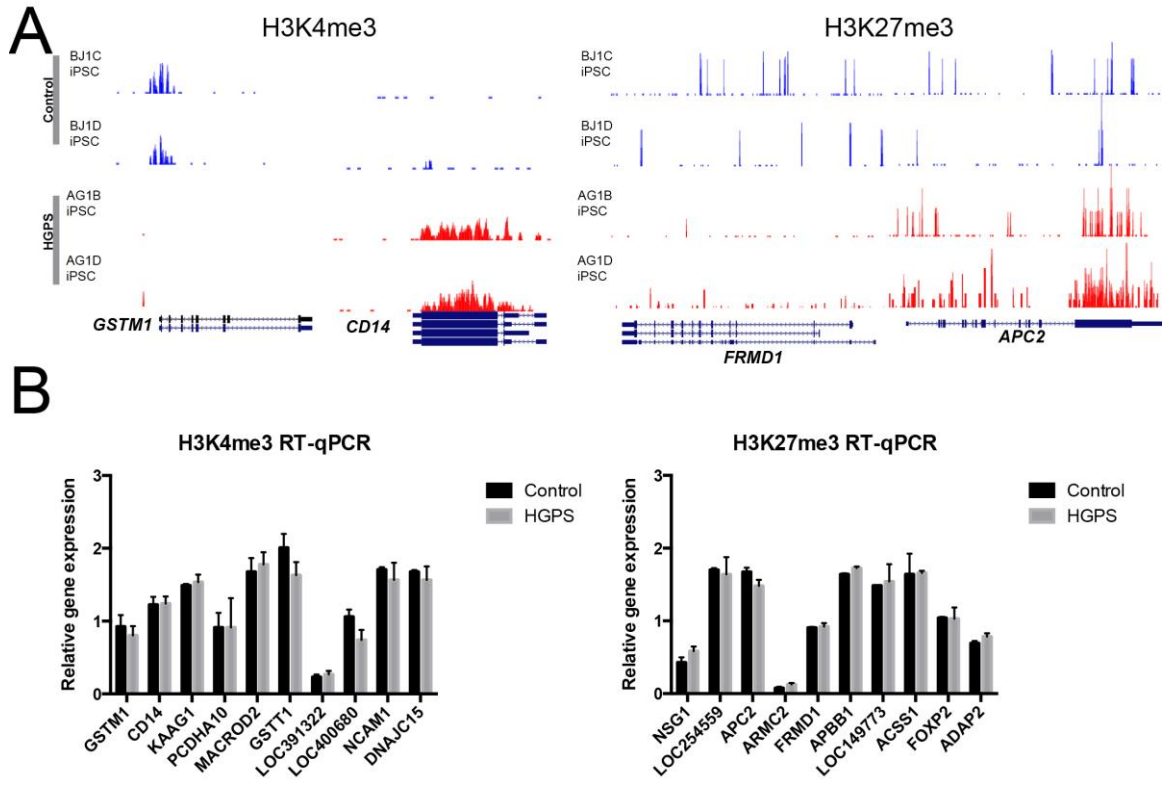

Figure 3.9. Altered epigenetic marks observed between normal and HGPS iPSCs do not impact transcriptional regulation of pluripotent cells. (A) Genome tracks of ChIP-seq data for H3K4me3 and H3K27me3 of two representative differentially enriched genes in normal and HGPS iPSCs. RefSeq gene tracks are shown below the profiles. **(B)** qPCR of differentially enriched genes between Control and HGPS iPSCs demonstrating that all differentially enriched genes were not differentially expressed between control and HGPS iPSCs. All statistical analyses were done using the two-tailed t-test. A minimum of 2 biological replicates was performed for qPCR analyses. Reprinted from John Wiley and Sons – Aging Cell – Reprogramming progeria fibroblasts re-establishes a normal epigenetic landscape, Z. Chen, W.L.Stanford et. al., 2017.

Chapter 3.2 – HGPS iPSCs differentiated into VSMCs to model HGPS disease progression

3.2.1 HGPS and control VSMCs exhibit similar differentiation capacity into VSMCs

To model HGPS disease progression in VSMCs, I applied a direct differentiation strategy (Xie et al., 2007) to generate cultures of HGPS VSMCs from iPSCs (Figure 3.10A). To assess the efficiency of VSMC differentiation, we quantified the expression of VSMC-specific markers (Calponin, Smooth Muscle Actin (SMA), and SM22α) at both early (passage 7, P7) and late (P14) passages of HGPS and control VSMCs. The percentages of cells positive for VSMC markers were comparable across multiple genotypes and passages with human carotid artery VSMCs (CAVSMCs) (Figure 3.10B). Furthermore, physiological contraction in response to the cholinergic agonist carbachol was observed across both control and HGPS VSMCs.

Thus, these results indicate that both control and HGPS VSMCs readily differentiate into VSMCs at similar efficiency.

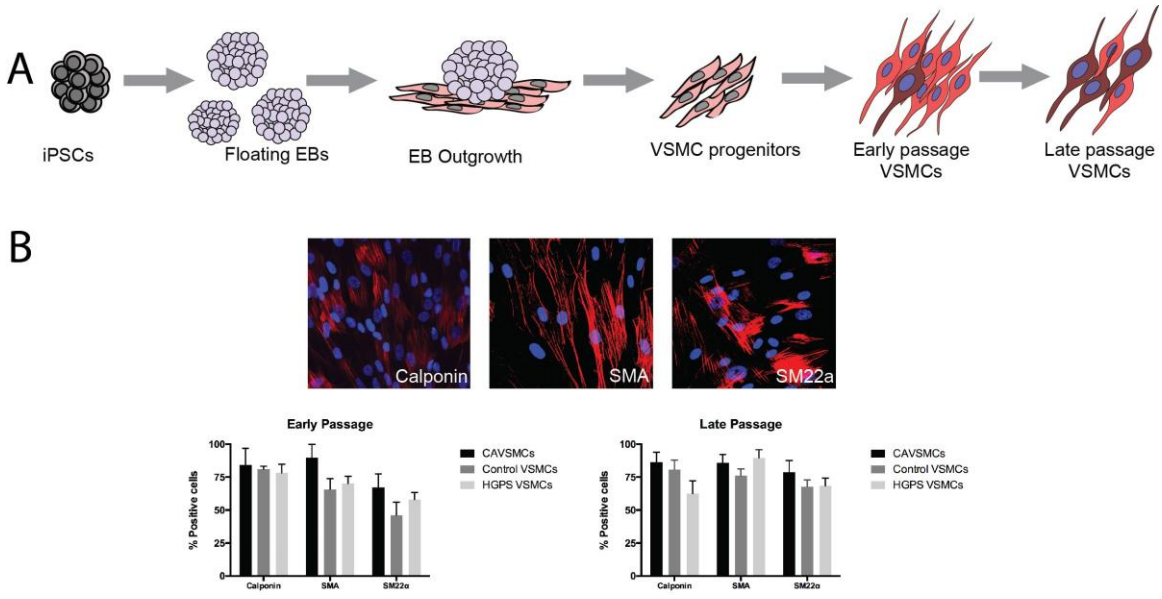

Figure 3.10. HGPS iPSC-derived VSMCs exhibit typical smooth muscle cell markers upon differentiation. (A) A schematic of the directed differentiation approach adopted to generate VSMCs from iPSCs through EB formation. **(B)** Differentiated VSMCs express typical VSMC markers such as Calponin, Smooth Muscle Actin (SMA), and Smooth Muscle 22 alpha (SM22alpha). Statistical analyses using ANOVA revealed no significance in terms of VSMC marker expression between the three groups of VSMCs. Reprinted from John Wiley and Sons – Aging Cell – Reprogramming progeria fibroblasts re-establishes a normal epigenetic landscape, Z. Chen, W.L.Stanford et. al., 2017.

3.2.2 HGPS VSMCs exhibit hallmarks of premature aging

Since HGPS fibroblasts typically exhibit nuclear defects including abnormal nuclear morphology (Goldman et al., 2004; Shumaker et al., 2006) which were rescued in iPSCs following reprogramming, I sought to assess these phenotypes in HGPS VSMCs when *LMNA* is re-expressed following differentiation. Using immunostaining

against Lamin A/C complimented with an unbiased Image J algorithm, I found that significantly more HGPS VSMCs display abnormal nuclear shape than control at both early and late passages (29% versus 3%, and 41% versus 6%, respectively) (Figure 3.11A). Concomitant with nuclear morphology defects, progerin^{+} VSMCs increased in proportion with passaging (Figure 3.11B). HGPS cells also accumulate elevated endogenous DNA damage, in particular double strand breaks (DSBs) with passage in culture (Goldman et al., 2004; Liu et al., 2005; Liu et al., 2006), which are typically indicated by the presence of cryptogenic foci marked by γH2A.X as part of the DDR signaling cascade. Using immunostaining, I found that HGPS VSMCs exhibit much higher levels of γH2A.X foci compared to control as previously reported in HGPS fibroblasts (Goldman et al., 2004; Taimen et al., 2009) (Figure 3.11C).

I next aimed to assess the extent of vascular aging in HGPS VSMCs. Excessive production of ROS is common in atherosclerotic plaques in normative aged vasculature and is a major cause of vascular inflammation, arterial remodeling and premature senescence (He and Zuo, 2015; Tavakoli and Asmis, 2012). Consistent with normative vascular aging, HGPS VSMCs exhibit a significant increase in ROS between early and late passages (22% versus 48%), in contrast to control VSMCs that remain less than 10% ROS-positive cells at corresponding passages (Figure 3.11D). Similarly, when I assessed the level of premature senescence by examining the percentage of cells staining for SA-βgal, I found that while the percentage of control VSMCs that expressed SA-βgal remained approximately 10% consistently through passaging, the percentage of SA-βgal+ HGPS VSMCs increased from 20% to

40% between early and late passages (Figure 3.11E). These results demonstrate that HGPS patient-derived VSMCs exhibit hallmark traits of accelerated vascular aging.

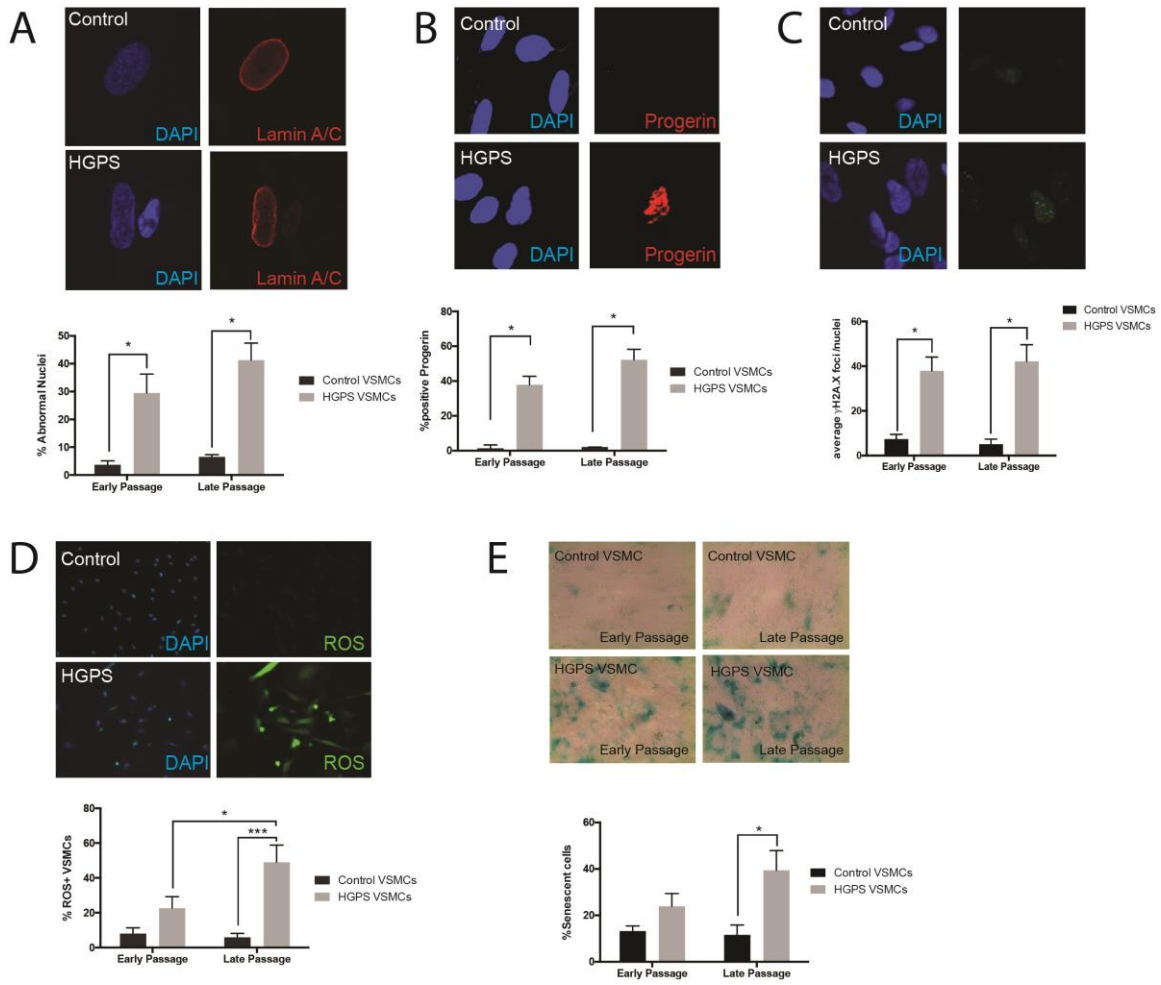

Figure 3.11. HGPS iPSC-derived VSMCs exhibit hallmark HGPS genomic defects (A) Representative confocal images of Lamin A/C staining demonstrate a 6-fold increase in defective nuclear morphology in HGPS VSMCs than control VSMCs. **(B-E)** Representative images of HGPS VSMCs exhibiting hallmark Progeria defects, including expressing the mutant protein progerin **(B)** and a markedly higher level of DNA damage γH2A.X foci **(C)** and ROS **(D)**. **(E)** HGPS VSMCs exhibit higher level of senescence marker SA-βGal compared to control **(E)**. Error bars represent SEM using student t-test. * indicates P<0.05, ** indicates P< 0.005, *** indicates P<0.001. A minimum of 3 biological replicates was performed for each experiment. Reprinted from John Wiley and Sons –

Aging Cell – Reprogramming progeria fibroblasts re-establishes a normal epigenetic landscape, Z. Chen, W.L.Stanford et. al., 2017.

To specifically examine whether HGPS vascular disease initiation can be modeled via VSMC differentiation *in vitro*, I measured the level of progerin accumulation in HGPS iPSCs as they differentiated into VSMCs from across several passages. RT-qPCR analysis revealed that in HGPS VSMC cultures, *progerin* mRNA transcripts increased significantly compared to undifferentiated iPSCs at the EB stage of differentiation and in passage 1 VSMC cultures (Figure 3.12A). Expectedly, *progerin* mRNA expression was negligible in hESCs and control iPSC-derived VSMC cultures. Using immunofluorescence staining with confocal imaging analyses, I identified that approximately 2% of HGPS EB cells contained detectable levels of progerin, while 10% of HGPS cells at passage 1 VSMC cultures had detectable levels of progerin (Figure 3.12B). More than 20% of HGPS VSMCs exhibited detectable levels of progerin by passage 4, while differentiated iPSC control cultures showed no progerin expression. Western Blot analysis also failed to detect progerin in undifferentiated iPSCs as well as control VSMCs, while progerin was detected by passage 1 of HGPS VSMC cultures (Figure 3.12C). Together, these results indicate that progerin expression begins to accumulate early in VSMC specification and increases in differentiated HGPS VSMCs.

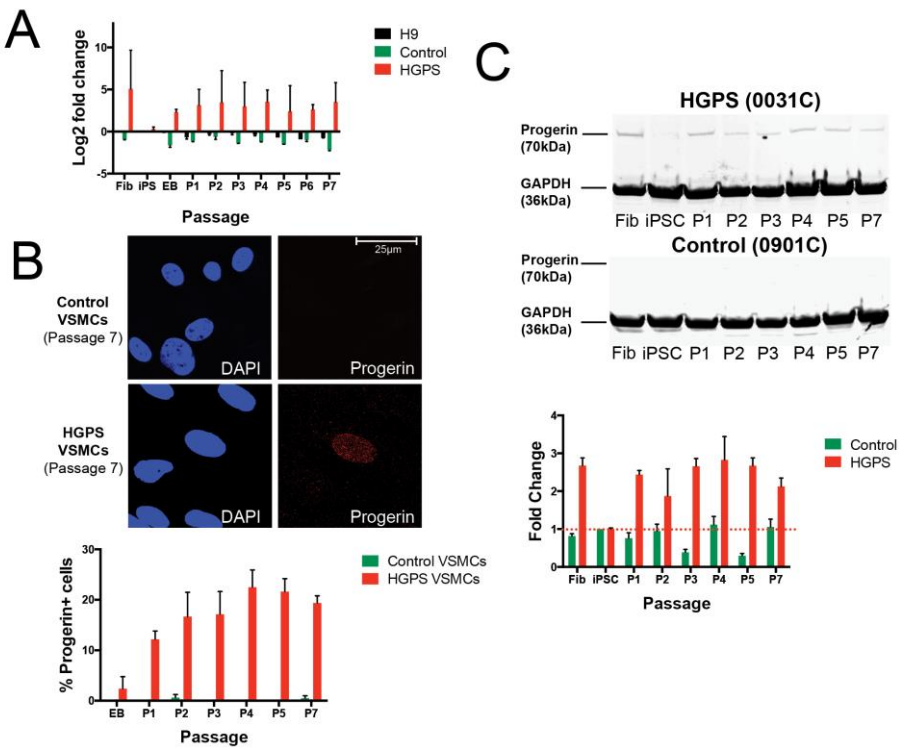

Figure 3.12. Differentiated HGPS VSMCs expressed progerin. (A) *Progerin* transcript levels assessed by qPCR showed *progerin* mRNA was not detected in control iPSCs and hESCs but is observed in HGPS EBs and early passage VSMCs. **(B)** Confocal analysis of progerin-positive cells in EB cultures, with increasing numbers in HGPS, but not control, VSMC cultures. **(C)** Western blot analysis of parental fibroblasts, undifferentiated (iPSC), EB outgrowth and increasing passages (P) of VSMC cultures. Progerin protein was not detected in HGPS iPSC cultures nor control cells but was detected in HGPS fibroblasts and VSMCs. Reprinted from John Wiley and Sons – Aging Cell – Reprogramming progeria fibroblasts re-establishes a normal epigenetic landscape, Z. Chen, W.L.Stanford et. al., 2017.

Using γH2A.X immunostaining to detect DSBs at each passage during VSMC differentiation, I found that there is an initial elevation in γH2A.X foci in both control and HGPS VSMCs in their EB outgrowth stage and at passage 1 (Figure 3.13), which

may indicate a link between DDR signaling and initiation of differentiation (Sherman et al., 2011). HGPS VSMCs showed a significant increase in γH2A.X foci at passage 4 that remained high. In contrast, control VSMCs demonstrated a low γH2A.X foci count from passage 2 (Figure 3.13). Overall, our differentiation data suggested that HGPS iPSCs differentiate into VSMCs that exhibit progressive HGPS phenotypes and can be used to monitor the progression of molecular and cellular phenotypes.

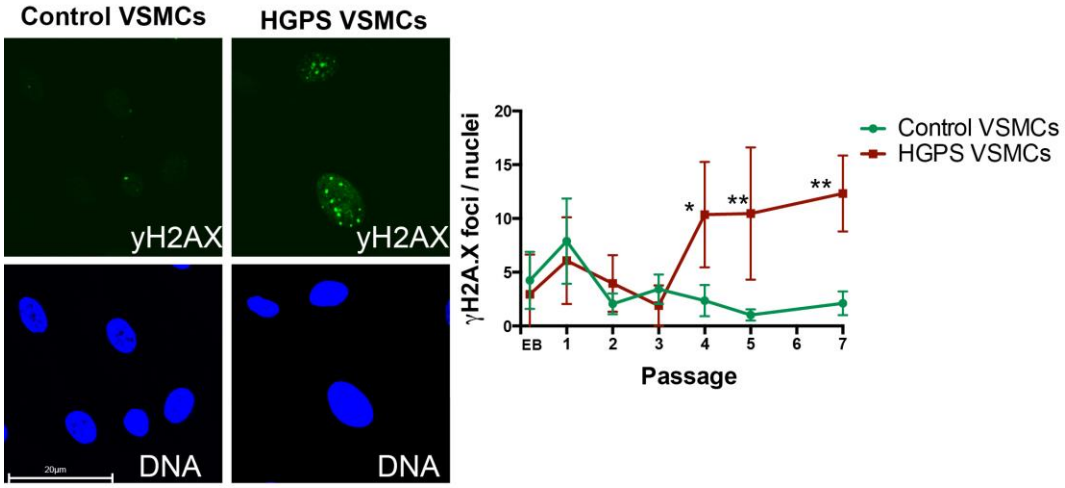

Figure 3.13. HGPS VSMCs exhibit passage-dependent increase in DNA damage when aged *in vitro*. Confocal imaging and analysis of γH2A.X foci in VSMC differentiation cultures (EBs and various passages (P) of VSMCs), showing that γH2A.X foci are comparable between control and HGPS cultures until passage 4 of VSMC cultures. Statistical significances were calculated using student's t-test. * indicates $P<0.05$, ** indicates $P< 0.005$. A minimum of 2 biological replicates was performed for each experiment. Reprinted from John Wiley and Sons – Aging Cell – Reprogramming progeria fibroblasts re-establishes a normal epigenetic landscape, Z. Chen, W.L.Stanford et. al., 2017.

Chapter 3.3 – HGPS VSMCs exhibit increased DNA damage due to elevated oxidative stress

3.3.1 HGPS VSMCs exhibit altered transcriptomic activation of cardiovascular remodeling and oxidative stress response

The presence of progerin in the nuclear lamina of HGPS fibroblasts has been reported to be correlated with transcriptomic changes, and that HGPS fibroblasts exhibit similar transcriptomic profiles to that in aged fibroblasts (Aliper et al., 2015; Fleischer et al., 2018). We sought to investigate whether HGPS VSMCs exhibit an age (passage)-dependent transcriptional profile via RNA-sequencing (RNA-seq) in two control and two HGPS VSMCs across early and late passages and whether transcriptomic changes reveal any programs pertaining to hallmark HGPS phenotypes. PCA on both control and HGPS VSMC lines revealed an expected segregation between male and female VSMC cultures (Figure 3.14A), as well as a separation between control and HGPS lines (Figure 3.14B). Differential expression analysis revealed a total of 1671 DEGs (*padj*<0.05) between early passage control and HGPS VSMCs, of which 1087 genes were upregulated and 585 genes were downregulated (Figure 3.14C&D). Similarly, 1801 DEGs were identified between control and HGPS VSMCs at late passage, of which 930 genes were downregulated, and 871 genes were upregulated in HGPS VSMCs (Figure 3.14C&D). Given the rapid progression of age-related pathologies in HGPS VSMCs, I examined alterations in passage dependent gene expression in both control and HGPS VSMCs. I found that 1406 DEGs were identified between early and late passages in HGPS VSMCs (Figure 3.15B). In contrast, only 108 DEGs were found between early and late passage in

control VSMCs (Figure 3.15A), suggesting that HGPS VSMCs exhibit strong passage-dependent transcriptomic aberrancies.

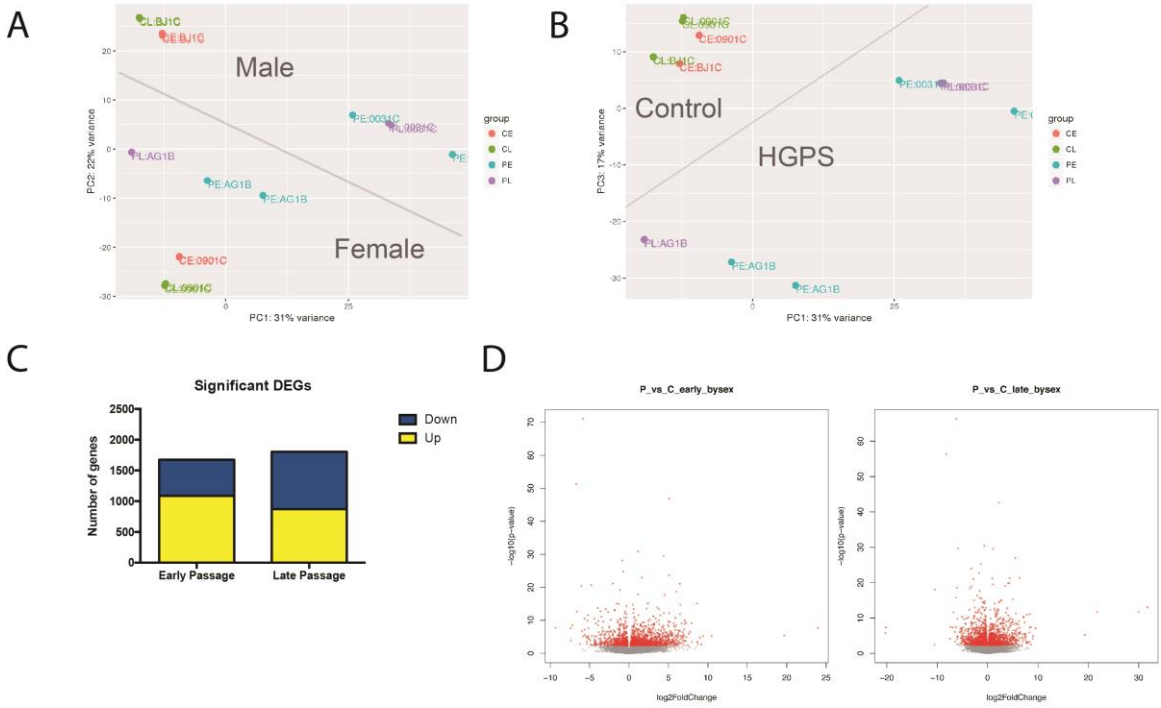

Figure 3.14 HGPS VSMCs exhibit transcriptomic dysregulation. (A) PCA of RNA-seq profiles of two control and two HGPS VSMC lines at both early and late passages. The combination of PC1 and PC2 demonstrated expected separation between all RNA-seq profiles based on sex. CE (red): Controls Early passage, CL (green): Controls Late passage, PE (blue): Progeria Early passage, PL (purple): Progeria Late passage. **(B)** PCA of all RNA-seq profiles demonstrating that combination of PC1 and PC3 show expected separation between control and HGPS VSMC RNA-seq profiles. **(C)** Number of total DEGs identified between control and HGPS VSMCs by RNA-seq analysis (FDR<0.05). **(D)** Volcano plot of RNA-seq data of control compared to HGPS VSMCs at early (left) and late (right) passages. DEGs are represented as red dots. PCA analysis and Volcano plots were generated by Christopher Porter.

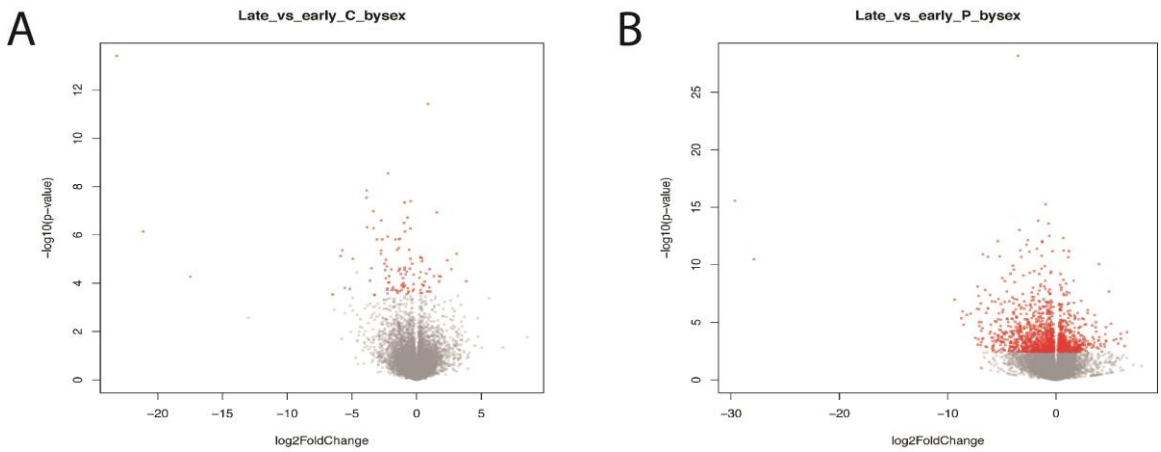

Figure 3.15 HGPS VSMCs exhibit passage-dependent transcriptomic aberrancies. (A) Volcano plot of RNA-seq data of control VSMCs at early (P7) versus late (P14) passages. **(B)** Volcano plot of RNA-seq data of HGPS VSMCs t early (P7) versus late (P14) passages. DEGs are represented as red dots. Volcano plots were generated by Christopher Porter.

To investigate which transcriptomic program(s) are altered in HGPS VSMCs, gene ontology (GO) analysis was performed on DEGs between control and HGPS VSMCs. At early passage, DEGs between control and HGPS VSMCs revealed a significant dysregulation of genes associated with "vasculogenesis" and "extracellular matrix organization" (Figure 3.16A). The list of DEGs was further divided between 'up' and 'down' regulated genes to which GO analysis was performed. A distinct enrichment of upregulated genes involved in vasculature development (Figure 3.17A) was observed, indicative of an activation of vascular remodeling program in early passage HGPS VSMCs. In contrast, downregulated genes predominantly enriched for response to "reactive oxygen species" and "cellular response to DNA damage" (Figure 3.17B), which suggests a dysregulation in DDR due to increased oxidative

stress. Interestingly, at late passage, GO terms that were predominantly enriched among downregulated genes were associated with "smooth muscle differentiation", "smooth muscle proliferation", and "regulation of stem cell differentiation" (Figure 3.17C), indicative of an arrest of the vascular remodeling and proliferation pathway at this passage, correlating with premature senescence observed in aged VSMC cultures (Costopoulos et al., 2008; Matthews et al., 2006; Sedelnikova et al., 2004; Wallis et al., 2004). GO terms associated with oxidative stress were enriched in both up and downregulated genes, suggesting an overall dysregulated oxidative stress response in late passage HGPS VSMCs (Figure 3.17D). Together, these results indicate that HGPS VSMCs exhibit perturbed vascular remodeling and redox response, which potentially contributes to elevated oxidative stress.

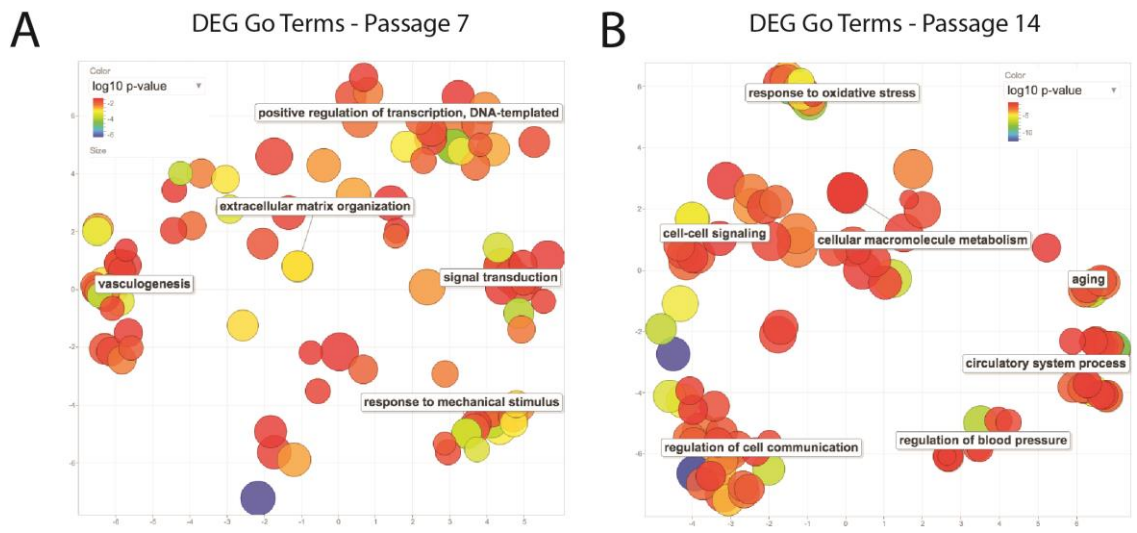

Figure 3.16 HGPS VSMCs exhibit altered transcriptional programs in vascular remodeling and oxidative stress. REViGO scatterplots of enriched GO Cluster representatives from RNA-seq datasets comparing control to HGPS VSMCs at both early (Passage 7) **(A)** and late (Passage 14) passages **(B)**.

The terms were plotted in a two-dimensional space following redundancy reduction of all GO terms. Bubble colour indicates log10 p-value. Bubble size indicates the relative frequency of the GO terms in the underlying reference EBI GOA database, where Bubbles of more general terms are larger.

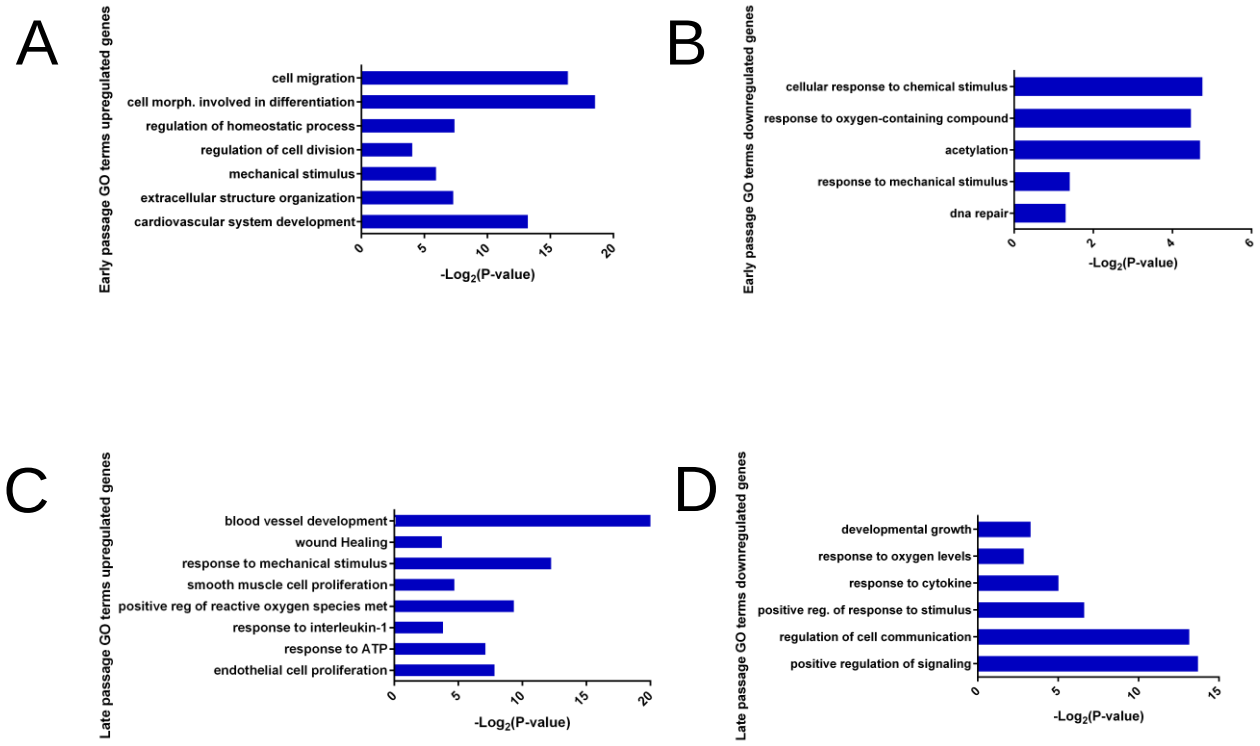

Figure 3.17 HGPS VSMCs exhibit passage-specific transcriptomic alterations. Enriched GO terms for genes upregulated and down regulated from RNA-seq datasets comparing control to HGPS VSMCs at early passages that are upregulated **(A)** and downregulated **(B)**, as well as GO cluster representatives from late passages that are upregulated **(C)** and downregulated **(D)**.

3.3.2 HGPS VSMCs exhibit elevated endogenous DNA damage due to oxidative stress

HGPS fibroblasts typically display an elevated DNA damage response as evidenced by the increased accumulation of γH2A.X in the nuclei (Constantinescu et al., 2010; Liu et al., 2013a; Liu et al., 2006). To examine the amount of endogenous DNA breaks in HGPS VSMCs, I performed the alkaline comet assay and observed that

HGPS VSMCs exhibit significantly higher Olive Tail moment compared to control cells at high passage (15.28 vs. 9.18) (Figure 3.18A). This indicates that HGPS VSMCs not only have elevated DNA damage, but DNA damage is not sufficiently repaired for the level of basal DNA damage to reach steady-state. Since HGPS VSMCs exhibit elevated ROS and dysregulated oxidative stress response, we next examined whether high ROS is inducing the DSBs via direct oxidation of DNA nucleotides. Guanines are highly susceptible to oxidation, resulting in formation of 8-oxo-7,8-dihydro-2-deoxyguanine (8-OxoG) DNA adducts that create lesions in the DNA and ultimately stalled replication forks (Mahmoudi et al., 2006). Using FITC-conjugated avidin which binds to 8-OxoG with high specificity (Struthers et al., 1998), we detected a significantly higher level of 8-OGG in HGPS VSMCs compared to control VSMCs (Figure 3.18B), underscoring the extent of DNA lesions present in HGPS VSMCs due to oxidative stress.

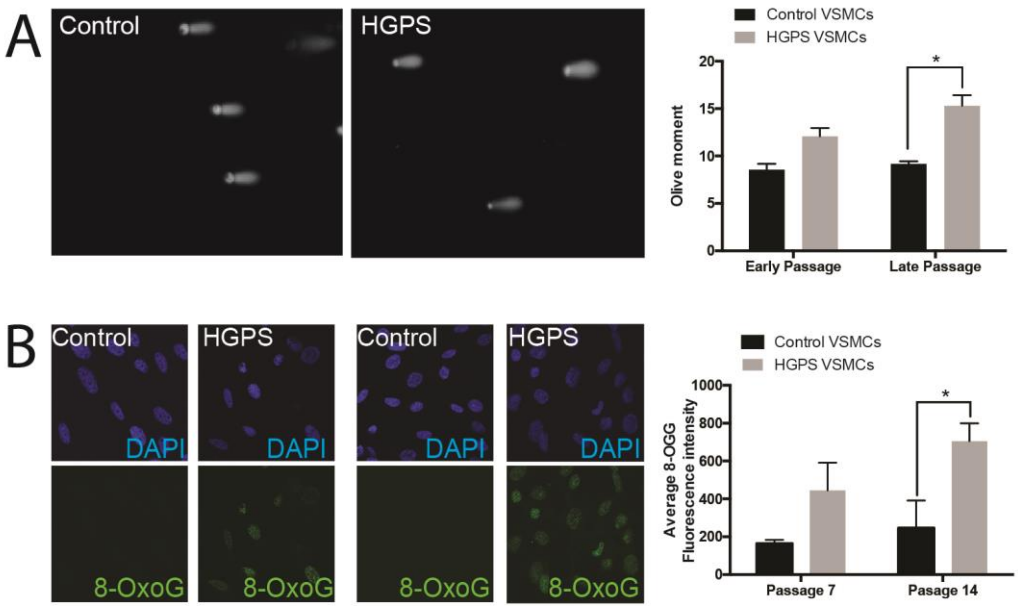

Figure 3.18. HGPS VSMCs exhibit elevated DSBs caused by increased oxidation. (A) HGPS VSMCs exhibit higher level of double stranded breaks via analysis using Comet Assay. **(B)** HGPS

VSMCs contain higher level of 8-Oxoguanine (8-OxoG) compared to control at late passage. Statistical significances were calculated using student's t-test. Error bars represent SEM. * indicates P<0.05. A minimum of 3 biological replicates was performed for each experiment at both early and late passages.

3.3.3 HGPS VSMCs show increased replicative stress and an altered double-strand break repair response

Since HGPS VSMCs exhibit replicative arrest and premature senescence, I next investigated whether DNA damage directly causes replicative stress. I performed accelerated native isolation of proteins on nascent DNA (aniPOND)(Leung et al., 2013) that allows the pull-down and analysis of purified replication fork proteins. Using this method, I probed for γH2A.X via western blot in both control and HGPS VSMCs and found that compared to control VSMCs, HGPS VSMCs exhibited much higher γH2A.X on nascent DNA at late passage (Figure 3.19A). This finding was further confirmed quantitatively using *in situ* Proximity Ligation Assay (PLA), demonstrating that HGPS VSMC nuclei contain much higher levels of BrdU-γH2A.X complexes than control VSMCs at later passage (Figure 3.19B), suggesting that elevated DNA damage causes replicative stress in HGPS VSMCs.

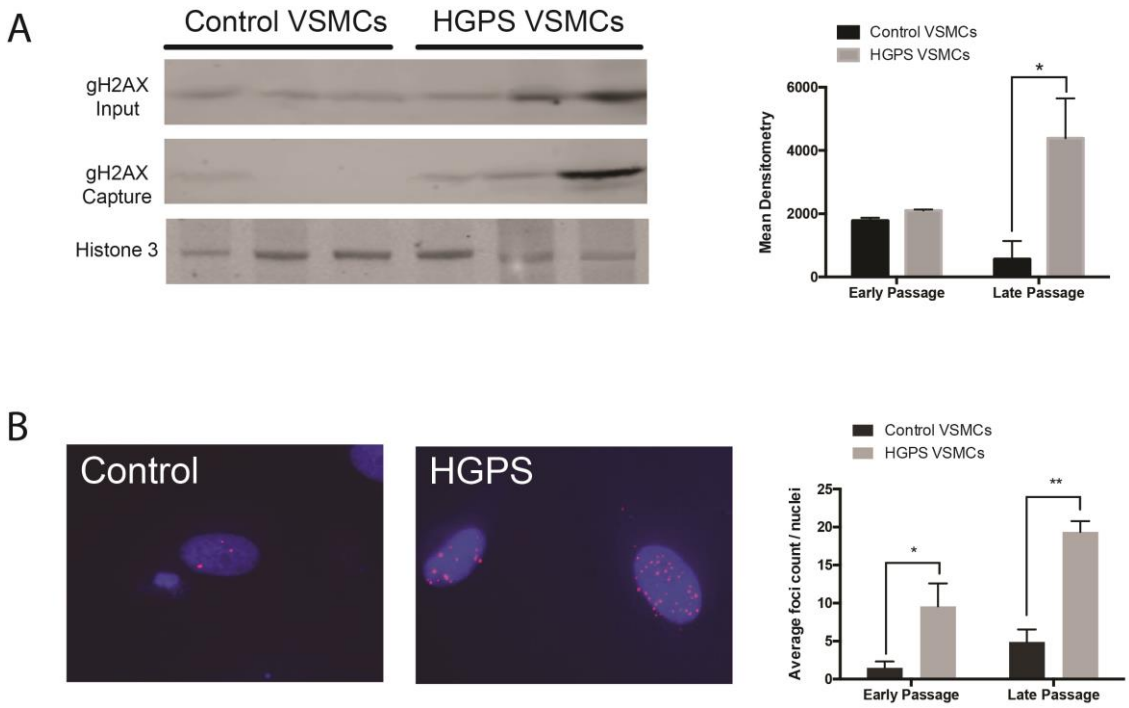

Figure 3.19. HGPS VSMCs exhibit replicative stress. **(A)** HGPS VSMCs have more γH2A.X accumulation on replicating DNA demonstrated by aniPOND. **(B)** HGPS VSMCs have more co-localization between BrdU and γH2A.X in the nucleus via PLA. Statistical significances were calculated using the student's t-test. Error bars represent SEM. * indicates P<0.05, ** indicates P< 0.005. A minimum of 3 biological replicates was performed for each experiment.

3.3.4 Elevated DNA damage can be rescued by FTI and N-acetyl cysteine administration

The prevailing therapeutic strategy for Progeria patients is treatment with Lonarfarnib, an FTI that blocks the farnesylation of prelamin A and progerin to prevent progerin from integrating into the nuclear lamina(Columbaro et al., 2005; Varela et al., 2008). To investigate whether progerin accumulation contributes to elevated endogenous DNA damage, we treated HGPS VSMCs with Lonafarnib and

examined the extent of rescue in HGPS nuclear morphology and DNA damage response. Consistent with previous studies (Capell et al., 2008; Yang et al., 2006), HGPS VSMCs exhibited improved nuclear morphology concomitant with a significant decrease of progerin-positive nuclei from 28% to 7% in HGPS VSMC cultures (Figure 3.20A&B). Similarly, we observed a significant drop in γH2A.X foci from 40 to 12 foci per nucleus in HGPS VSMCs following FTI administration relative to control VSMCs (Figure 3.20C), indicating that DNA damage response activation is at least partially caused by progerin accumulation in HGPS VSMCs.

To assess whether oxidative stress also contributes to DNA damage and replicative stress, we rescued ROS production by treating HGPS VSMCs with the ROS scavenger N-acetyl Cysteine (NAC). Following NAC treatment, not only did ROS-positive HGPS VSMCs decrease from 40% to 13% (Figure 3.20D), γH2A.X foci also dropped from 41 to 24 per nucleus in HGPS VSMCs (Figure 3.20E), suggesting that elevated ROS, in tandem with progerin accumulation, causes extensive DNA damage in HGPS VSMCs.

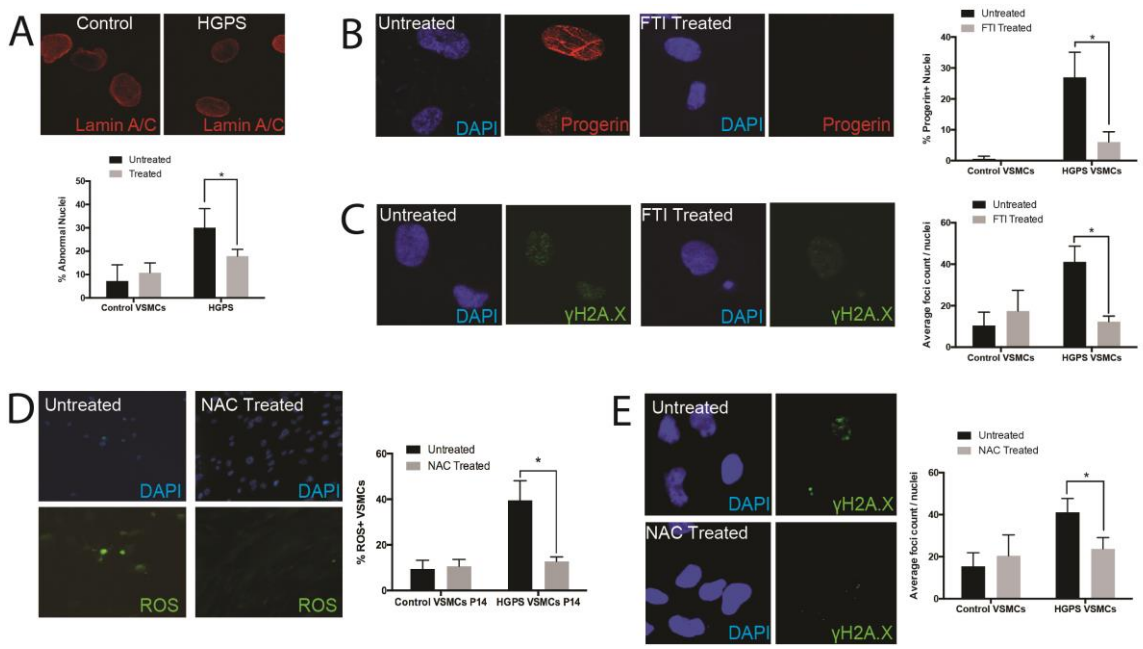

Figure 3.20. Treatment with FTI and NAC decreased endogenous DNA damage in HGPS VSMCs. **(A-C)** FTI treatment improved nuclear defects in HGPS VSMCs including **(A)** rescuing abnormal nuclear morphology via Lamin A/C staining, **(B)** decreased Progerin accumulation, and **(C)** decreased DNA damage marker γH2A.X foci. Calculated values represent mean ± SEM (n=4, 2x for each cell line per test group at each passage). **(D-E)** NAC treatment decreased cellular ROS levels **(D)** as well as γH2A.X foci **(E)** in HGPS VSMCs. Calculated values represent mean ± SEM (n=6, 2x for 3 cell lines per test group at each passage).

Chapter 3.4 – HGPS VSMCs exhibit altered Histone 4 Lysine 16 abundance due to abnormal engagement with DDR

3.4.1 Persistent DNA damage in HGPS VSMCs is due to engagement in NHEJ repair on replicating DNA

As HGPS VSMCs exhibit replicative stress, demonstrated by the accumulation of

γH2A.X foci at replication sites, I sought to investigate mechanisms underlying this phenomenon by identifying differential protein dynamics involved in replication fork progression in HGPS VSMCs through the utilization of aniPOND coupled with mass spectrometry. Using STRING analysis, protein-protein interaction networks of the replication-fork proteome were defined based on the list of differentially enriched proteins between control and HGPS VSMCs ($p<0.05$, Fisher's exact test) from both early and late passages (Figure 3.21A). I observed an emergence of protein clusters associated with the NHEJ DDR pathway in HGPS VSMC replication forks at both early and late passage (Figure 3.21A), which include proteins such as XRCC5, XRCC6, DNA PKC, PARP1, and 53BP1 in HGPS VSMCs in contrast to control (Table 3.2). In addition, GO analysis revealed an enrichment of terms associated with DNA damage (Figure 3.21B), indicative of elevated DDR occurring on replicating DNA in HGPS VSMCs that could drive replicative stress.

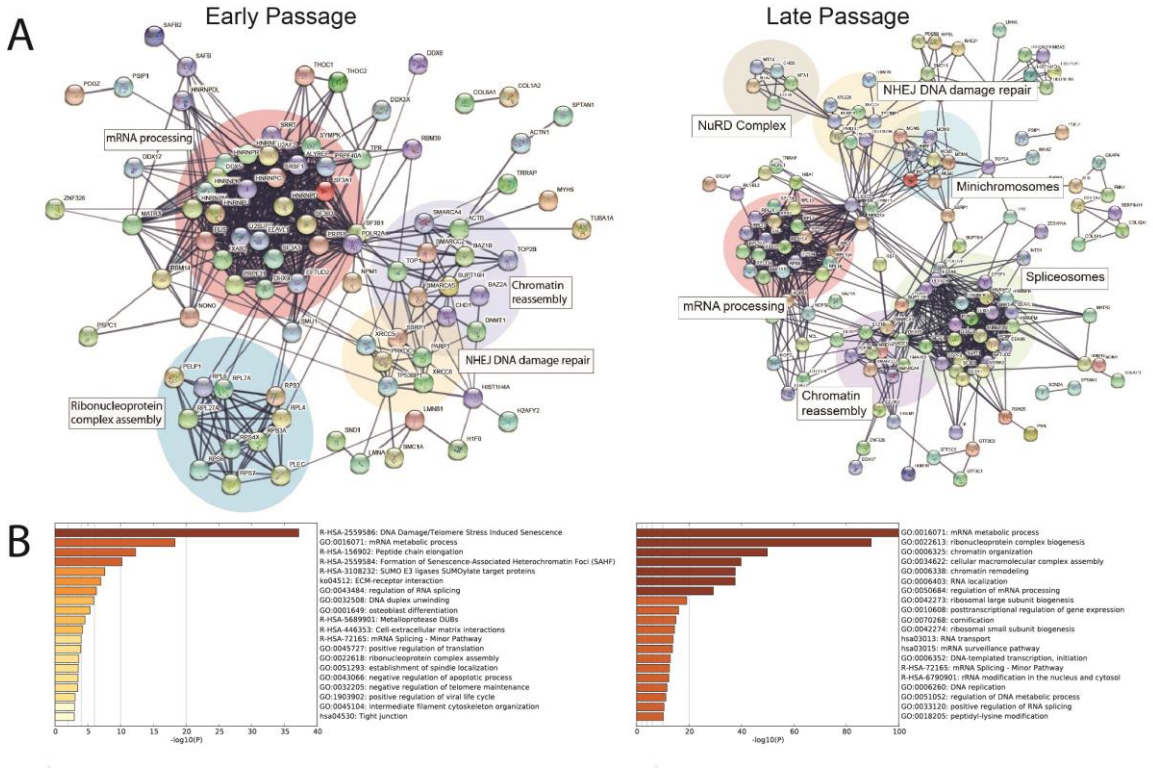

Figure 3.21. HGPS VSMCs exhibit abnormal engagement with NHEJ repair on replicating DNA. (A) STRING interactome analysis of differentially abundant proteins from aniPOND mass spectrometry analysis from early (passage 7) (left) and late passage (passage 14) (right). The confidence level was set to 0.5 (medium). The thickness of the blue lines connecting various proteins represents the level of confidence with which functional partners can be predicted. **(B)** Metascape-generated heat map of GO enriched terms of differentially enriched proteins from aniPOND mass spectrometry analysis from both passage 7 (left) and passage 14 (right). Colours indicate p-values of the GO terms.

	Early Passage		Late Passage	
NHEJ Protein	Control VSMCs	HGPS VSMCs	Control VSMCs	HGPS VSMCs
53BP1	3	13	2	20
Ku70	3	15	0	13
Ku80	3	18	1	12
DNA PKC	65	155	18	46
PARP1	20	48	3	17

Table 3.2 Spectra count of proteins involved in NHEJ repair based on aniPOND mass spectrometry analysis using scaffold comparing 2 control and 2 HGPS VSMCs at both early (P7) and late passage (P14).

DSBs can be repaired by either the error-prone NHEJ pathway or the error-free HR pathway (Misteli and Scaffidi, 2005). To investigate whether NHEJ is persistently activated in HGPS VSMCs, we performed immunostaining for DNA-Pkc and 53BP1, since the phosphorylation of H2A.X by DNA-Pkc is required for NHEJ DDR activation (Urushihara et al., 2012), and 53BP1 is a checkpoint protein recruited at sites of DNA damage to promote NHEJ repair (Callen et al., 2013). High content imaging showed a significant increase in both DNA-PKc and 53BP1 in HGPS VSMCs (Figure 3.22A). Moreover, PLA analysis revealed a significant increase in 53BP1 on newly replicating DNA in HGPS VSMCs (Figure 3.22B), confirming that that HGPS cells engage the NHEJ machinery to repair breaks arising during DNA replication, promoting genomic instability.

Based upon the enrichment of 53BP1, DNA-PKcs, Ku70 and Ku80 with newly replicated DNA in HGPS VSMCs, we wanted to determine whether 53BP1 is associated with DSBs that arise during S-phase. Normally, these breaks are repaired by HR repair and the cell utilizes histone methylation, histone acetylation, and histone ubiquitylation to control the binding of 53BP1 to DNA near DSB sites (Harrigan et al., 2011; Lukas et al., 2011). BRCA1, a key protein in HR repair, and 53BP1 compete for association with DSBs. In the absence of exogenous damage, two types of DSBs are commonly seen in cells. In G1, a small number of abnormally large foci are formed and resolved in S-phase. These breaks are reportedly associated with under-replicated DNA arising at fragile sites in the genome (Harrigan et al., 2011; Lukas et al., 2011). The second type of DSB observed occurs during S-phase. S-phase cells frequently have multiple foci throughout the cell that reflect the presence of DSBs generated during DNA replication. Normally, these DSBs are negative for 53BP1 but positive for BRCA1 (Wang et al., 2002). When logarithmically growing HGPS VSMCs were immunostained against 53BP1 and BRCA1, it was observed that these cells commonly had large G1 foci enriched in 53BP1, similar to the control VSMCs. However, there was a striking accumulation of 53BP1 in the numerous foci that arise during S-phase (Figure 3.22C), suggesting that HGPS VSMCs abnormally engage the error-prone NHEJ machinery during DSB repair.

To further test whether HGPS VSMCs engage more with NHEJ machinery, VSMCs were exposed to ionizing radiation (IR) to examine the assembly of 53BP1 and

BRCA1 into the foci that arise around DSBs. NHEJ machinery assembles comparatively fast to repair DSBs within the first hour post IR. In contrast, HR requires a longer time to assemble the machinery and takes maximally 3-6 hours post damage. When we examined the ratio between 53BP1 and BRCA1 at early and later time points, we found that expectedly, control VSMCs showed a decrease in 53BP1/BRCA1 ratio per individual DSB focus over time (Figure 3.22D). However, HGPS VSMCs showed more DSBs with high 53BP1 over time (Figure 3.22D). This finding was consistent with increased NHEJ engagement I previously observed and also demonstrated a decrease in HR pathway engagement in HGPS VSMCs.

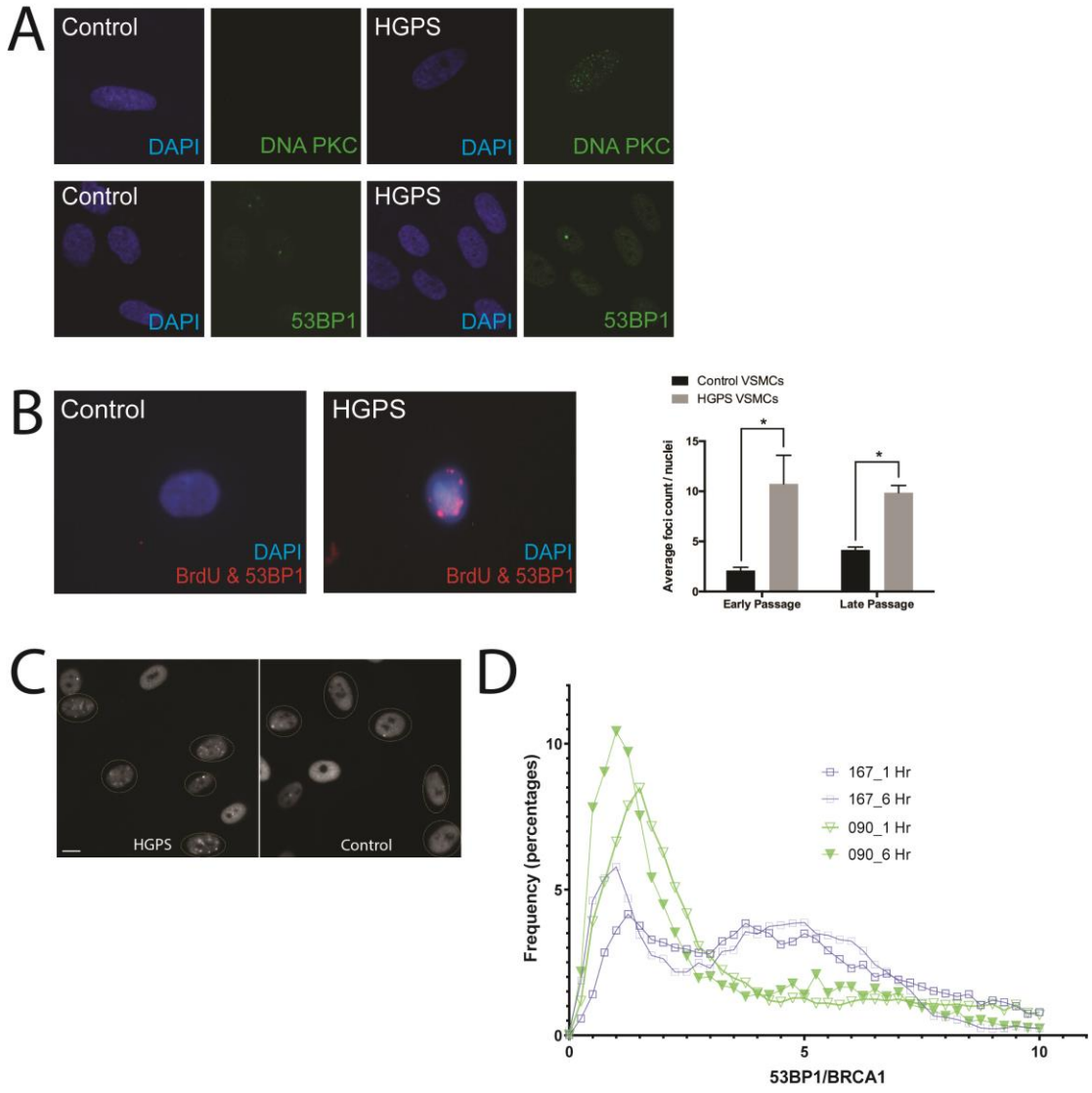

Figure 3.22 HGPS VSMCs exhibit increased engagement with NHEJ machinery during S-phase. **(A)** Representative confocal images showing immunofluorescence staining of DNA PKC and 53BP1 in control and HGPS VSMCs. **(B)** (left) Representative images of PLA staining between BrdU and 53BP1 in control and HGPS VSMCs (left). Red dots represent positive ligation between BrdU and 53BP1. (right) Bar graphs representing average count by ImageJ of PLA foci between control and HGPS VSMCs at early and late passages. Values represent mean +/-SEM (n=2, 2 lines per passage per test group). **(C)** Representative confocal image of VSMC nucleus stained with 53BP1 during S-phase. Cells were identified as S-phased based on 53BP1 foci size. **(D)** Ratio of 53BP1/BRCA1 in control versus

HGPS VSMCs following ionization. The ionization experiments and analyses were performed by Darin McDonald and Michael Hendzel.

3.4.2 HGPS VSMCs exhibit global Histone 4 Lysine 16 acetylation (H4K16ac) loss due to defective acetyltransferase MOF abundance

NHEJ protein 53BP1 binds to nucleosomes at DNA DSBs by engaging with a constitutive histone modification (mono or trimethylated K20 of histone H4) and a DNA damage-induced modification, ubiquitylation of lysine 13 or 15 on histone H2A (Hsiao and Mizzen, 2013). Histone acetylation of lysine residues at or near these modification sites are inhibitory to 53BP1 loading. The best-characterized inhibitory acetylation is that of histone H4 K16, which interferes with the binding of the 53BP1 Tudor domain to methylated H4K20. This acetylation is deposited by the histone acetyltransferase MOF. MOF and its corresponding H4K16 acetylation have previously been reported to be reduced in the ZMPSTE24 mouse model of HGPS (Krishnan et al., 2011). Recently, lamin A/C has been shown to be a target of acetylation by MOF, and that MOF depletion leads to catastrophic genomic defects including weakened nuclear lamina stability (Karoutas et al., 2019). Therefore, I hypothesized that altered MOF activity would compromise the H4K16 acetylation level in HGPS VSMCs.

To investigate whether H4K16ac levels are indeed lowered in HGPS VSMCs relative to control cell lines, I performed immunostaining and observed a significant reduction in H4K16ac in HGPS VSMCs compared to control (Figure 3.23A). I also examined whether there is a correlation between progerin accumulation and

H4K16ac level by plotting progerin expression versus H4K16 acetylation. Strikingly, high acetylation was almost exclusively observed in low progerin expressing cells whereas elevated progerin expression correlates with decreased acetylation (Figure 3.23B), demonstrating that loss of H4K16 acetylation in HGPS VSMCs is associated with progerin accumulation.

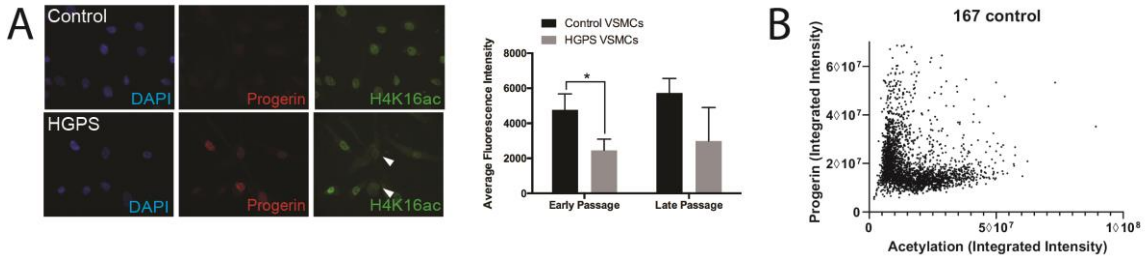

3.23 HGPS VSMCs exhibit H4K16ac loss in progerin+ cells. (A) *Left:* Representative images of immunofluorescence staining targeting progerin and H4K16ac in control and HGPS VSMCs. *Right:* Quantitative analysis of H4K16ac fluorescence intensity between control and HGPS VSMCs across both early (Passage 7) and late (Passage 14) passages. **(B)** Correlation plot from high content-imaging analysis between Progerin (x-axis) and H4K16ac (y-axis) in HGPS VSMCs. Statistical significances were calculated using student's t-test. Error bars represent SEM. * indicates $P<0.05$. A minimum of 3 biological replicates was performed for each experiment. Correlation plot and analysis were done by Michael Hendzel's lb.

To interrogate whether decreased H4K16 acetylation mediated increased NHEJ activity in HGPS VSMCs, MOF was transiently knocked down in control VSMCs using dicer-substrate siRNA, and NHEJ levels were measured via 53BP1 expression. I observed that a 60% knockdown of MOF (Figure 3.24A) led to a decrease in global H4K16ac level by 2-fold (Figure 3.24B) and significantly increased 53BP1 foci in

control VSMCs (Figure 3.24C), suggesting that reduced H4K16 acetylation would facilitate 53BP1 binding. This is consistent with the aberrant 53BP1 binding to DNA damage sites in replicating chromatin observed in HGPS VSMCs associated with loss of H4K16ac.

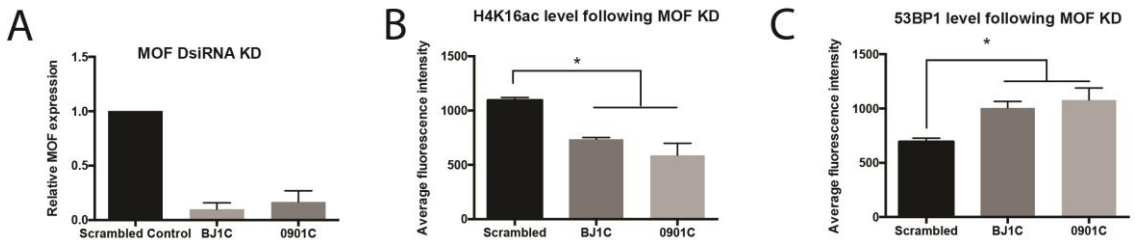

Figure 3.24 Depletion in MOF led to increased 53BP1 accumulation in normal VSMCs. (A) Relative MOF mRNA expression in two control VSMCs (BJ1C and 0901C) compared to scrambled control following MOF partial knockdown using DsiRNA knockdown strategy. Values represent average expression ± SD (n=2, 2 times per line). **(B)** High-content imaging fluorescence quantification showing a decrease in H4K16ac in control VSMCs compared to scrambled control following MOF DsiRNA knockdown. Values represent average fluorescence intensity ± SD (n=2, 2 times per line). **(C)** High-content imaging fluorescence quantification demonstrating an increase in 53BP1 expression following MOF knockdown. Values represent average fluorescence intensity ± SD (n=2, 2 times per line).

To examine whether global loss of H4K16ac is due to loss of MOF, I analyzed the expression of MOF via high content imaging and found a modest reduction in MOF expression in HGPS cells compared to control at late passage (Figure 3.25A). To determine if MOF was sufficiently recruited at replication forks to impart H4K16 acetylation in HGPS VSMCs, I performed PLA against MOF and BrdU in HGPS VSMCs. A striking loss of MOF on nascent DNA in HGPS VSMCs was observed compared to

control VSMCs (Figure 3.25C). I next determined whether progerin accumulation in the nuclear lamina affected MOF activity, since the nuclear lamina is known to regulate epigenetic landscape by interacting with histone modifiers such as acetyltransferases (Taipale et al., 2005). Indeed, HGPS VSMCs exhibited loss of interaction between lamin A and MOF (Figure 3.25E), indicating that progerin accumulation impairs the interaction between the nuclear lamina and MOF, and ultimately leads to the decreased MOF activity on nascent DNA in HGPS VSMCs. Interestingly, when we examined whether acetylation level can be rescued by treating HGPS VSMCs with histone deacetylase inhibitor trichostatin A (TSA), I observed an increase in H4K16ac level in HGPS VSMCs (Figure 3.25B), demonstrating that hypoacetylation in HGPS VSMCs could be reversed via deacetylase inhibition. Overall, I demonstrated a correlative link between defective nuclear lamina with loss of acetylation via decreased MOF recruitment.

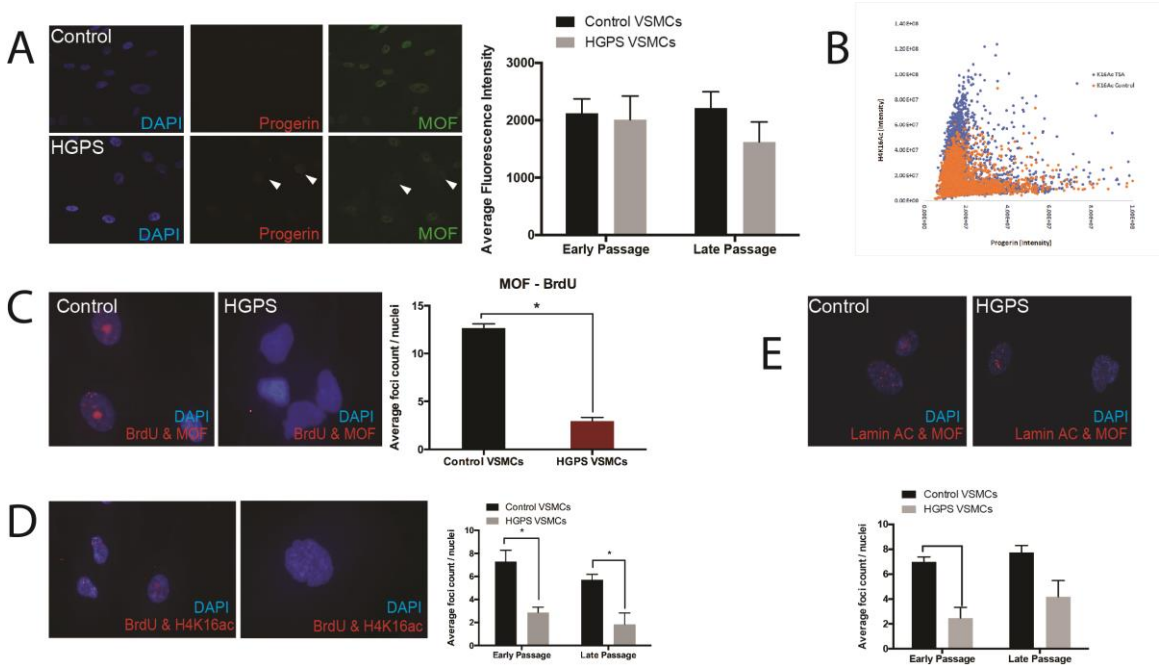

3.24. Decreased histone acetyltransferase MOF is correlated with reduced H4K16ac. (A) (Left) Representative confocal images of immunofluorescence staining for progerin (red) and MOF (green) proteins in control and HGPS VSMCs. (Right) Bar graphs representing average fluorescence intensity of MOF in both control and HGPS VSMCs at early and late passages. **(B)** Correlation plot from high content immunofluorescence imaging analysis between Progerin and H4K16ac expression in HGPS VSMC line 1671Q (orange) following TSA treatment (Blue). Each dot represents expression from a single cell. **(C)** *Left:* Representative images of PLA staining between BrdU and MOF in control and HGPS VSMCs. Each red dot represents positive ligation between BrdU and MOF. *Right:* Bar graphs representing average count of red dots by ImageJ showing colocalization of MOF and BrdU between control and HPGS VSMCs at early and late passages. **(D)** *Left:* Representative images of PLA staining between BrdU and H4K16ac in control and HGPS VSMCs. Each red dot represents positive ligation between BrdU and H4K16ac. *Right*: Bar graphs representing average signal count using ImageJ demonstrating colocalization between H4K16ac and BrdU in control versus HGPS VSMCs at both early and late passages. **(E)** *Left:* Representative images of PLA staining between Lamin A/C and MOF in control and HGPS VSMCs. Red dots represent positive ligation between Lamin A/C and MOF. *Right:* Bar graphs representing average count of red dots counted by ImageJ analysis showing colocalization of Lamin A/C and MOF in both control and HGPS VSMCs at early and late passages. Statistical significances were calculated using student's t-test. Error bars represent SEM. * indicates $P<0.05$. A minimum of 3 biological replicates was performed for each experiment. TSA treatment and analysis were performed by Michael Hendzel.

CHAPTER 4 – DISCUSSION

Aging is as a major risk factor for the development of cardiovascular disease and is associated with the onset of clinical diseases such as atherosclerosis, hypertension and heart failure as a consequence of alterations in the molecular profile of blood vessels. Therefore, the cellular and molecular mechanisms underlying age-related changes in the vasculature represent promising targets for new and improved treatments.

HGPS is an accelerated aging disease caused by a spontaneous point mutation in the *LMNA* gene. LMNA mutation leads to the accumulation of progerin, the mutant version of the Lamin A protein in the INM, which ultimately induces downstream abnormalities in nuclear structure and cellular function. Since HGPS associated cardiovascular damage mimics aspects of normative vascular aging, understanding the molecular mechanisms through which progerin damages the cardiovascular system provides novel insights into therapeutic targets of age-dependent vascular damage affecting normative CVDs.

Reprogramming HGPS fibroblasts produced bona-fide iPSCs and reset the epigenetic landscape

VSMC dysfunction is a key contributor to the pathophysiology of atherosclerosis in both HGPS and vascular aging. To enable analysis of disease initiation and progression, disease modeling using reprogrammed patient iPSCs requires the

erasure of any pathological features of the patient cells. It is evident from previous reports that the nuclear lamina is essential for normal heterochromatin organization and that progerin accumulation interferes with nuclear architecture and chromatin spatial distribution (Scaffidi and Misteli, 2005; Shumaker et al., 2006). Indeed, I observed nuclear architectural abnormalities and irregular chromatin distribution within HGPS fibroblasts. To elucidate the mechanism driving VSMC deterioration in HGPS, I validated a library of HGPS patient fibroblast-derived iPSCs and differentiated them into VSMCs to study HGPS vascular pathology. Overall, HGPS fibroblast-derived iPSCs reverted back to a normal pluripotent state despite the compromised genomic state of the donor HGPS fibroblasts. Upon reprogramming and the downregulation of Lamin A and progerin, HGPS iPSCs exhibit no gross nuclear morphological defects as observed in their parental fibroblasts. iPSCs exhibited a smooth nuclear perimeter similar to control iPSCs and hESCs, implicating that nuclear architectural defects were rescued upon silencing of progerin via reprogramming.

The nuclear lamina serves as an anchorage site for heterochromatin and thus a repressive environment for gene expression (Favale et al., 2007; Lammerding et al., 2004; Puckelwartz et al., 2011). Accumulation of progerin disrupts lamin network integrity and consequently causes transcriptional dysregulation in HGPS cells. I found that the gene expression profiles of reprogrammed HGPS statistically resemble control iPSCs and hESCs had no differentially expressed genes identified

between the two groups, despite the aberrant transcriptomic profiles found in donor fibroblasts.

The use of iPSCs to model age-related diseases including HGPS have been heavily adopted by previous studies. To date, my data is the first study using a systematic approach to demonstrate that despite initial compromised genomic state in donor fibroblasts, the morphological nuclear defects and transcriptomic as well as the epigenetic landscape were ameliorated following reprogramming. Despite the apparent efficacy of reprogramming to abolish the HGPS phenotype, certain improvements would further validate the complete reprogramming and rejuvenation of aged HGPS fibroblast to a healthy ESC state. Firstly, emerging studies suggested that iPSCs may harbour more genetic and epigenetic abnormalities than hESCs and their original somatic cells following reprogramming, potentially retaining residual methylation signatures from their tissue of origin (Pera, 2011). For instance, iPSCs derived from mouse neural progenitors contained methylomic signatures at loci essential for hematopoietic differentiation, resulting in a decreased potential to differentiate into hematopoietic cell lineages (Kim et al., 2010). HGPS fibroblasts exhibit a profound loss in histone-covalent modifications and compromised epigenetic landscape (Goldman et al., 2004; Shumaker et al., 2006). We observed a loss of both H3K4me3 and H3K27me3 histone marks in HGPS fibroblasts, which were restored to normal levels in the derived iPSCs. Genome-wide enrichment profiles of both marks showed little variance between HGPS and control iPSCs, further confirming that the epigenome in our iPSC clones

were restored. Interestingly, differentially methylated regions in HGPS iPSCs were predominantly clustered outside gene promoters, which could affect distal enhancer activities and impact downstream gene expression. These regions could represent epigenetic memory retention from the parental fibroblasts and may impact any differentiated cell phenotypes. Future experiments incorporating more sensitive technologies such as RNA-seq combined with ATAC-seq could shed light on differences in regional enhancers and its impact on differential gene expression in iPSCs.

HGPS cells display severe telomere shortening, which are elongated in iPSCs following reprogramming (Liu et al., 2011). However, in recent reports comparing iPSC to hESCs, variability in telomere length and telomerase expression was observed in iPSCs in comparison to hESCs in a passage-dependent manner (Vaziri et al., 2010; Wang et al., 2012). It would be important to identify telomere length in HGPS iPSCs to examine whether telomere length has been restored via reprogramming. Finally, mitochondrial function and metabolism were found to be different between aged somatic cells versus ESCs, including variable oxidative stress in somatic cells and a greater reliance on anaerobic glycolysis in ESCs (Prigione et al., 2010). Therefore, additional experiments should determine whether the reprogramming process resets the metabolic and oxidative stress signature in HGPS iPSCs.

HGPS iPSCs can differentiate into VSMCs that exhibit hallmark vascular aging phenotypes

To study vascular complications in HGPS patients, I differentiated HGPS iPSCs into VSMCs. I observed that HGPS iPSCs differentiate into VSMCs at a similar efficiency as control iPSCs. Following differentiation, HGPS VSMCs exhibited progerin accumulation at mRNA and protein level, increased abnormal nuclear morphology, increased DNA damage response, elevated ROS, and premature senescence, which are all phenotypes observed in normative vascular aging. During differentiation, both control and HGPS VSMCs exhibited an initial spike in γH2A.X expression, which could be indicative of an increase in DNA aberrations during iPSC differentiation, since DDR pathways have been shown to regulate differentiation processes from undifferentiated hESCs and iPSCs into various lineages including neural progenitors and B lymphocytes (Bredemeyer et al., 2008; Mujoo et al., 2017). However, HGPS VSMCs exhibit an initial decline in DNA damage similarly to control VSMCs, followed by an increase in γH2A.X despite comparable progerin levels in HGPS VSMCs across all passages. It is possible that progerin associated DNA damage and DDR required some time accumulate to observable levels in older HGPS VSMCs. Nonetheless, the progressive increase in DNA damage and DDR I observed is corroborated by elevated DNA damage in atherosclerotic plaques from both HGPS and normal aged individuals, demonstrating HGPS iPSCs can be differentiated into disease-relevant cell types to analyze disease progression.

The differentiation of iPSCs into vascular lineages is a multistep process that involves mesoderm formation, further differentiation into vascular progenitors followed finally by maturation. Early differentiation of human PSCs in VSMCs is controlled by major signaling pathways including the temporal activation of BMP, TGF-β/Activin/Nodal, WNT and FGF, giving rise to cardiovascular lineage progenitors which can then be specifically differentiated into VSMCs (Yang et al., 2008). An important aspect of deriving VSMCs from pluripotent stem cells is through EB formation followed by monolayer formation in the presence of varying cocktails of factors throughout differentiation (Xie et al., 2007). This method was adopted to derive HGPS VSMCs since EB formation partially mimics early embryonic development, where expression of essential regulatory factors occur in a similar sequence to embryogenesis (Nishikawa et al., 2007). Following EB formation, EB outgrowths were grown in media containing FBS and growth factors such as βFGF and IGF-1 to enrich for the proliferation and maturation of VSMCs. I observed that VSMCs differentiated using this method expressed high levels of smooth muscle cell markers at a comparable level to the control, demonstrating the efficacy of this method to derive VSMCs. On the other hand, one of the limitations using EB differentiation system is that the cell lineage heterogeneity within EBs and between EBs is common due to the inability for EBs to reproduce axial specification or patterning during differentiation (Sinha et al., 2006). Thus, the EB outgrowth can vary considerably, which may impact biological HGPS progression or the final VSMC phenotype. In addition, VSMCs vary greatly in terms of their origin and terminal phenotype. VSMCs are heterogenic in origin and can undergo phenotypic changes in

response to environmental signals (Majesky and Mummery, 2012). Identifying specific markers to define the varying terminal VSMC phenotypes post-differentiation would ensure that VSMCs of the same type are compared. A serum-free and chemical defined method could be an alternative approach to resolve the complexity of VSMC differentiation specificity to obtain a more reproducible population of VSMCs for disease modeling.

Transcription aberrancies in HGPS VSMCs capture typical atherosclerotic progression

In early stages of vascular aging, VSMCs undergo phenotypic switch from a quiescent to proliferative state due to the dysfunction of cell cycle checkpoint proteins and overexpression or activation of growth factors that induce uninhibited cell division (Bennett, 1999; Capell et al., 2007; Costopoulos et al., 2008). Diseased VSMCs during vascular aging also respond abnormally to mechanical stress, which induces altered gene expression and changes in the biophysical properties of the nucleus (Swift et al., 2013). Similarly, I observed that, following differentiation, HGPS VSMCs exhibited passage-dependent transcriptomic aberrancies upon the expression of progerin. At early passages, HGPS VSMCs exhibited downregulated in transcriptomic programs such as *cell cycle regulation* and *response to mechanical stimulus*, consistent with the molecular changes observed in early vascular aging. Downregulated *cell cycle regulation* genes such as *THOC5* and *NR4A1* have been previously implicated in suppressing mitogen-induced smooth muscle dedifferentiation and proliferation (Hinze et al., 2013; Yuan et al., 2018), illustrating

the hyperproliferative identity HGPS VSMCs adopt at early stage of disease progression. HGPS VSMCs also exhibit alterations in mechanical stimulus response genes, including *SUN1*, which was previously reported to have dysregulated binding with the nuclear lamina in progeroid studies (Chen et al., 2012; Chen et al., 2014). *SUN1* is a component of the LINC complex within the nuclear membrane and is essential for nuclear mechanotransduction (Capell and Collins, 2006; Wilson and Foisner, 2010). The downregulation of *SUN1* in HGPS VSMCs may drive abnormal nuclear morphology as well as increase sensitivity to mechanical stress. HGPS VSMCs exhibited an activation of *vasculature morphogenesis* and *collagen metabolic processes* genes, capturing the transcriptomic changes driving vascular remodeling and the calcification that takes place during early atherosclerosis.

In contrast, late passage HGPS VSMCs exhibited a downregulation of *smooth muscle proliferation*, concomitant with an upregulation of the *immune response* and an overall dysregulation of *oxidative stress response* genes. These changes phenocopied late stage vascular aging and atherosclerosis where VSMCs undergo senescence and exhibit increased proinflammatory cytokine release in tandem with increased oxidative insults. It is commonly known that atherosclerosis is a chronic inflammatory disorder where pro- and anti-inflammatory immune responses are generated around the vascular lesion sites (Costopoulos et al., 2008; Gorenne et al., 2006; Wang et al., 2007). Consistent with this observation, HGPS VSMCs exhibit an upregulation in immune response genes such as *IL6*, *TRPM4*, and *CAMK4,* which were previously reported to play a role in atherosclerotic progression (Galkina and

Ley, 2009; Lacolley et al., 2012). It is also interesting to note that HGPS VSMCs showed a downregulation in the *regulation of autophagy*, including decreased expression of *TSC1* and *ATG7*, supporting previous findings that demonstrated HGPS fibroblasts and other laminopathies exhibit alterations in mTOR signaling and increased autophagy (Cenni et al., 2011; Talaei et al., 2013). Overall, the differential gene signatures observed at early and late passages in HGPS VSMCs compared to controls revealed a pathological progression of VSMC deterioration that phenocopied vascular changes in atherosclerosis on a transcriptomic level, which further validates HGPS VSMCs as a valuable resource for modeling normative aging.

Oxidative stress induces DNA damage in HGPS VSMCs

Altered ROS metabolism has been a common byproduct in both normative vascular aging and progeroid laminopathies, where accumulation of farnesylated prelamin A induces excessive ROS and reduced levels of antioxidant enzymes (Richards et al., 2011; Viteri et al., 2010). My RNA-seq analyses revealed that HGPS VSMCs exhibit significant perturbations in the transcriptomic programs involved in oxidative stress response at both early and late passage. At early passage, HGPS VSMCs exhibit a down-regulation in *ROS response* programs, suggesting a misregulation of ROS maintenance. At later passage, GO terms for *response to oxidative stress* were observed to be both up and downregulated as compared to control, indicating an overall imbalance of the redox response that contributes to the overall increase in ROS and cellular inflammation. Recent studies on the direct link between defective nuclear lamina with elevated ROS revealed that progerin has a stronger affinity for

redox regulators such as NRF2 than lamins, thereby entrapping NRF2 at the nuclear membrane and impairing its ability to maintain redox homeostasis(Kubben et al., 2016). Our RNA-seq data indicated an upregulation in NRF2 expression in HGPS VSMCs compared to control at late passage. This could be a result of NRF2 mislocalization at the nuclear periphery, which would induce increased NRF2 expression in a feed-forward loop. Nonetheless, the entrapment of redox regulatory proteins in tandem with dysregulation in oxidative stress transcriptional programs could contribute to the rapid deterioration in HGPS VSMCs. This finding highlights the importance of lamins in regulating gene expression and protein localization and reveals the oxidative stress pathway as an attractive target for developing therapeutic strategies to treat HGPS VSMCs and normative aged vasculature.

Increased DNA damage is common in both HGPS VSMCs as well as atherosclerotic plaques from normal individuals. Since it is well established that cells with defective nuclear lamina exhibit elevated DNA damage, a majority of previous HGPS studies targeted progerin accumulation by administering HGPS patients with FTI, which was shown to moderately improve cardiovascular health (Gordon et al., 2012). The major deleterious effect of elevated ROS is persistent DNA damage leading to cellular dysfunction and diseases. I investigated whether persistently increased oxidation activity in HGPS VSMCs is directly altering DNA and thereby creating DNA breaks. I found that HGPS VSMCs exhibit elevated cellular ROS that induced direct DNA damage by oxidizing nucleotides to create DNA lesions. Furthermore, treating HGPS VSMCs with the ROS scavenger NAC significantly decreased DNA damage,

highlighting the influence of ROS imbalance on DNA damage in vascular aging. To my knowledge, this is the first report of ROS directly inducing DNA lesions in the context of vascular aging. We hypothesize administering both FTI and molecular reagents targeting oxidative stress pathways could synergistically improve the outcomes of both HGPS and CVDs.

HGPS VSMCs exhibit abnormal engagement with NHEJ

The misregulation of DSB repair has been previously implicated in HGPS. Progeroid fibroblasts accumulate basal levels of DNA damage as shown by the elevated presence of γH2AX foci and persistent activation of DDR checkpoint kinases (Liu et al., 2005; Liu et al., 2006). Recent studies have shed light on abnormal downstream DDR signalling events that could cause persistent DNA damage in HGPS cells. Liu et al. reported that HGPS patient-derived fibroblasts exhibit reduced expression of DNAPK holoenzyme, consisting of DNA PKcs/XRCC5/XRCC6 (Liu et al., 2011). Similarly, a recent study by Zhang et al. revealed that HGPS iPSC-derived smooth muscle cells exhibited an abnormal activation of NHEJ as a result of progerin accumulation suppressing PARP1 expression (Zhang et al., 2014). Here, I determined that HGPS VSMCs exhibited an overall loss of DNA PKcs at the protein level. Interestingly, HGPS VSMCs exhibit an abundance of protein clusters involved in NHEJ repair on newly replicated DNA. These proteins were not upregulated at a transcriptomic level, suggesting that they are likely mislocalized rather than misregulated. We also observed that HGPS VSMCs showed higher 53BP1 to BRCA1 foci ratio post-IR treatment, suggesting that HGPS VSMCs engage with NHEJ

machinery more than HR and thereby contributing to the increased level of unrepaired DNA damage in HGPS cells. I also found an increased abundance of minichromosome maintenance proteins (MCMs) in HGPS VSMCs at later passage. MCMs constitute the core of replicative DNA helicase and are required for processive DNA replication. More importantly, the presence of MCMs at replications forks has been implicated to have a role in protecting against DNA damage during replicative stress (Drissi et al., 2018; Ibarra et al., 2008). It is suspected that the elevated MCM level in HGPS VSMCs could be a response mechanism in the presence of persistent DNA damage. Future experiments using lamin-ChIP could reveal whether defective nuclear lamina interaction with NHEJ proteins would contribute to the elevated NHEJ repair activity in HGPS.

Dysregulated DDR activity drives defective epigenetic landscape in HGPS VSMCs

Strong correlative evidence suggested that persistent DNA damage leads to defective epigenetic inheritance as DDR involves the remodeling of chromatin compaction at damaged sites (Margueron and Reinberg, 2010). The enrichment for chromatin remodelers such as SMARCA4 and SMARCA5 as well as components of the NuRD complex on newly replicated DNA in HGPS VSMCs suggest an increase in chromatin decondensation in the presence of NHEJ machinery recruitment, thereby demonstrating a causal link between DNA damage and epigenetic drift in HGPS cells. Interestingly, the NuRD complex was reported to be reduced in both HGPS cells and cells from aged individuals (Pegoraro et al., 2009). The enrichment of NuRD

complex components on replicating DNA may be a response to elevated endogenous DNA damage in HGPS cells. Further experiments utilizing FTI treatment could resolve whether progerin directly impacts their expression or localization on nascent DNA.

The impairment of DDR may be a consequence of an altered epigenetic landscape. The histone deacetylase MOF is required to promote HR repair in S-phase by acetylating H4K16, which interferes with the binding of 53BP1 to the DNA, in part through the disruption of a salt bridge between H4K16 and Glu1551 in the 53BP1 Tudor domain (Gupta et al., 2014). Concomitantly, H4K16 acetylation increases BRCA1 recruitment to DNA damage foci and activates downstream recruitment of HR repair machinery (Escribano-Diaz et al., 2013). Our immunofluorescence analyses reveal a loss of H4K16ac levels with decreased MOF expression in HGPS VSMCs, indicating that the decreased acetylation levels in tandem with abnormal accumulation of 53BP1 at DSB sites exacerbated the build-up of DNA damage. Furthermore, the global hypoacetylated state could have altered the transcriptomic landscape as reflected by RNA-seq. H4K16ac ChIP-seq would help identify differentially enriched genes to help resolve whether altered acetylation landscape and histone modifications contributes to the profound transcriptomic differences observed in HGPS VSMCs.

The role of histone acetylation and their regulation on gene expression have been studied in the context of atherosclerosis. In rat VSMCs *in vitro*, histone deacetylase

(HDAC) activity inhibits the expression of inflammatory genes and delay atherosclerotic progression (Choi et al., 2005). It is interesting to note that H4K16ac is required to promote VSMC differentiation by facilitating the binding of serum response factor (SRF) to CarG binding site in VSMC differentiation marker genes, which is crucial to inhibit VSMC phenotypic switch to a more proliferative state in response to vascular injury (Cao et al., 2005). However, the cause of deacetylation in atherosclerosis remains elusive. I identified MOF as a binding partner of nuclear lamina in VSMCs and demonstrated that progerin decreased lamin-MOF binding. Mattioli et al. similarly reported that prelamin A has a much lower affinity to HDAC2 compared to mature lamin A, a defect which can be reverted by HDAC inhibitors with statin (Mattioli et al., 2018). These observations build upon previous observations to show that the nuclear lamina maintains vascular health via acetylation-mediated regulation. Furthermore, HGPS cells showed defective modulation of HDAC2 substrates, including H3K9ac and H4K16ac during oxidative stress response, underpinning the importance of redox homeostasis in governing vascular epigenetic maintenance. Targeting the modulation of interaction between lamin A/C with acetyltransferases/deacetylases suggest a potential therapeutic approach in CVDs, which warrants further investigation.

CHAPTER 5 – CONCLUSION & FUTURE DIRECTIONS

The work presented in this dissertation describes an *in vitro* model system that uses a panel of disease relevant iPSCs with restored epigenetic landscape to generate VSMCs that recapitulated the essential phenotypes of HGPS vascular pathology. Furthermore, this thesis established a paradigm for the role of nuclear lamina in driving loss of global acetylation via defective NHEJ in the context of vascular aging, which will directly aid the identification of novel therapeutic approaches in HGPS as well as CVDs.

It is worth investigating whether defective acetylation landscape is VSMC-specific or is a systemic phenomenon. For instance, the presence of progerin in other cell types such as endothelial cells suggest that progerin accumulation in these cells may play a role in the development of cardiovascular defects in conjunction with defective VSMCs (Gimbrone and Garcia-Cardena, 2016). Yet very little is known regarding the molecular mechanism driving endothelial dysfunction in HGPS patients. Developing a HGPS iPSC-derived EC model could uncover any common underlying aberrancies between VSMCs and ECs. In addition, despite exhibiting systematic premature aging, HGPS patients does not display any cognitive impairments, which was attributed to mir-9 negatively regulating lamin A and progerin expression in neural cells (Jung et al., 2012; Nissan et al., 2012). Examining whether mir-9 rescues the defective epigenetic landscape in HGPS neural cells could pave a road to new therapeutic approaches using miRNA to rescue genomic instability in HGPS as well as CVDs.

Moreover, it remains unclear whether disease pathophysiology observed in VSMC monolayer system can be faithfully recapitulated in *in vivo* mouse models. Numerous progeria mouse models have been developed over the past 15 years. Although none of these models fully recapitulates HGPS symptoms, they provide an invaluable tool for identifying molecular and cellular mechanisms underlying progeria. *Lmna*^{G609G} knock-in mice develop numerous classic HGPS phenotypes, including extreme VSMC loss in the aortic arch (Osorio et al., 2011). Isolating primary VSMCs from these mice to measure NHEJ protein level and acetylation loss would help validate this disease mechanism in an *in vivo* context.

Since HGPS is a monogenic disease caused by a single point mutation in the *LMNA* gene, CRISPR/Cas9-targeted therapies hold considerable promises. Recently, Santiago-Fernandez et.al reported that using CRISPR/Cas9 system to render progerin non-functional can dramatically improve the physiological health and life span of progeroid mice (Santiago-Fernandez et al., 2019). Our lab is currently using CRISPR/Cas9 technology to ameliorate the point mutation in HGPS iPSC lines. We aim to differentiate these cells into VSMCs to investigate whether HGPS phenotypes can be rescued. Ideally, by using this strategy to correct the point mutation in VSMCs at varying points during VSMC specification, we aim to elucidate the correlation between progerin accumulation and the onset of each disease phenotype.

Experimentally, additional tests could uncover further mechanistic insights into epigenetic defects in HGPS VSMCs. For example, MOF depletion assay could be improved using multiple siRNA targets to avoid off-target effects. In addition, experiments including Lamin A/C ChIP-seq would reveal whether MOF association with nuclear lamina is affected by progerin accumulation in HGPS VSMCs. Finally, a drug screen using chemical compounds targeting epigenetic targets (using prelamin-A accumulation and localization as readout) would further deduce whether restoring epigenetic landscape in HGPS VSMCs can restore HGPS-related cellular phenotypes.

CHAPTER 6 – REFERENCES

Aliper, A.M., Csoka, A.B., Buzdin, A., Jetka, T., Roumiantsev, S., Moskalev, A., and Zhavoronkov, A. (2015). Signaling pathway activation drift during aging: Hutchinson-Gilford Progeria Syndrome fibroblasts are comparable to normal middle-age and old-age cells. Aging *7*, 26-37.

Bennett, M.R. (1999). Apoptosis of vascular smooth muscle cells in vascular remodelling and atherosclerotic plaque rupture. Cardiovascular research *41*, 361-368.

Bennett, M.R., Macdonald, K., Chan, S.W., Boyle, J.J., and Weissberg, P.L. (1998). Cooperative interactions between RB and p53 regulate cell proliferation, cell senescence, and apoptosis in human vascular smooth muscle cells from atherosclerotic plaques. Circulation research *82*, 704-712.

Blondel, S., Jaskowiak, A.L., Egesipe, A.L., Le Corf, A., Navarro, C., Cordette, V., Martinat, C., Laabi, Y., Djabali, K., de Sandre-Giovannoli, A*., et al.* (2014). Induced pluripotent stem cells reveal functional differences between drugs currently investigated in patients with hutchinson-gilford progeria syndrome. Stem Cells Transl Med *3*, 510-519.

Bredemeyer, A.L., Helmink, B.A., Innes, C.L., Calderon, B., McGinnis, L.M., Mahowald, G.K., Gapud, E.J., Walker, L.M., Collins, J.B., Weaver, B.K*., et al.* (2008). DNA double-strand breaks activate a multi-functional genetic program in developing lymphocytes. Nature *456*, 819-823.

Broers, J.L., Kuijpers, H.J., Ostlund, C., Worman, H.J., Endert, J., and Ramaekers, F.C. (2005). Both lamin A and lamin C mutations cause lamina instability as well as loss of internal nuclear lamin organization. Experimental cell research *304*, 582-592.

Bunting, S.F., Callen, E., Wong, N., Chen, H.T., Polato, F., Gunn, A., Bothmer, A., Feldhahn, N., Fernandez-Capetillo, O., Cao, L*., et al.* (2010). 53BP1 inhibits homologous recombination in Brca1-deficient cells by blocking resection of DNA breaks. Cell *141*, 243-254.

Callen, E., Di Virgilio, M., Kruhlak, M.J., Nieto-Soler, M., Wong, N., Chen, H.T., Faryabi, R.B., Polato, F., Santos, M., Starnes, L.M*., et al.* (2013). 53BP1 mediates productive and mutagenic DNA repair through distinct phosphoprotein interactions. Cell *153*, 1266-1280.

Cao, D., Wang, Z., Zhang, C.L., Oh, J., Xing, W., Li, S., Richardson, J.A., Wang, D.Z., and Olson, E.N. (2005). Modulation of smooth muscle gene expression by association of histone acetyltransferases and deacetylases with myocardin. Mol Cell Biol *25*, 364-376.

Cao, K., Graziotto, J.J., Blair, C.D., Mazzulli, J.R., Erdos, M.R., Krainc, D., and Collins, F.S. (2011). Rapamycin reverses cellular phenotypes and enhances mutant protein clearance in Hutchinson-Gilford progeria syndrome cells. Sci Transl Med *3*, 89ra58.

Capell, B.C., and Collins, F.S. (2006). Human laminopathies: nuclei gone genetically awry. Nature reviews Genetics *7*, 940-952.

Capell, B.C., Collins, F.S., and Nabel, E.G. (2007). Mechanisms of cardiovascular disease in accelerated aging syndromes. Circulation research *101*, 13-26.

Capell, B.C., Erdos, M.R., Madigan, J.P., Fiordalisi, J.J., Varga, R., Conneely, K.N., Gordon, L.B., Der, C.J., Cox, A.D., and Collins, F.S. (2005). Inhibiting farnesylation of progerin prevents the characteristic nuclear blebbing of Hutchinson-Gilford progeria syndrome. Proceedings of the National Academy of Sciences of the United States of America *102*, 12879-12884.

Capell, B.C., Olive, M., Erdos, M.R., Cao, K., Faddah, D.A., Tavarez, U.L., Conneely, K.N., Qu, X., San, H., Ganesh, S.K.*, et al.* (2008). A farnesyltransferase inhibitor prevents both the onset and late progression of cardiovascular disease in a progeria mouse model. Proceedings of the National Academy of Sciences of the United States of America *105*, 15902-15907.

Cenni, V., Capanni, C., Columbaro, M., Ortolani, M., D'Apice, M.R., Novelli, G., Fini, M., Marmiroli, S., Scarano, E., Maraldi, N.M.*, et al.* (2011). Autophagic degradation of farnesylated prelamin A as a therapeutic approach to lamin-linked progeria. Eur J Histochem *55*, e36.

Chang, W.Y., Andrews, J., Carter, D.E., and Dagnino, L. (2006). Differentiation and injury-repair signals modulate the interaction of E2F and pRB proteins with novel target genes in keratinocytes. Cell cycle *5*, 1872-1879.

Chang, W.Y., Lavoie, J.R., Kwon, S.Y., Chen, Z., Manias, J.L., Behbahani, J., Ling, V., Kandel, R.A., Stewart, D.J., and Stanford, W.L. (2013). Feeder-independent derivation of induced-pluripotent stem cells from peripheral blood endothelial progenitor cells. Stem Cell Res *10*, 195-202.

Chapman, J.R., Sossick, A.J., Boulton, S.J., and Jackson, S.P. (2012). BRCA1-associated exclusion of 53BP1 from DNA damage sites underlies temporal control of DNA repair. Journal of cell science *125*, 3529-3534.

Chen, C.Y., Chi, Y.H., Mutalif, R.A., Starost, M.F., Myers, T.G., Anderson, S.A., Stewart, C.L., and Jeang, K.T. (2012). Accumulation of the inner nuclear envelope protein Sun1 is pathogenic in progeric and dystrophic laminopathies. Cell *149*, 565-577.

Chen, Z.J., Wang, W.P., Chen, Y.C., Wang, J.Y., Lin, W.H., Tai, L.A., Liou, G.G., Yang, C.S., and Chi, Y.H. (2014). Dysregulated interactions between lamin A and SUN1 induce abnormalities in the nuclear envelope and endoplasmic reticulum in progeric laminopathies. Journal of cell science *127*, 1792-1804.

Choi, J.H., Nam, K.H., Kim, J., Baek, M.W., Park, J.E., Park, H.Y., Kwon, H.J., Kwon, O.S., Kim, D.Y., and Oh, G.T. (2005). Trichostatin A exacerbates atherosclerosis in low density lipoprotein receptor-deficient mice. Arteriosclerosis, thrombosis, and vascular biology *25*, 2404-2409.

Chojnowski, A., Ong, P.F., Wong, E.S., Lim, J.S., Mutalif, R.A., Navasankari, R., Dutta, B., Yang, H., Liow, Y.Y., Sze, S.K*., et al.* (2015). Progerin reduces LAP2alpha-telomere association in Hutchinson-Gilford progeria. eLife *4*.

Columbaro, M., Capanni, C., Mattioli, E., Novelli, G., Parnaik, V.K., Squarzoni, S., Maraldi, N.M., and Lattanzi, G. (2005). Rescue of heterochromatin organization in Hutchinson-Gilford progeria by drug treatment. Cellular and molecular life sciences : CMLS *62*, 2669-2678.

Constantinescu, D., Csoka, A.B., Navara, C.S., and Schatten, G.P. (2010). Defective DSB repair correlates with abnormal nuclear morphology and is improved with FTI treatment in Hutchinson-Gilford progeria syndrome fibroblasts. Experimental cell research *316*, 2747-2759.

Constantinescu, D., Gray, H.L., Sammak, P.J., Schatten, G.P., and Csoka, A.B. (2006). Lamin A/C expression is a marker of mouse and human embryonic stem cell differentiation. Stem cells *24*, 177-185.

Correia-Melo, C., and Passos, J.F. (2015). Mitochondria: Are they causal players in cellular senescence? Biochim Biophys Acta *1847*, 1373-1379.

Costopoulos, C., Liew, T.V., and Bennett, M. (2008). Ageing and atherosclerosis: Mechanisms and therapeutic options. Biochemical pharmacology *75*, 1251-1261.

d'Adda di Fagagna, F., Reaper, P.M., Clay-Farrace, L., Fiegler, H., Carr, P., Von Zglinicki, T., Saretzki, G., Carter, N.P., and Jackson, S.P. (2003). A DNA damage checkpoint response in telomere-initiated senescence. Nature *426*, 194-198.

Dahl, K.N., Scaffidi, P., Islam, M.F., Yodh, A.G., Wilson, K.L., and Misteli, T. (2006). Distinct structural and mechanical properties of the nuclear lamina in Hutchinson-Gilford progeria syndrome. Proceedings of the National Academy of Sciences of the United States of America *103*, 10271-10276.

De Vos, W.H., Houben, F., Kamps, M., Malhas, A., Verheyen, F., Cox, J., Manders, E.M., Verstraeten, V.L., van Steensel, M.A., Marcelis, C.L.*, et al.* (2011). Repetitive disruptions of the nuclear envelope invoke temporary loss of cellular compartmentalization in laminopathies. Human molecular genetics *20*, 4175-4186.

Dechat, T., Pfleghaar, K., Sengupta, K., Shimi, T., Shumaker, D.K., Solimando, L., and Goldman, R.D. (2008). Nuclear lamins: major factors in the structural organization and function of the nucleus and chromatin. Genes & development *22*, 832-853.

Dimri, G.P., Lee, X., Basile, G., Acosta, M., Scott, G., Roskelley, C., Medrano, E.E., Linskens, M., Rubelj, I., Pereira-Smith, O.*, et al.* (1995). A biomarker that identifies senescent human cells in culture and in aging skin in vivo. Proceedings of the National Academy of Sciences of the United States of America *92*, 9363-9367.

Dorado, B., and Andres, V. (2017). A-type lamins and cardiovascular disease in premature aging syndromes. Curr Opin Cell Biol *46*, 17-25.

Driscoll, M.K., Albanese, J.L., Xiong, Z.M., Mailman, M., Losert, W., and Cao, K. (2012). Automated image analysis of nuclear shape: what can we learn from a prematurely aged cell? Aging *4*, 119-132.

Drissi, R., Chauvin, A., McKenna, A., Levesque, D., Blais-Brochu, S., Jean, D., and Boisvert, F.M. (2018). Destabilization of the MiniChromosome Maintenance (MCM) complex modulates the cellular response to DNA double strand breaks. Cell cycle *17*, 2593-2609.

Durik, M., Kavousi, M., van der Pluijm, I., Isaacs, A., Cheng, C., Verdonk, K., Loot, A.E., Oeseburg, H., Bhaggoe, U.M., Leijten, F.*, et al.* (2012). Nucleotide excision DNA repair is associated with age-related vascular dysfunction. Circulation *126*, 468-478.

Eriksson, M., Brown, W.T., Gordon, L.B., Glynn, M.W., Singer, J., Scott, L., Erdos, M.R., Robbins, C.M., Moses, T.Y., Berglund, P.*, et al.* (2003). Recurrent de novo point mutations in lamin A cause Hutchinson-Gilford progeria syndrome. Nature *423*, 293-298.

Escribano-Diaz, C., Orthwein, A., Fradet-Turcotte, A., Xing, M., Young, J.T., Tkac, J., Cook, M.A., Rosebrock, A.P., Munro, M., Canny, M.D.*, et al.* (2013). A cell cycle-dependent regulatory circuit composed of 53BP1-RIF1 and BRCA1-CtIP controls DNA repair pathway choice. Molecular cell *49*, 872-883.

Favale, N.O., Sterin Speziale, N.B., and Fernandez Tome, M.C. (2007). Hypertonic-induced lamin A/C synthesis and distribution to nucleoplasmic speckles is mediated by TonEBP/NFAT5 transcriptional activator. Biochemical and biophysical research communications *364*, 443-449.

Fawcett, D.W. (1966). On the occurrence of a fibrous lamina on the inner aspect of the nuclear envelope in certain cells of vertebrates. Am J Anat *119*, 129-145.

Fleischer, J.G., Schulte, R., Tsai, H.H., Tyagi, S., Ibarra, A., Shokhirev, M.N., Huang, L., Hetzer, M.W., and Navlakha, S. (2018). Predicting age from the transcriptome of human dermal fibroblasts. Genome Biol *19*, 221.

Gabriel, D., Roedl, D., Gordon, L.B., and Djabali, K. (2015). Sulforaphane enhances progerin clearance in Hutchinson-Gilford progeria fibroblasts. Aging cell *14*, 78-91.

Galkina, E., and Ley, K. (2009). Immune and inflammatory mechanisms of atherosclerosis (*). Annu Rev Immunol *27*, 165-197.

Ghosh, S., Liu, B., Wang, Y., Hao, Q., and Zhou, Z. (2015). Lamin A Is an Endogenous SIRT6 Activator and Promotes SIRT6-Mediated DNA Repair. Cell reports *13*, 1396-1406.

Gibbs-Seymour, I., Markiewicz, E., Bekker-Jensen, S., Mailand, N., and Hutchison, C.J. (2015). Lamin A/C-dependent interaction with 53BP1 promotes cellular responses to DNA damage. Aging cell *14*, 162-169.

Gimbrone, M.A., Jr., and Garcia-Cardena, G. (2016). Endothelial Cell Dysfunction and the Pathobiology of Atherosclerosis. Circulation research *118*, 620-636.

Goldman, R.D., Shumaker, D.K., Erdos, M.R., Eriksson, M., Goldman, A.E., Gordon, L.B., Gruenbaum, Y., Khuon, S., Mendez, M., Varga, R.*, et al.* (2004).

Accumulation of mutant lamin A causes progressive changes in nuclear architecture in Hutchinson-Gilford progeria syndrome. Proceedings of the National Academy of Sciences of the United States of America *101*, 8963-8968.

Gonzalo, S., Kreienkamp, R., and Askjaer, P. (2017). Hutchinson-Gilford Progeria Syndrome: A premature aging disease caused by LMNA gene mutations. Ageing Res Rev *33*, 18-29.

Gordon, L.B., Kleinman, M.E., Miller, D.T., Neuberg, D.S., Giobbie-Hurder, A., Gerhard-Herman, M., Smoot, L.B., Gordon, C.M., Cleveland, R., Snyder, B.D.*, et al.* (2012). Clinical trial of a farnesyltransferase inhibitor in children with Hutchinson-Gilford progeria syndrome. Proceedings of the National Academy of Sciences of the United States of America *109*, 16666-16671.

Gordon, L.B., Massaro, J., D'Agostino, R.B., Sr., Campbell, S.E., Brazier, J., Brown, W.T., Kleinman, M.E., Kieran, M.W., and Progeria Clinical Trials, C. (2014). Impact of farnesylation inhibitors on survival in Hutchinson-Gilford progeria syndrome. Circulation *130*, 27-34.

Gorenne, I., Kavurma, M., Scott, S., and Bennett, M. (2006). Vascular smooth muscle cell senescence in atherosclerosis. Cardiovascular research *72*, 9-17.

Gruenbaum, Y., and Medalia, O. (2015). Lamins: the structure and protein complexes. Curr Opin Cell Biol *32*, 7-12.

Guelen, L., Pagie, L., Brasset, E., Meuleman, W., Faza, M.B., Talhout, W., Eussen, B.H., de Klein, A., Wessels, L., de Laat, W.*, et al.* (2008). Domain organization of human chromosomes revealed by mapping of nuclear lamina interactions. Nature *453*, 948-951.

Gupta, A., Hunt, C.R., Hegde, M.L., Chakraborty, S., Chakraborty, S., Udayakumar, D., Horikoshi, N., Singh, M., Ramnarain, D.B., Hittelman, W.N.*, et al.* (2014). MOF phosphorylation by ATM regulates 53BP1-mediated double-strand break repair pathway choice. Cell reports *8*, 177-189.

Guzik, T.J., Chen, W., Gongora, M.C., Guzik, B., Lob, H.E., Mangalat, D., Hoch, N., Dikalov, S., Rudzinski, P., Kapelak, B.*, et al.* (2008). Calcium-dependent NOX5 nicotinamide adenine dinucleotide phosphate oxidase contributes to vascular oxidative stress in human coronary artery disease. J Am Coll Cardiol *52*, 1803-1809.

Harada, T., Swift, J., Irianto, J., Shin, J.W., Spinler, K.R., Athirasala, A., Diegmiller, R., Dingal, P.C., Ivanovska, I.L., and Discher, D.E. (2014). Nuclear

lamin stiffness is a barrier to 3D migration, but softness can limit survival. The Journal of cell biology *204*, 669-682.

Harrigan, J.A., Belotserkovskaya, R., Coates, J., Dimitrova, D.S., Polo, S.E., Bradshaw, C.R., Fraser, P., and Jackson, S.P. (2011). Replication stress induces 53BP1-containing OPT domains in G1 cells. The Journal of cell biology *193*, 97-108.

Hatch, E.M., Fischer, A.H., Deerinck, T.J., and Hetzer, M.W. (2013). Catastrophic nuclear envelope collapse in cancer cell micronuclei. Cell *154*, 47-60.

He, F., and Zuo, L. (2015). Redox Roles of Reactive Oxygen Species in Cardiovascular Diseases. Int J Mol Sci *16*, 27770-27780.

Heidenreich, P.A., Trogdon, J.G., Khavjou, O.A., Butler, J., Dracup, K., Ezekowitz, M.D., Finkelstein, E.A., Hong, Y., Johnston, S.C., Khera, A.*, et al.* (2011). Forecasting the future of cardiovascular disease in the United States: a policy statement from the American Heart Association. Circulation *123*, 933-944.

Hennekam, R.C. (2006). Hutchinson-Gilford progeria syndrome: review of the phenotype. Am J Med Genet A *140*, 2603-2624.

Herbig, U., Jobling, W.A., Chen, B.P., Chen, D.J., and Sedivy, J.M. (2004). Telomere shortening triggers senescence of human cells through a pathway involving ATM, p53, and p21(CIP1), but not p16(INK4a). Molecular cell *14*, 501-513.

Hinze, A.V., Mayer, P., Harst, A., and von Kugelgen, I. (2013). P2X1 receptor-mediated inhibition of the proliferation of human coronary smooth muscle cells involving the transcription factor NR4A1. Purinergic Signal *9*, 677-686.

Hirano, Y., Hizume, K., Kimura, H., Takeyasu, K., Haraguchi, T., and Hiraoka, Y. (2012). Lamin B receptor recognizes specific modifications of histone H4 in heterochromatin formation. The Journal of biological chemistry *287*, 42654-42663.

Hotta, A., Cheung, A.Y.L., Farra, N., Garcha, K., Chang, W.Y., Stanford, W.L., and Ellis, J. (2009). EOS lentiviral vector selection system for human induced pluripotent stem cells. . Nature protocols *4*, 1828-1844.

Hsiao, K.Y., and Mizzen, C.A. (2013). Histone H4 deacetylation facilitates 53BP1 DNA damage signaling and double-strand break repair. J Mol Cell Biol *5*, 157-165.

Ibarra, A., Schwob, E., and Mendez, J. (2008). Excess MCM proteins protect human cells from replicative stress by licensing backup origins of replication. Proceedings of the National Academy of Sciences of the United States of America *105*, 8956-8961.

Jung, H.J., Coffinier, C., Choe, Y., Beigneux, A.P., Davies, B.S., Yang, S.H., Barnes, R.H., 2nd, Hong, J., Sun, T., Pleasure, S.J.*, et al.* (2012). Regulation of prelamin A but not lamin C by miR-9, a brain-specific microRNA. Proceedings of the National Academy of Sciences of the United States of America *109*, E423-431.

Karoutas, A., Szymanski, W., Rausch, T., Guhathakurta, S., Rog-Zielinska, E.A., Peyronnet, R., Seyfferth, J., Chen, H.R., de Leeuw, R., Herquel, B.*, et al.* (2019). The NSL complex maintains nuclear architecture stability via lamin A/C acetylation. Nature cell biology *21*, 1248-1260.

Kennedy, B.K., Barbie, D.A., Classon, M., Dyson, N., and Harlow, E. (2000). Nuclear organization of DNA replication in primary mammalian cells. Genes & development *14*, 2855-2868.

Kim, K., Doi, A., Wen, B., Ng, K., Zhao, R., Cahan, P., Kim, J., Aryee, M.J., Ji, H., Ehrlich, L.I.*, et al.* (2010). Epigenetic memory in induced pluripotent stem cells. Nature *467*, 285-290.

Kovacic, J.C., Moreno, P., Hachinski, V., Nabel, E.G., and Fuster, V. (2011). Cellular senescence, vascular disease, and aging: Part 1 of a 2-part review. Circulation *123*, 1650-1660.

Krishnan, V., Chow, M.Z., Wang, Z., Zhang, L., Liu, B., Liu, X., and Zhou, Z. (2011). Histone H4 lysine 16 hypoacetylation is associated with defective DNA repair and premature senescence in Zmpste24-deficient mice. Proceedings of the National Academy of Sciences of the United States of America *108*, 12325-12330.

Kubben, N., Adriaens, M., Meuleman, W., Voncken, J.W., van Steensel, B., and Misteli, T. (2012). Mapping of lamin A- and progerin-interacting genome regions. Chromosoma *121*, 447-464.

Kubben, N., Zhang, W., Wang, L., Voss, T.C., Yang, J., Qu, J., Liu, G.H., and Misteli, T. (2016). Repression of the Antioxidant NRF2 Pathway in Premature Aging. Cell *165*, 1361-1374.

Lacolley, P., Regnault, V., Nicoletti, A., Li, Z., and Michel, J.B. (2012). The vascular smooth muscle cell in arterial pathology: a cell that can take on multiple roles. Cardiovascular research *95*, 194-204.

Lacolley, P., Regnault, V., Segers, P., and Laurent, S. (2017). Vascular Smooth Muscle Cells and Arterial Stiffening: Relevance in Development, Aging, and Disease. Physiol Rev *97*, 1555-1617.

Lammerding, J., Schulze, P.C., Takahashi, T., Kozlov, S., Sullivan, T., Kamm, R.D., Stewart, C.L., and Lee, R.T. (2004). Lamin A/C deficiency causes defective nuclear mechanics and mechanotransduction. The Journal of clinical investigation *113*, 370-378.

Larrieu, D., Vire, E., Robson, S., Breusegem, S.Y., Kouzarides, T., and Jackson, S.P. (2018). Inhibition of the acetyltransferase NAT10 normalizes progeric and aging cells by rebalancing the Transportin-1 nuclear import pathway. Sci Signal *11*.

Lee, D.C., Welton, K.L., Smith, E.D., and Kennedy, B.K. (2009). A-type nuclear lamins act as transcriptional repressors when targeted to promoters. Experimental cell research *315*, 996-1007.

Lee, H.Y., and Oh, B.H. (2010). Aging and arterial stiffness. Circ J *74*, 2257-2262.

Leung, K.H., Abou El Hassan, M., and Bremner, R. (2013). A rapid and efficient method to purify proteins at replication forks under native conditions. BioTechniques *55*, 204-206.

Lieber, M.R. (2010). The mechanism of double-strand DNA break repair by the nonhomologous DNA end-joining pathway. Annu Rev Biochem *79*, 181-211.

Lin, F., and Worman, H.J. (1993). Structural organization of the human gene encoding nuclear lamin A and nuclear lamin C. The Journal of biological chemistry *268*, 16321-16326.

Link, J., Leubner, M., Schmitt, J., Gob, E., Benavente, R., Jeang, K.T., Xu, R., and Alsheimer, M. (2014). Analysis of meiosis in SUN1 deficient mice reveals a distinct role of SUN2 in mammalian meiotic LINC complex formation and function. PLoS genetics *10*, e1004099.

Liu, B., Wang, J., Chan, K.M., Tjia, W.M., Deng, W., Guan, X., Huang, J.D., Li, K.M., Chau, P.Y., Chen, D.J.*, et al.* (2005). Genomic instability in laminopathy-based premature aging. Nature medicine *11*, 780-785.

Liu, B., Wang, Z., Ghosh, S., and Zhou, Z. (2013a). Defective ATM-Kap-1-mediated chromatin remodeling impairs DNA repair and accelerates senescence in progeria mouse model. Aging cell *12*, 316-318.

Liu, B., Wang, Z., Zhang, L., Ghosh, S., Zheng, H., and Zhou, Z. (2013b). Depleting the methyltransferase Suv39h1 improves DNA repair and extends lifespan in a progeria mouse model. Nature communications *4*, 1868.

Liu, G.H., Barkho, B.Z., Ruiz, S., Diep, D., Qu, J., Yang, S.L., Panopoulos, A.D., Suzuki, K., Kurian, L., Walsh, C.*, et al.* (2011). Recapitulation of premature ageing with iPSCs from Hutchinson-Gilford progeria syndrome. Nature *472*, 221-225.

Liu, Y., Rusinol, A., Sinensky, M., Wang, Y., and Zou, Y. (2006). DNA damage responses in progeroid syndromes arise from defective maturation of prelamin A. Journal of cell science *119*, 4644-4649.

Liu, Y., Wang, Y., Rusinol, A.E., Sinensky, M.S., Liu, J., Shell, S.M., and Zou, Y. (2008). Involvement of xeroderma pigmentosum group A (XPA) in progeria arising from defective maturation of prelamin A. FASEB journal : official publication of the Federation of American Societies for Experimental Biology *22*, 603-611.

Lombardi, M.L., Jaalouk, D.E., Shanahan, C.M., Burke, B., Roux, K.J., and Lammerding, J. (2011). The interaction between nesprins and sun proteins at the nuclear envelope is critical for force transmission between the nucleus and cytoskeleton. The Journal of biological chemistry *286*, 26743-26753.

Luijsterburg, M.S., de Krijger, I., Wiegant, W.W., Shah, R.G., Smeenk, G., de Groot, A.J.L., Pines, A., Vertegaal, A.C.O., Jacobs, J.J.L., Shah, G.M.*, et al.* (2016). PARP1 Links CHD2-Mediated Chromatin Expansion and H3.3 Deposition to DNA Repair by Non-homologous End-Joining. Molecular cell *61*, 547-562.

Lukas, C., Savic, V., Bekker-Jensen, S., Doil, C., Neumann, B., Pedersen, R.S., Grofte, M., Chan, K.L., Hickson, I.D., Bartek, J.*, et al.* (2011). 53BP1 nuclear bodies form around DNA lesions generated by mitotic transmission of chromosomes under replication stress. Nature cell biology *13*, 243-253.

Lund, E., Oldenburg, A.R., Delbarre, E., Freberg, C.T., Duband-Goulet, I., Eskeland, R., Buendia, B., and Collas, P. (2013). Lamin A/C-promoter interactions specify chromatin state-dependent transcription outcomes. Genome research *23*, 1580-1589.

Mahen, R., Hattori, H., Lee, M., Sharma, P., Jeyasekharan, A.D., and Venkitaraman, A.R. (2013). A-type lamins maintain the positional stability of DNA damage repair foci in mammalian nuclei. PloS one *8*, e61893.

Mahmoudi, M., Mercer, J., and Bennett, M. (2006). DNA damage and repair in atherosclerosis. Cardiovascular research *71*, 259-268.

Majesky, M.W., Dong, X.R., Regan, J.N., and Hoglund, V.J. (2011). Vascular smooth muscle progenitor cells: building and repairing blood vessels. Circulation research *108*, 365-377.

Majesky, M.W., and Mummery, C.L. (2012). Smooth muscle diversity from human pluripotent cells. Nature biotechnology *30*, 152-154.

Margueron, R., and Reinberg, D. (2010). Chromatin structure and the inheritance of epigenetic information. Nature reviews Genetics *11*, 285-296.

Matthews, C., Gorenne, I., Scott, S., Figg, N., Kirkpatrick, P., Ritchie, A., Goddard, M., and Bennett, M. (2006). Vascular smooth muscle cells undergo telomere-based senescence in human atherosclerosis: effects of telomerase and oxidative stress. Circulation research *99*, 156-164.

Mattioli, E., Andrenacci, D., Garofalo, C., Prencipe, S., Scotlandi, K., Remondini, D., Gentilini, D., Di Blasio, A.M., Valente, S., Scarano, E.*, et al.* (2018). Altered modulation of lamin A/C-HDAC2 interaction and p21 expression during oxidative stress response in HGPS. Aging cell *17*, e12824.

McClintock, D., Ratner, D., Lokuge, M., Owens, D.M., Gordon, L.B., Collins, F.S., and Djabali, K. (2007). The mutant form of lamin A that causes Hutchinson-Gilford progeria is a biomarker of cellular aging in human skin. PloS one *2*, e1269.

McCord, R.P., Nazario-Toole, A., Zhang, H., Chines, P.S., Zhan, Y., Erdos, M.R., Collins, F.S., Dekker, J., and Cao, K. (2013). Correlated alterations in genome organization, histone methylation, and DNA-lamin A/C interactions in Hutchinson-Gilford progeria syndrome. Genome research *23*, 260-269.

Merideth, M.A., Gordon, L.B., Clauss, S., Sachdev, V., Smith, A.C., Perry, M.B., Brewer, C.C., Zalewski, C., Kim, H.J., Solomon, B.*, et al.* (2008). Phenotype and course of Hutchinson-Gilford progeria syndrome. The New England journal of medicine *358*, 592-604.

Misteli, T., and Scaffidi, P. (2005). Genome instability in progeria: when repair gets old. Nature medicine *11*, 718-719.

Moon, S.K., Thompson, L.J., Madamanchi, N., Ballinger, S., Papaconstantinou, J., Horaist, C., Runge, M.S., and Patterson, C. (2001). Aging, oxidative responses, and proliferative capacity in cultured mouse aortic smooth muscle cells. Am J Physiol Heart Circ Physiol *280*, H2779-2788.

Mujoo, K., Pandita, R.K., Tiwari, A., Charaka, V., Chakraborty, S., Singh, D.K., Hambarde, S., Hittelman, W.N., Horikoshi, N., Hunt, C.R.*, et al.* (2017). Differentiation of Human Induced Pluripotent or Embryonic Stem Cells Decreases the DNA Damage Repair by Homologous Recombination. Stem Cell Reports *9*, 1660-1674.

Nishikawa, S., Jakt, L.M., and Era, T. (2007). Embryonic stem-cell culture as a tool for developmental cell biology. Nat Rev Mol Cell Biol *8*, 502-507.

Nissan, X., Blondel, S., Navarro, C., Maury, Y., Denis, C., Girard, M., Martinat, C., De Sandre-Giovannoli, A., Levy, N., and Peschanski, M. (2012). Unique preservation of neural cells in Hutchinson- Gilford progeria syndrome is due to the expression of the neural-specific miR-9 microRNA. Cell reports *2*, 1-9.

O'Donnell, C.J., and Nabel, E.G. (2008). Cardiovascular genomics, personalized medicine, and the National Heart, Lung, and Blood Institute: part I: the beginning of an era. Circ Cardiovasc Genet *1*, 51-57.

O'Hagan, H.M., Mohammad, H.P., and Baylin, S.B. (2008). Double strand breaks can initiate gene silencing and SIRT1-dependent onset of DNA methylation in an exogenous promoter CpG island. PLoS genetics *4*, e1000155.

Olive, M., Harten, I., Mitchell, R., Beers, J.K., Djabali, K., Cao, K., Erdos, M.R., Blair, C., Funke, B., Smoot, L.*, et al.* (2010). Cardiovascular pathology in Hutchinson-Gilford progeria: correlation with the vascular pathology of aging. Arteriosclerosis, thrombosis, and vascular biology *30*, 2301-2309.

Osorio, F.G., Navarro, C.L., Cadinanos, J., Lopez-Mejia, I.C., Quiros, P.M., Bartoli, C., Rivera, J., Tazi, J., Guzman, G., Varela, I.*, et al.* (2011). Splicing-directed therapy in a new mouse model of human accelerated aging. Sci Transl Med *3*, 106ra107.

Pegoraro, G., Kubben, N., Wickert, U., Gohler, H., Hoffmann, K., and Misteli, T. (2009). Ageing-related chromatin defects through loss of the NURD complex. Nature cell biology *11*, 1261-1267.

Pera, M.F. (2011). Stem cells: The dark side of induced pluripotency. Nature *471*, 46-47.

Prigione, A., Fauler, B., Lurz, R., Lehrach, H., and Adjaye, J. (2010). The senescence-related mitochondrial/oxidative stress pathway is repressed in human induced pluripotent stem cells. Stem cells *28*, 721-733.

Puckelwartz, M.J., Depreux, F.F., and McNally, E.M. (2011). Gene expression, chromosome position and lamin A/C mutations. Nucleus *2*, 162-167.

Ragnauth, C.D., Warren, D.T., Liu, Y., McNair, R., Tajsic, T., Figg, N., Shroff, R., Skepper, J., and Shanahan, C.M. (2010). Prelamin A acts to accelerate smooth muscle cell senescence and is a novel biomarker of human vascular aging. Circulation *121*, 2200-2210.

Ramachandran, P., Palidwor, G.A., Porter, C.J., and Perkins, T.J. (2013). MaSC: mappability-sensitive cross-correlation for estimating mean fragment length of single-end short-read sequencing data. Bioinformatics *29*, 444-450.

Richards, S.A., Muter, J., Ritchie, P., Lattanzi, G., and Hutchison, C.J. (2011). The accumulation of un-repairable DNA damage in laminopathy progeria fibroblasts is caused by ROS generation and is prevented by treatment with N-acetyl cysteine. Human molecular genetics *20*, 3997-4004.

Rober, R.A., Weber, K., and Osborn, M. (1989). Differential timing of nuclear lamin A/C expression in the various organs of the mouse embryo and the young animal: a developmental study. Development *105*, 365-378.

Rothkamm, K., Kruger, I., Thompson, L.H., and Lobrich, M. (2003). Pathways of DNA double-strand break repair during the mammalian cell cycle. Mol Cell Biol *23*, 5706-5715.

Rowe, R.G., and Daley, G.Q. (2019). Induced pluripotent stem cells in disease modelling and drug discovery. Nature reviews Genetics *20*, 377-388.

Sancar, A., Lindsey-Boltz, L.A., Unsal-Kacmaz, K., and Linn, S. (2004). Molecular mechanisms of mammalian DNA repair and the DNA damage checkpoints. Annu Rev Biochem *73*, 39-85.

Santiago-Fernandez, O., Osorio, F.G., Quesada, V., Rodriguez, F., Basso, S., Maeso, D., Rolas, L., Barkaway, A., Nourshargh, S., Folgueras, A.R.*, et al.* (2019). Development of a CRISPR/Cas9-based therapy for Hutchinson-Gilford progeria syndrome. Nature medicine *25*, 423-426.

Scaffidi, P., and Misteli, T. (2005). Reversal of the cellular phenotype in the premature aging disease Hutchinson-Gilford progeria syndrome. Nature medicine *11*, 440-445.

Scaffidi, P., and Misteli, T. (2006). Lamin A-dependent nuclear defects in human aging. Science *312*, 1059-1063.

Sedelnikova, O.A., Horikawa, I., Zimonjic, D.B., Popescu, N.C., Bonner, W.M., and Barrett, J.C. (2004). Senescing human cells and ageing mice accumulate DNA lesions with unrepairable double-strand breaks. Nature cell biology *6*, 168-170.

Shah, P.P., Donahue, G., Otte, G.L., Capell, B.C., Nelson, D.M., Cao, K., Aggarwala, V., Cruickshanks, H.A., Rai, T.S., McBryan, T.*, et al.* (2013). Lamin B1 depletion in senescent cells triggers large-scale changes in gene expression and the chromatin landscape. Genes & development *27*, 1787-1799.

Shen, L., Shao, N.Y., Liu, X., Maze, I., Feng, J., and Nestler, E.J. (2013). diffReps: detecting differential chromatin modification sites from ChIP-seq data with biological replicates. PloS one *8*, e65598.

Sherman, M.H., Bassing, C.H., and Teitell, M.A. (2011). Regulation of cell differentiation by the DNA damage response. Trends Cell Biol *21*, 312-319.

Shevchenko, A., Tomas, H., Havlis, J., Olsen, J.V., and Mann, M. (2006). In-gel digestion for mass spectrometric characterization of proteins and proteomes. Nat Protoc *1*, 2856-2860.

Shumaker, D.K., Dechat, T., Kohlmaier, A., Adam, S.A., Bozovsky, M.R., Erdos, M.R., Eriksson, M., Goldman, A.E., Khuon, S., Collins, F.S.*, et al.* (2006). Mutant nuclear lamin A leads to progressive alterations of epigenetic control in premature aging. Proceedings of the National Academy of Sciences of the United States of America *103*, 8703-8708.

Sinha, S., Wamhoff, B.R., Hoofnagle, M.H., Thomas, J., Neppl, R.L., Deering, T., Helmke, B.P., Bowles, D.K., Somlyo, A.V., and Owens, G.K. (2006). Assessment of contractility of purified smooth muscle cells derived from embryonic stem cells. Stem cells *24*, 1678-1688.

Smith, E.D., Kudlow, B.A., Frock, R.L., and Kennedy, B.K. (2005). A-type nuclear lamins, progerias and other degenerative disorders. Mechanisms of ageing and development *126*, 447-460.

Solovei, I., Wang, A.S., Thanisch, K., Schmidt, C.S., Krebs, S., Zwerger, M., Cohen, T.V., Devys, D., Foisner, R., Peichl, L.*, et al.* (2013). LBR and lamin A/C sequentially tether peripheral heterochromatin and inversely regulate differentiation. Cell *152*, 584-598.

Struthers, L., Patel, R., Clark, J., and Thomas, S. (1998). Direct detection of 8-oxodeoxyguanosine and 8-oxoguanine by avidin and its analogues. Anal Biochem *255*, 20-31.

Swift, J., Ivanovska, I.L., Buxboim, A., Harada, T., Dingal, P.C., Pinter, J., Pajerowski, J.D., Spinler, K.R., Shin, J.W., Tewari, M.*, et al.* (2013). Nuclear lamin-A scales with tissue stiffness and enhances matrix-directed differentiation. Science *341*, 1240104.

Taimen, P., Pfleghaar, K., Shimi, T., Moller, D., Ben-Harush, K., Erdos, M.R., Adam, S.A., Herrmann, H., Medalia, O., Collins, F.S.*, et al.* (2009). A progeria mutation reveals functions for lamin A in nuclear assembly, architecture, and chromosome organization. Proceedings of the National Academy of Sciences of the United States of America *106*, 20788-20793.

Taipale, M., Rea, S., Richter, K., Vilar, A., Lichter, P., Imhof, A., and Akhtar, A. (2005). hMOF histone acetyltransferase is required for histone H4 lysine 16 acetylation in mammalian cells. Mol Cell Biol *25*, 6798-6810.

Takahashi, K., Tanabe, K., Ohnuki, M., Narita, M., Ichisaka, T., Tomoda, K., and Yamanaka, S. (2007). Induction of pluripotent stem cells from adult human fibroblasts by defined factors. Cell *131*, 861-872.

Talaei, F., van Praag, V.M., and Henning, R.H. (2013). Hydrogen sulfide restores a normal morphological phenotype in Werner syndrome fibroblasts, attenuates oxidative damage and modulates mTOR pathway. Pharmacol Res *74*, 34-44.

Tavakoli, S., and Asmis, R. (2012). Reactive oxygen species and thiol redox signaling in the macrophage biology of atherosclerosis. Antioxidants & redox signaling *17*, 1785-1795.

Tennant, M., and McGeachie, J.K. (1990). Blood vessel structure and function: a brief update on recent advances. Aust N Z J Surg *60*, 747-753.

Tsai, T.N., Kirton, J.P., Campagnolo, P., Zhang, L., Xiao, Q., Zhang, Z., Wang, W., Hu, Y., and Xu, Q. (2012). Contribution of stem cells to neointimal formation of decellularized vessel grafts in a novel mouse model. The American journal of pathology *181*, 362-373.

Urushihara, Y., Kobayashi, J., Matsumoto, Y., Komatsu, K., Oda, S., and Mitani, H. (2012). DNA-PK inhibition causes a low level of H2AX phosphorylation and homologous recombination repair in Medaka (Oryzias latipes) cells. Biochemical and biophysical research communications *429*, 131-136.

Varela, I., Pereira, S., Ugalde, A.P., Navarro, C.L., Suarez, M.F., Cau, P., Cadinanos, J., Osorio, F.G., Foray, N., Cobo, J.*, et al.* (2008). Combined treatment with statins and aminobisphosphonates extends longevity in a mouse model of human premature aging. Nature medicine *14*, 767-772.

Vaziri, H., Chapman, K.B., Guigova, A., Teichroeb, J., Lacher, M.D., Sternberg, H., Singec, I., Briggs, L., Wheeler, J., Sampathkumar, J.*, et al.* (2010). Spontaneous reversal of the developmental aging of normal human cells following transcriptional reprogramming. Regen Med *5*, 345-363.

Verstraeten, V.L., Broers, J.L., van Steensel, M.A., Zinn-Justin, S., Ramaekers, F.C., Steijlen, P.M., Kamps, M., Kuijpers, H.J., Merckx, D., Smeets, H.J.*, et al.* (2006). Compound heterozygosity for mutations in LMNA causes a progeria syndrome without prelamin A accumulation. Human molecular genetics *15*, 2509-2522.

Virmani, R., Avolio, A.P., Mergner, W.J., Robinowitz, M., Herderick, E.E., Cornhill, J.F., Guo, S.Y., Liu, T.H., Ou, D.Y., and O'Rourke, M. (1991). Effect of aging on aortic morphology in populations with high and low prevalence of hypertension and atherosclerosis. Comparison between occidental and Chinese communities. The American journal of pathology *139*, 1119-1129.

Viteri, G., Chung, Y.W., and Stadtman, E.R. (2010). Effect of progerin on the accumulation of oxidized proteins in fibroblasts from Hutchinson Gilford progeria patients. Mechanisms of ageing and development *131*, 2-8.

Walker, E., Chang, W.Y., Hunkapiller, J., Cagney, G., Garcha, K., Torchia, J., Krogan, N.J., Reiter, J.F., and Stanford, W.L. (2010). Polycomb-like 2 associates with PRC2 and regulates transcriptional networks during mouse embryonic stem cell self-renewal and differentiation. Cell stem cell *6*, 153-166.

Wallis, C.V., Sheerin, A.N., Green, M.H., Jones, C.J., Kipling, D., and Faragher, R.G. (2004). Fibroblast clones from patients with Hutchinson-Gilford progeria can senesce despite the presence of telomerase. Experimental gerontology *39*, 461-467.

Wang, B., Matsuoka, S., Carpenter, P.B., and Elledge, S.J. (2002). 53BP1, a mediator of the DNA damage checkpoint. Science *298*, 1435-1438.

Wang, F., Yin, Y., Ye, X., Liu, K., Zhu, H., Wang, L., Chiourea, M., Okuka, M., Ji, G., Dan, J.*, et al.* (2012). Molecular insights into the heterogeneity of telomere reprogramming in induced pluripotent stem cells. Cell Res *22*, 757-768.

Wang, M., Zhang, J., Jiang, L.Q., Spinetti, G., Pintus, G., Monticone, R., Kolodgie, F.D., Virmani, R., and Lakatta, E.G. (2007). Proinflammatory profile within the grossly normal aged human aortic wall. Hypertension *50*, 219-227.

Wilson, K.L., and Foisner, R. (2010). Lamin-binding Proteins. Cold Spring Harb Perspect Biol *2*, a000554.

Worman, H.J. (2012). Nuclear lamins and laminopathies. The Journal of pathology *226*, 316-325.

Xie, C.Q., Zhang, J., Villacorta, L., Cui, T., Huang, H., and Chen, Y.E. (2007). A highly efficient method to differentiate smooth muscle cells from human embryonic stem cells. Arteriosclerosis, thrombosis, and vascular biology *27*, e311-312.

Xiong, Z.M., Choi, J.Y., Wang, K., Zhang, H., Tariq, Z., Wu, D., Ko, E., LaDana, C., Sesaki, H., and Cao, K. (2016). Methylene blue alleviates nuclear and mitochondrial abnormalities in progeria. Aging cell *15*, 279-290.

Xiong, Z.M., LaDana, C., Wu, D., and Cao, K. (2013). An inhibitory role of progerin in the gene induction network of adipocyte differentiation from iPS cells. Aging *5*, 288-303.

Yang, L., Soonpaa, M.H., Adler, E.D., Roepke, T.K., Kattman, S.J., Kennedy, M., Henckaerts, E., Bonham, K., Abbott, G.W., Linden, R.M.*, et al.* (2008). Human cardiovascular progenitor cells develop from a KDR+ embryonic-stem-cell-derived population. Nature *453*, 524-528.

Yang, S.H., Meta, M., Qiao, X., Frost, D., Bauch, J., Coffinier, C., Majumdar, S., Bergo, M.O., Young, S.G., and Fong, L.G. (2006). A farnesyltransferase inhibitor improves disease phenotypes in mice with a Hutchinson-Gilford progeria syndrome mutation. The Journal of clinical investigation *116*, 2115-2121.

Ye, Q., and Worman, H.J. (1996). Interaction between an integral protein of the nuclear envelope inner membrane and human chromodomain proteins homologous to Drosophila HP1. The Journal of biological chemistry *271*, 14653-14656.

Yin, H., and Pickering, J.G. (2016). Cellular Senescence and Vascular Disease: Novel Routes to Better Understanding and Therapy. Can J Cardiol *32*, 612-623.

Yuan, X., Zhang, T., Yao, F., Liao, Y., Liu, F., Ren, Z., Han, L., Diao, L., Li, Y., Zhou, B.*, et al.* (2018). THO Complex-Dependent Posttranscriptional Control

Contributes to Vascular Smooth Muscle Cell Fate Decision. Circulation research *123*, 538-549.

Zettler, M.E., Prociuk, M.A., Austria, J.A., Massaeli, H., Zhong, G., and Pierce, G.N. (2003). OxLDL stimulates cell proliferation through a general induction of cell cycle proteins. Am J Physiol Heart Circ Physiol *284*, H644-653.

Zhang, H., Xiong, Z.M., and Cao, K. (2014). Mechanisms controlling the smooth muscle cell death in progeria via down-regulation of poly(ADP-ribose) polymerase 1. Proceedings of the National Academy of Sciences of the United States of America *111*, E2261-2270.

Zhang, J., Lian, Q., Zhu, G., Zhou, F., Sui, L., Tan, C., Mutalif, R.A., Navasankari, R., Zhang, Y., Tse, H.F.*, et al.* (2011). A human iPSC model of Hutchinson Gilford Progeria reveals vascular smooth muscle and mesenchymal stem cell defects. Cell stem cell *8*, 31-45.

Zhang, W., Li, J., Suzuki, K., Qu, J., Wang, P., Zhou, J., Liu, X., Ren, R., Xu, X., Ocampo, A.*, et al.* (2015). Aging stem cells. A Werner syndrome stem cell model unveils heterochromatin alterations as a driver of human aging. Science *348*, 1160-1163.

Zhou, Y., Zhou, B., Pache, L., Chang, M., Khodabakhshi, A.H., Tanaseichuk, O., Benner, C., and Chanda, S.K. (2019). Metascape provides a biologist-oriented resource for the analysis of systems-level datasets. Nature communications *10*, 1523.

Zuela, N., Bar, D.Z., and Gruenbaum, Y. (2012). Lamins in development, tissue maintenance and stress. EMBO Rep *13*, 1070-1078.